Cytoskeletons as Polar Landmarks

Characterization of bactofilin homologs in *Myxococcus xanthus*

Dissertation

zur Erlangung des Doktorgrades

der Naturwissenschaften

(Dr. rer. nat.)

dem

Fachbereich Biologie

der Philipps-Universität Marburg

vorgelegt

von

Lin Lin

aus Yongchun, P. R. China

Marburg (Lahn), September 2013

Vom Fachbereich Biologie der Philipps-Universität Marburg (Hochschulkennziffer: 1180)
als Dissertation angenommen am: 30.10.2013

Erstgutachter: Jun.-Prof. Dr. Martin Thanbichler
Zweitgutachter: Prof. Dr. Lotte Søgaard-Andersen

Tag der mündlichen Prüfung am: 22.11.2013

Die Untersuchungen zur vorliegenden Arbeit wurden von Oktober 2010 bis September 2013 am Max-Planck-Institut für terrestrische Mikrobiologie unter der Leitung von Jun.-Prof. Dr. Martin Thanbichler durchgeführt.

Publications involved in this thesis:

Lin, L. and Thanbichler, M. (2013) Nucleotide-independent cytoskeletal scaffolds in bacteria. *Cytoskeleton (Hoboken)* 70, 409–423.

Bulyha, I., Lindow, S., **Lin, L.**, Bolte, K., Wuichet, K., Kahnt, J., van der Does, C., Thanbichler, M., and Sogaard-Andersen, L. (2013) Two small GTPases act in concert with the bactofilin cytoskeleton to regulate dynamic bacterial cell polarity. *Dev Cell* 25, 119-131.

Lin, L., Harms, A., Kahnt, J., Søgaard-Andersen, L., and Thanbichler, M. Bactofilins as polar cytoskeletons stabilize the chromosome segregation machinery in *Myxococcus xanthus*. In preparation.

Dedicated to people who I love

ABSTRACT

Bacteria, similar to eukaryotes, possess cytoskeletons that are involved in the temporal and spatial organization of various cellular processes, including cell division, cell morphogenesis, cell polarity, as well as DNA partitioning. Out of these elements, the tubulin homolog FtsZ, the actin homolog MreB, and intermediate filament-like (IF) proteins are widespread in many bacterial lineages. In addition, in recent years, an increasing number of non-canonical cytoskeletons have been identified in bacteria. These include a new class of cytoskeletal proteins, named bactofilins, which was originally discovered in *Caulobacter crescentus*. Bactofilins are widely distributed among bacteria and show no similarity in either sequence or structure to other known cytoskeletal proteins. Interestingly, many species possess two or more bactofilin alleles, indicating multiple gene duplication events and functional diversification. In *Myxococcus xanthus*, it has been shown that BacP, one of its four bactofilin homologs, forms bipolar filaments and appears to be essential for positioning a cell polarity factor, SofG; by constrast, BacM, another bactofilin homolog, is involved in cell morphogenesis. In this work, we demonstrate that BacP, together with two other bactofilin homologs, BacO and BacN, plays an important role in stabilizing the chromosome segregation machinery in this organism. We show that BacN-P copolymerize into bipolar filaments to mediate the proper arrangement of ParA and ParB, which are key components of chromosome segregation in *M. xanthus*. In the absence of BacN-P, both proteins mislocalize, which further affects proper chromosome segregation. We further identified BadA, a ParB-like nuclease homolog that acts along with BacN-P in this mechanism, possibly by interacting with ParA directly. Taken together, bactofilins serve as landmark structures at the cell poles in *M. xanthus*, positioning and stabilizing subpolar or polar protein complexes. This scaffolding function is similar to that of PopZ in *C. crescentus* or DivIVA in Gram-positive bacteria, despite the lack of sequence similarity among proteins. This similarity revealed a common theme in cell pole organization: landmark proteins form a higher-order structure that serves as an assembly platform for other proteins, thereby mediating their polar localization.

ZUSAMMENFASSUNG

Bakterien besitzen, ähnlich wie Eukaryoten, Zytoskelettelemente, die an der zeitlichen und räumlichen Organisation von zellulären Prozessen beteiligt sind und beispielsweise eine Rolle bei der Zellteilung, Chromosomensegregation, Zellmorphogenese sowie bei der Bestimmung der Zellpolarität spielen. Zu den wohl am weitesten verbreiteten Vertretern der bakteriellen Zytoskelettelemente zählen das Tubulin-Homolog FtsZ, das Actin-Homolog MreB und die Intermediärfilament-ähnlichen (IF) Proteine. Darüber hinaus wurde in den letzten Jahren eine Vielzahl von nicht-kanonischen Zytoskelettelementen identifiziert, zu denen unter anderem die sogenannten Bactofiline gehören, welche kürzlich für *Caulobacter crescentus* erstmals beschrieben wurden. Bactofiline sind unter Mikroorganismen weit verbreitet, zeigen jedoch weder auf Sequenz- noch auf Strukturebene eine Ähnlichkeit zu bekannten Zytoskelettelementen. Darüber hinaus besitzt eine Vielzahl von Bakterienspezies zwei oder mehr paraloge Proteine dieser Protein-Klasse. Dies ist vermutlich auf mehrere Genduplikationsereignisse zurück zu führen und deutet auf eine funktionelle Diversifizierung der Bactofiline hin. Ein Bespiel für die funktionelle Vielfalt dieser Zytoskelettelemente wurde kürzlich für die beiden Baktofilin-Homologe BacP und BacM aus *Myxococcus xanthus* erbracht. Während BacP bipolare Filamente ausbildet und essentiell für die Positionierung des Zellpolaritätsfaktors SofG ist, nimmt BacM Einfluss auf die Ausprägung der Zellform. Im Rahmen dieser Arbeit konnte nachgewiesen werden, dass in *M. xanthus* BacP zusammen mit zwei weiteren paralogen Proteinen, BacO und BacN, zudem eine entscheidende Funktion bei der Stabilisierung des Chromosomensegregationsapparates übernimmt. Es wurde gezeigt, dass BacN-P in bipolare Filamente co-polymerisieren und dabei die korrekte Anordnung der Proteine ParA und ParB koordinieren, welche eine essentielle Rolle bei der bakteriellen DNA-Segregation übernehmen. Die Abwesenheit von BacN-P führt zu einer fehlerhaften Lokalisation von ParA und ParB in der Zelle und beeinträchtigt somit die korrekte Verteilung des genetischen Materials im Zuge der Zellteilung. Protein-Interaktionsstudien haben darüber hinaus zur Identifizierung von BadA geführt, einer ParB-ähnlichen Nuklease, welche vermutlich direkt mit ParA interagiert und gemeinsam mit BacN-P den korrekten Ablauf der DNA-Segregation ermöglicht. Zusammenfassend lässt sich feststellen, dass Bactofiline in *M. xanthus* als eine Art molekulare Plattform betrachtet werden können, die für die korrekte Positionierung und Stabilisierung von polaren und subpolaren Proteinkomplexen verantwortlich sind. Trotz fehlender Sequenzähnlichkeit wurde eine ähnliche gerüstbildende Funktion bereits für PopZ aus *C. crescentus* und für das in Gram-positiven Bakterien vorkommende Protein DivIVA postuliert. Diese funktionelle Analogie legt daher die Vermutung nahe, dass die Anwesenheit von Proteinen, die in übergeordnete makromolekulare Strukturen polymerisieren können und dadurch die Assemblierung und polare Lokalisation von Proteinen vermitteln, eine weitverbreitete Strategie zur subzellulären Organisation der Polregion in Bakterien ist.

TABLE OF CONTENTS

1 INTRODUCTION

Cytoskeletons have been shown to be essential for proper temporal and spatial subcellular organization in all life forms, including bacteria. Since the first prokaryotic cytoskeletal protein, FtsZ, was identified, the family of bacterial cytoskeletal elements has been greatly expanded. Although barely any homolog was found in prokaryotes by aligning primary sequences, compelling evidence has been provided that bacteria contain homologs of all three main eukaryotic cytoskeletal elements, including tubulins, actins and intermediate filaments [2, 46, 94, 140]. Moreover, there are also a number of cytoskeletal elements that are bacteria-specific and mostly nucleotide-independent [92]. Like in eukaryotes, bacterial cytoskeletons have been demonstrated to widely contribute to diverse cellular processes, including cell morphogenesis, cell motility, cell division as well as intracellular transport. The following sections will focus on the scaffolding function provided by cytoskeletons for different cellular processes in bacterial cells.

1.1 Bacterial cytoskeletons as subcellular landmarks

In general, cytoskeletons not only generate mechanical force for cell movement and the maintenance of cell shape, or provide structural or physical support for the communication with the outer environment, but often build scaffolds serving as landmarks at particular subcellular positions, which then further recruit target proteins or molecules to spatially organize the cellular contents [42]. This mechanism provides platforms for the coordination of the localization and dynamics of multi-protein complexes, especially for sets of proteins that are functionally related. In bacteria, several cytoskeletal proteins have been demonstrated to have a central role in subcellular organization by providing this scaffolding function at various positions within the cell.

1.1.1 FtsZ: the central structure for divisome

FtsZ, a tubulin-like protein that is widely conserved among bacteria, is an essential cell-division protein that assembles into the ring-like structure at the future division site [8, 17, 25, 143]. This ring-shaped structure, called the Z-ring, serves as the foundation of the divisome, and recruits many other cell division proteins and peptidoglycan synthesis-related enzymes during cell division [50, 135] (Figure 1.1). In *Escherichia coli*, a rod-shaped Gram-negative bacterium, several proteins were shown to be very important for divisome assembly, including the actin homolog FtsA [24], the DNA translocase FtsK [4], the ABC transporter-like FtsEX [121], the inner membrane protein ZipA [55], as well as ZapA-D [34, 54, 56, 95, 135]. Among them, FtsA and ZipA have been shown to be essential for stabilizing the FtsZ proto-ring [109]. In addition, the divisome complex also recruits proteins such as the FtsQLB complex [14], the lipid II

flippase FtsW [45, 99], as well as the late essential division protein FtsN which were shown to bind peptidoglycan synthases such as PBP3 and PBP1B to drive septal PG remodeling [116, 138]. In the divisome, the transpeptidase PBP3 is essential for septal PG synthesis [111, 135]. PBP3 was also shown to interact with a bifunctional PG synthase, PBP1B, which in turn interacts with an outer membrane protein, LpoB, that stimulates its transpeptidase activity [7, 107, 134]. Formation of the divisome is a highly coordinated process, meaning that components are recruited to the Z-ring in a defined temporal order [95, 135]. The Z-ring was shown to be very dynamic and to provide the main driving force for cytokinesis [1, 91, 118]. Although not forming tubular structures, FtsZ protofilaments share a highly similar arrangement of subunits with tubulins, which assemble into microtubules in eukaryotes [17, 102, 104].

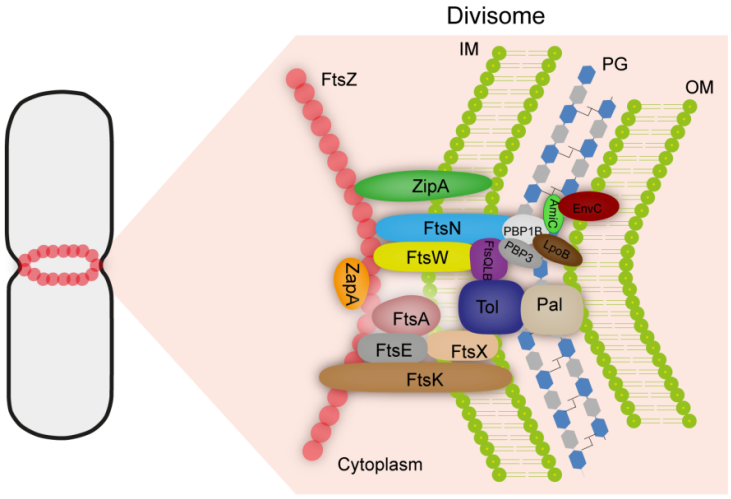

Figure 1.1: The *E. coli* divisome. Schematic representation of the divisome, assembled on the FtsZ ring, at a late stage of cell division. See introduction for more details. Modified from [135].

1.1.2 MreB: structural support for the elongasome

MreB, an actin homolog, routinely serves as a cell-shape determinant providing structural support for the peptidoglycan (PG) synthesis machinery, especially in rod-shaped bacteria [17, 21, 25, 106, 110]. *In vitro*, MreB polymerizes into actin-like protofilaments in the presence of ATP [140]; *in vivo*, by contrast, it forms discrete patches that move along a helical-like track at the inner face of the cytoplasmic membrane and coordinate the synthesis of the cell wall, by recruiting multiple peptidoglycan synthesis enzymes and controlling the distribution of PG biosynthesis [19, 20, 29, 41, 47, 71, 142]. For instance, in *E. coli*, MreB is directly associated with inner-membrane proteins MreC and MreD [81]. It was also shown that MreB itself could interact with the inner membrane through a helix in its N-terminal region as well as via an integral membrane protein, RodZ [120, 141]. MreB filaments also interact with another integral membrane protein, RodA, which is directly associated with the essential PG synthetic enzyme, PBP2, involved in lateral cell wall elongation [27, 67, 135, 148]. PBP1A, one of the two major bifunctional PG synthases, is also recruited into the elongasome complex, in which it interacts

with LpoA, an outer membrane lipoprotein that stimulates its transpeptidase activity to promote the attachment of newly synthesized PG to sacculi [107, 134, 135] (Figure 1.2).

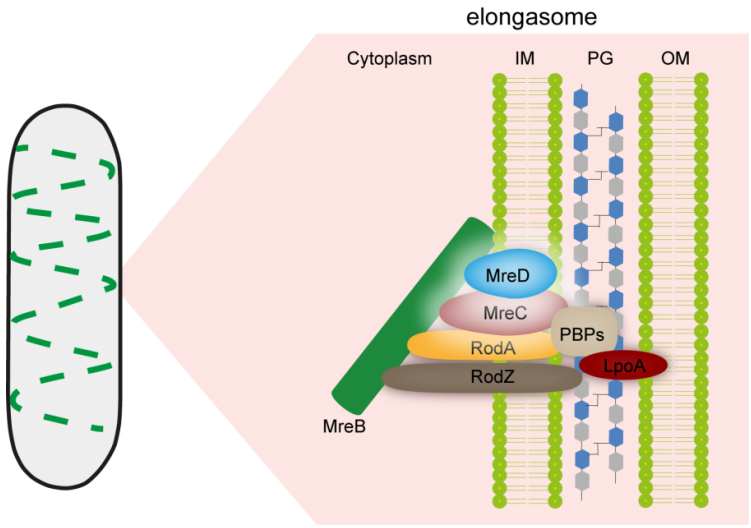

Figure 1.2: The *E. coli* elongasome. Schematic representation of the elongasome complex, assembled on MreB, during cell elongation. See introduction for more details. Modified from [135].

1.1.3 Polar cytoskeletal landmarks in bacteria

Our knowledge of the subcellular organization of the divisome by FtsZ as well as the elongasome by MreB has recently expanded greatly. However, information on the organization of the cell poles is relatively limited. Bacterial cell poles recruit a surprisingly large number of proteins involved in a wide range of cellular processes, such as cell motility, chemotaxis and chromosome segregation. With so many proteins in these crowded regions, the establishment of polar landmarks is crucial for tight regulation of polar protein localization and dynamics. The small number of landmark proteins identified so far in bacterial species reveals that unlike FtsZ or MreB, these proteins are much less conserved or even species-specific. However, most of them appear to be able to form multimers or even higher-order structures, exhibiting a cytoskeleton-like behavior. In Gram-positive bacteria, DivIVA was shown to be such a polar scaffolding protein in several species (Figure 1.3A). DivIVA in *Bacillus subtilis* has been shown to oligomerize into ordered lattice-like structures and possibly attach to negatively curved membrane regions preferentially at both cell poles and the cell division plane [19, 88, 105, 114, 126]. While septal DivIVA scaffolds recruit the cell division inhibitor MinCDJ [12, 108], during sporulation, polar DivIVA interacts with polar proteins such as the chromosome anchoring protein RacA to ensure the attachment of the chromosomal origin region to pre-spore cell poles [5, 149]. DivIVA is also found in actinomycetes and involved in a number of cellular processes [40, 59, 90]. For instance, in *Corynebacterium glutamicum*, DivIVA has been shown to anchor the chromosome segregation protein ParB to ensure the attachment of *oriC* at the cell poles [31]. This interaction has also been observed in some other actinomycetes species [31]. In *Mycobacterium tuberculosis*, ParA and ParB, both of which are key components in

chromosome segregation, show interactions with DivIVA [31, 48]. In *Streptomyces coelicolor*, ParB also seems to associate with DivIVA [31]. Interestingly, in *S. coelicolor*, another tip-organizing center protein, Scy, has been identified [28, 63]. Scy, a cytoskeletal element, together with DivIVA, establishes the polarity centers that coordinate the characteristic apical growth of this organism [63]. Scy also interacts with ParA, which together with ParB then promotes chromosome segregation [28]. Moreover, Scy also shows association with FilP, a regulatory coiled-coil-rich protein involved in polar cell wall biogenesis [63]. Therefore, both Scy and DivIVA cooperate to build a tip-organizing scaffold. In Gram-negative bacteria, a well-studied example of polar landmarks is PopZ from *Caulobacter crescentus*, a pole-organizing protein that anchors the ParB-*ori* complex and thus is critical for proper chromosome dynamics (Figure 1.3B) [10, 36]. Moreover, PopZ is also required to position two transmembrane histidine kinases, CckA and DivJ, which are important for cell cycle regulation and stalk biogenesis [11, 36]. PopZ is able to self-multimerize into a polymeric network at the cell pole in a cell-cycle-dependent manner [10, 36, 85]. The PopZ matrix was proposed to assemble in cytoplasmic regions with low DNA content [10, 11, 36].

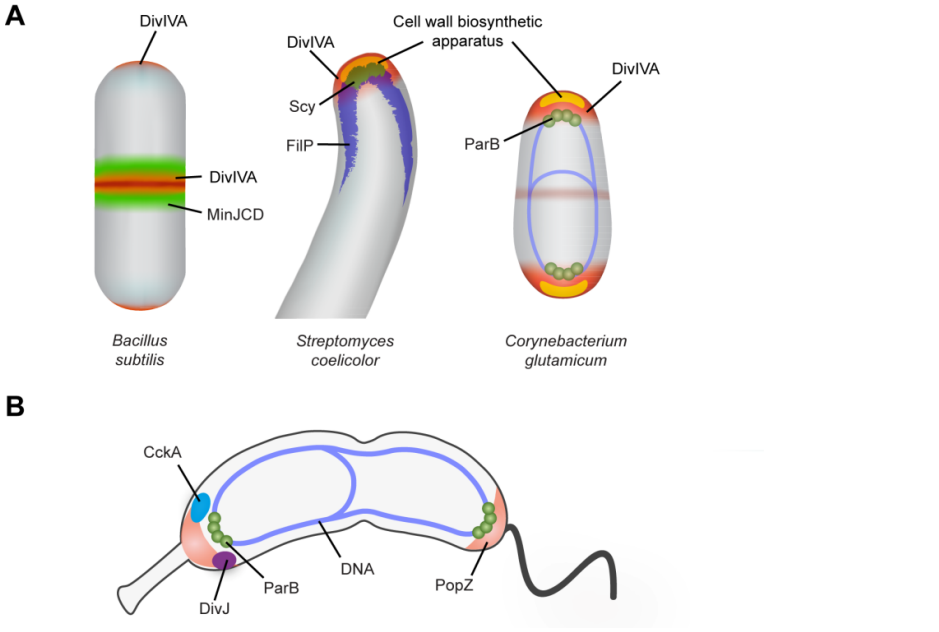

Figure 1.3: Polar scaffolding proteins among bacterial species. (A) Schematic representation of the subcellular localization of DivIVA and its interaction partners in *B. subtilis* (left panel), *S. coelicolor* (middle panel), and *C. glutamicum* (right panel), respectively. (B) Schematic representation of the subcellular localization of PopZ and proteins tethered to the PopZ matrix in *C. crescentus*.

1.2 Bactofilins: a class of non-canonical cytoskeletal elements in bacteria

Bactofilins are a widespread class of non-canonical cytoskeletal elements, which was first discovered and characterized in *C. crescentus* [82]. They are characterized by a DUF583

domain, later denoted as bactofilin domain, which is usually surrounded by short non-conserved N- and C- terminal regions [82]. Bactofilin domains are enriched in β-strands, indicating a β-sheet-rich structure (Figure 1.4). Interestingly, bactofilins are not only widely distributed among the bacterial phylogeny, but also frequently duplicated within genomes [82]. Moreover, although bactofilins are mostly small in size (~20 kDa), some homologs have long N- or C-terminal extensions, which likely confer the functional specificity. *In vitro*, bactofilins are able to polymerize spontaneously into stable filaments without any cofactor, similar to intermediate-filament-like proteins [78, 82]. The function of bactofilins in most bacteria still remains mysterious. However, investigations in a few species have supported the idea that bactofilins are likely to play a wide range of roles in different organisms.

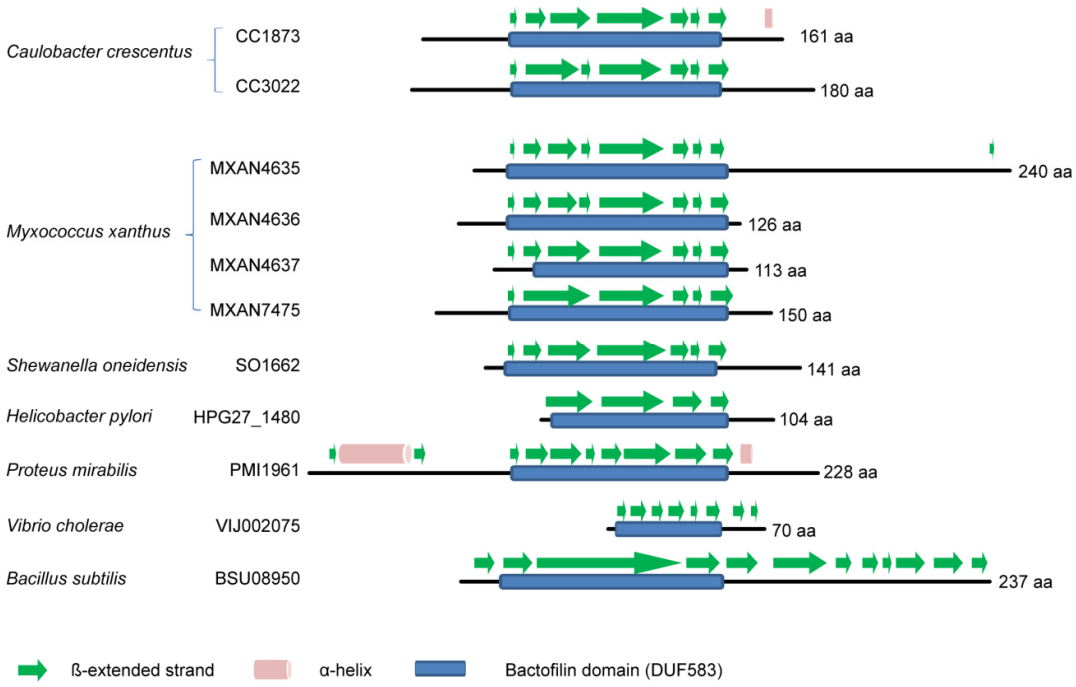

Figure 1.4: Domain organization of bactofilin homologs in different species. The positions of the bactofilin domain were determined by NCBI domain prediction. Secondary structures were predicted by the PSIPRED server [13, 70, 96].

1.2.1 Bactofilins in *C. crescentus*

In *C. crescentus*, bactofilins were discovered when screening for proteins involved in stalk biogenesis based on localization and transcriptional profiling [82]. Two DUF583 domain-containing proteins, BacA and BacB, were revealed to colocalize to the stalk base, while being diffuse in swarmer cells, indicating that despite their constitutive expression during the cell cycle, BacAB appear to localize dynamically [82]. At the stalked pole, BacAB form membrane-associated filaments that recruit a peptidoglycan biosynthetic enzyme, PbpC, which is a membrane protein that is likely involved in stalk PG synthesis. In the absence of BacAB or PbpC, *C. crescentus* cells form significantly shorter stalks, suggesting an accessory function of BacAB/PbpC in stalked pole PG synthesis or modification [82]. It was shown that the

overproduction of BacA or BacB leads to the formation of ribbon-like structures that extend along the cell envelope, resulting in a striking cell shape defect with hyper-curvature [82]. However, how BacAB are targeted to cell membranes still remains unclear.

Meanwhile, it was also shown that both BacA and BacB are able to polymerize into stable polymers and bundles in the absence of any cofactor *in vitro*, similar to intermediate-filament like proteins [82]. Moreover, filaments are visible under physiologically relevant conditions, i. e. in high salt buffer, and appear to be resistant to stringent treatments such as chelating agents and pH changes [82].

1.2.2 Bactofilins in other bacteria

Despite the limited knowledge about bactofilins, the few studies available to date suggest a functional diversification of bactofilin homologs in different organisms. For instance, in *Helicobacter pylori*, the only bactofilin homolog, CcmA, has been shown to be essential for the helical cell shape of this organism [129]. Upon deletion of *ccmA*, *H. pylori* loses its helical cell shape, which is crucial for its pathogenicity; therefore, CcmA is considered to be an important virulence factor [129]. It was also suggested that CcmA may function in concert with three LytM-type endopeptidase, Csd1-3, to regulate the hydrolysis of PG crosslinks [129]. In another bacterium, *Proteus mirabilis*, the only bactofilin homolog (CcmA), exists in two forms: the full-length protein with an N-terminal transmembrane helix, and an N-terminal truncated version [58]. The deletion of *ccmA* or the synthesis of a C-terminally truncated protein leads to significantly reduced swarming motility, as well as a large fraction of curved cells in the population [58]. A similar involvement of bactofilins in motility is also observed in *Vibrio parahaemolyticus*, in which the bactofilin homolog together with a LytM endopeptidase was shown to be up-regulated during swarming [49]. In addition, two bactofilin homologs in *B. subtilis* were proposed to be required for swimming motility [113].

1.2.3 Bactofilins in *M. xanthus*

Bactofilins appear not only to be functionally diverse across species, but also to be able to play distinct roles within species. For example in *Myxococcus xanthus*, a Gram-negative bacterium with a complex life cycle, it has been reported that one of the four bactofilin homologs, named BacM, is important for proper cell shape maintenance, while the other three seem to be involved in other cellular processes [16, 78, 82]. BacM was shown to form fibres that are highly resistant to a number of treatments such as high salt concentrations and detergents [78, 82]. *In vivo*, BacM forms intracellular helical cables throughout the cell, but ~25% of cells also have a rod-like structure near the cell poles [78]. The absence of BacM results in an unusual cell morphology with kinks or curls in a subset of cells [78]. Moreover, the deletion of *bacM* also significantly increases the sensitivity of this bacterium toward antibiotics that interfere with PG biogenesis [78]. Therefore, one can speculate that BacM may be involved in general cell wall biogenesis in *M. xanthus*. On the other hand, another bactofilin homolog, BacP, has recently been revealed to form polar cytoskeletal structures and recruit a small GTPase, SofG, which acts together with the small GTPase MglA to regulate cell polarity [16] (Figure 1.5). Cell polarity is crucial for the temporal and spatial regulation of type IV pili assembly or

disassembly, which in turn is essential for the so-called social motility of this bacterium, in which cells move coordinately in groups, driven by type IV-pili-mediated cell-cell contacts [15]. Type IV pili are assembled at the leading cell pole; during reversal, cells switch their assembly to the new leading cell pole (i.e., the old lagging pole) [15]. To accomplish this switch, a set of type IV pili-related proteins has to relocate to the opposite cell pole [15]. SofG, a Ras-like GTPase, is an important polarity factor that initially establishes the localization of type IV pili-associated proteins such as the PilB (the extension ATPase) and PilT (the retraction ATPase) at the cell pole [16]. It has been demonstrated that the subpolar localization of the single SofG cluster within the cell is crucial for its function [16]. BacP, which forms bipolar filaments *in vivo*, was shown to interact directly with SofG [16]. By associating with one of the BacP patches, SofG is able to form a cluster and then shuttle over the BacP patch to the pole in a GTPase activity-dependent manner; and it was suggested that this shuttling was important for recruiting PilB and PilT to the cell pole [16]. The mechanism underlying the movement of SofG on the BacP patch remains to be clarified. In particular, it is not clear if this shuttling is coupled to the depolymerization of BacP filaments; however, it has been observed that BacP patches seem to be shorter in the presence of SofG than without SofG [16]. After polar recruitment by SofG/BacP, PilB and PilT are sorted to the leading pole and lagging pole, respectively, by the MglA/MglB module, in which MglA acts as Ras-like GTPase while MglB is the corresponding GTPase-activating protein (GAP) [89, 97, 155]. At this time, active GTP-bound MglA and PilB localize at the leading cell pole; while the majority of MglB and PilT molecules are at the lagging pole [15, 16, 89, 97, 155]. However, it is not clear if these BacP patches exclusively interact with SofG, or whether they rather act as polar hubs for different polar proteins.

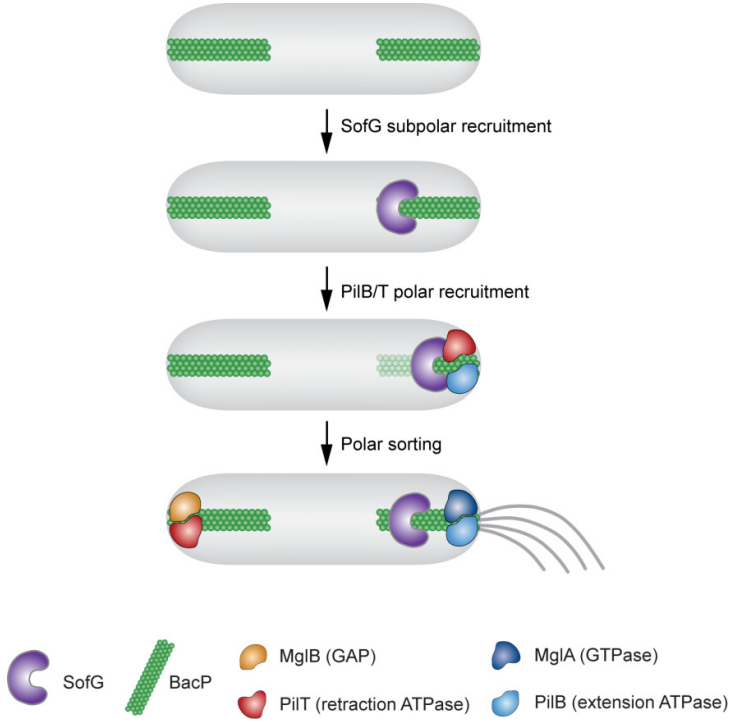

Figure 1.5: Polar recruitment of PilB and PilT by the SofG/BacP module in *M. xanthus*. See Introduction for more details. Modified from [16].

1.3 Chromosome segregation in bacteria

Unlike in eukaryotes where chromosomes segregate after replication is accomplished, chromosome segregation in many bacterial species occurs while DNA replication is still ongoing. This implies that the replication and segregation programs have to be tightly regulated and coordinated. Moreover, it appears that across species, there is no universal mechanism that contributes to the segregation, meaning that there are different mechanisms involved in chromosome segregation in different bacteria. In many cases, within species, multiple processes are implicated in chromosome segregation, where the disruption of individual ones often causes only partial defects but does not abolish segregation completely; this indicates the high degree of independence and redundancy of the different processes involved [115]. However, there are several systems that have been shown to contribute to chromosome segregation to different extents in a range of bacteria. These mechanisms include the structural maintenance of chromosome (SMC) complex, the DNA translocase FtsK, as well as the ParAB-*parS* segregation system [115]. The mechanism of action of the SMC complex is still incompletely understood. However, it seems SMC acts with the ParAB system to facilitate proper chromosome organization and segregation [53, 98, 115, 128]. On the other hand, FtsK preferentially interacts with the *ter* region of the chromosome, guiding the terminal region to the septum, and then coordinating the last step of chromosome segregation and cell division, such as chromosome decatenation and dimer resolution [9]. In contrast to FtsK, the ParAB-*parS* system plays an important role in positioning and segregating the *oriC* region of the chromosome, which will be discuss in detail in the following section.

1.3.1 The ParAB-*parS* partitioning system in plasmid segregation

The ParAB-*parS* system is the most widely used segregation mechanism in low-copy plasmids, including the F and P1 plasmids [35, 145]. This DNA partitioning system consists of three key components: (1) an ATPase named ParA, possibly responsible for ensuring the directionality of the segregation process; (2) a centromere-like DNA sequence, *parS*; (3) and the partitioning protein ParB, which can bind and move *parS* sites during segregation [35, 115, 144]. In general, ParB binds to *parS* sites to form a partitioning complex, while ParA binds to DNA nonspecifically and provides the energy to drive segregation; moreover, ParB or nonspecific DNA can stimulate the ATPase activity of ParA and release it from nucleoid [26, 64, 147]. However, how ParA dynamics link with DNA movement remains elusive. There are two proposed hypotheses based on different lines of evidence: (1) the 'ParA filament pulling' model in which the polymerization and depolymerization of ParA filaments is responsible for the plasmid segregation [117]; (2) the 'diffusion-ratchet' model in which the segregation directionality depends on the ParA-ParB interaction, rather than the ParA polymerization; moreover, ParA uses nucleoids as the matrix [64, 144, 146].

1.3.2 The ParAB-*parS* in bacterial chromosome segregation

There are a number of bacterial species with ParAB-*parS* system encoded in their genomes. Accumulating knowledge on ParAB-*parS* systems from different species suggests that this mechanism also participates, to a varying extent, in the chromosome segregation in a number of species. However, the ParAB system also exhibits a high functional flexibility, as evidenced by its involvement in other cellular processes such as cell division and sporulation [115].

During ParAB-*parS*-dependent chromosome segregation, the ParB-*parS* complex in most cases initially localizes to a cell pole and gets duplicated when DNA replication initiates; during the segregation process, one of the two copies then travels through the cell and eventually reaches the opposite cell pole, as mostly studied in species like *C. crescentus* [112, 122] (Figure 1.6). In *C. crescentus*, both ParA and ParB are essential for viability, probably due to the involvement of ParB in cytokinesis [101, 130]. The overexpression of ParA leads to similar defect as the depletion of ParB, which inhibits cell division and Z ring formation and leads to filamentous cells and mini cells [100, 101]. Interestingly, the cell division defect caused by the overexpression of *parA* can be alleviated by the overexpression of *parB* [101], indicating the importance of maintaining the proper ratio of ParA to ParB. During chromosome segregation in *C. crescentus, parS* acts as a centromeric DNA sequence that is located near the *oriC* region on the chromosome, and is tethered through ParB to the cell pole by the polar landmark protein PopZ [10, 36, 112]. At the beginning of chromosome replication, the ParB/*parS* complex at the old pole is released from the PopZ matrix and moves to a position located at a short distance from the cell pole; meanwhile, duplication of the origin region leads to the formation of two ParB/*parS* complexes; during chromosome segregation, these partitioning complexes interact with ParA, which directs the two ParB/*parS* complexes towards opposite cell poles [112, 122, 123]. Once the newly duplicated ParB/*parS* complex reaches the opposite cell pole, it is immobilized by PopZ again [10, 36]. It has been proposed that *Caulobacter* ParA forms a linear polymer-like structure both *in vivo* and *in vitro*; this supported the hypothesis that ParA depolymerization might be the driving force for DNA segregation [112]. However, this hypothesis is controversial and required further verification.

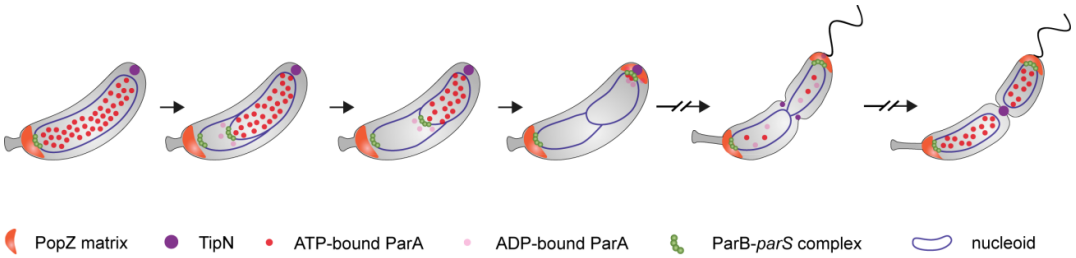

Figure 1.6: Schematic representation of *Caulobacter* chromosome segregation. See Introduction for more details. Modified from [122].

In *B. subtilis*, Soj (ParA) and Spo0J (ParB) were shown to play a minor role in chromosome segregation. For instance, the inactivation of Soj alone shows no obvious chromosome segregation effect, while inactivating Spo0J leads to an increased number of anucleate cells

(~100-fold increase) [66, 87]. However, Spo0J is responsible for tethering *oriC* to the cell pole before sporulation [6, 149]. Moreover, the deletion of both *soj* and *smc* leads to a synthetic phenotype, with a significant increase in the production of anucleate cells [87]. Also, Spo0J/*parS* was shown to interact with SMC [53]. Similarly, in *Streptococcus pneumoniase*, ParB/*parS* also exhibits a tight connection with SMC and contributes to chromosome segregation [98]. These findings all further support the contribution of Soj-Spo0J and SMC in chromosome organization and segregation. Interestingly, when the ratio of Soj to Spo0J is increased in the cell, DNA replication is promoted in *B. subtilis*, suggesting a possible link between DNA replication and the Soj-Spo0J partitioning system [103].

An often-observed consequence of the absence or inactivation of ParA or ParB is a significant increase in the number of anucleate cells in the population. For instance, in *Mycobacterium smegmatis*, the deletion of *parB* leads to the production of ~10% anucleate cells; overproduction of ParB, by contrast, affects the growth rate, but not chromosome segregation [68]. ParB was shown to bind to *parS* sequences both *in vivo* and *in vitro* in this species [68]. On the other hand, the absence of ParA not only results in the production of ~30% anucleate cells, but also leads to a cell growth delay as well as an increase in the number of elongated cells [48]. Moreover, the overexpression of *parA* causes similar effect as *parB* deletion, with 9.3% anucleate cells and more elongated cells [48]. Interestingly, the deletion of *parB* can suppress the chromosome segregation defect caused by the absence of *parA*, while the other phenotypic defect is not altered [48]. Similar effect has been observed in another actinobacterial species, *C. glutamicum*, where the absence of ParA or ParB leads to the production of ~18% or 43% anucleate cells, respectively [30]. The loss of ParA and ParB was also shown to influence the growth rate in minimal medium [30]. Additionally, in this species, chromosome segregation has also been shown to influence division site selection, with ~10% of cells having septa placed over chromosomes in the absence of *parA* or *parB* [32]. Similarly, in *Pseudomonas aeruginosa*, the disruption of *parAB* has severely affects both chromosome segregation and organization [139]. Strains without either ParA or ParB exhibit slower growth and produce more than 20% anucleate cells [139]. Moreover, the distribution and localization of the *oriC* and *ter* loci is severely altered, further indicating a major role of ParAB in chromosome organization [139].

The *parAB* genes are also found in the linear chromosome of another actinomycete member, *S. coelicolor*, in which ParAB were observed to be involved in the partitioning of chromosomal DNA during sporulation; however, the disruption of *parAB* has no obvious effect on cell growth or spore development [75].

ParAB-*parS* was also found to play roles in *Vibrio cholerae*, which possesses two circular chromosomes. Each chromosome encodes its own *par* operon, with distinct contribution and dynamics [43, 44, 153]. In the case of chromosome I, the $ParAB_I$-$parS_I$ system is important for the polar localization of $oriC_I$, although its inactivation has no obvious effect on the efficiency of chromosome segregation [44, 73]. $ParB_I$ was found to bind $parS_I$ at the cell pole and segregate asymmetrically from one pole to the other; while ParA forms a dynamic cloud-like structure between cell pole and the $ParB_I$/$parS_I$ complex [44]. Upon the deletion of $parA_I$, thte two $ParB_I$/$parS_I$ complexes disassociate from cell poles, and often localizes either closed to cell center or at the quarter positions of the cell [44]. Moreover, in the absence of $ParA_I$, $ParB_I$/$parS_I$ complexes show irregular bidirectional movement, indicating a defect in the segregation process [44]. It was shown that $ParB_I$ colocalizes with $ParA_I$ either at the cell poles or at the end of

$ParA_I$ clouds. Moreover, the dynamic directional movement of $ParB_I$/*parS*$_I$ complexes during segregation exhibit a mitotic-like pattern, with the dynamic $ParA_I$ structure providing directionality to the segregation process [44]. In addition to a significant defect on *oriC*$_I$ polar positioning, the loss of $ParB_I$ causes an increase in the number of *oriC*$_I$ copies, suggesting a connection with DNA replication [73]. However, the absence of $ParAB_I$/*parS*$_I$ has no appreciable impact on cell growth [73]. In contrast, the loss of $ParAB_{II}$-*parS*$_{II}$ leads to severe growth defect, with two thirds of the cells showing irregular sizes and shapes and more condensed nucleoids [44, 73, 153]. It has been demonstrated that $ParAB_{II}$ is essential for the maintenance of chromosome II, as a frequent loss of this chromosome is observed in the absence of *parAB*$_{II}$ genes [153]. A *parAB*$_{II}$ mutant also exhibits severe defects in chromosome II localization and segregation [153], consistent with the plasmid-like properties of this small replicon [115].

Recently, the ParAB/*parS* system has also been investigated in the rod-shaped bacterium, *M. xanthus*, where it was found to be essential for cell viability [57]. In *M. xanthus*, both *parA* and *parB* are essential; and the depletion of ParB leads to a significant defect in cell growth, as well as to the production of anucleate cells and cells with division sites placed over the nucleoid, indicating that ParB is essential for chromosome segregation [57]. Furthermore, ParB localizes dynamically in the cell and remains attached to the edges of nucleoids after chromosome segregation, localizing at a short distance from the corresponding cell poles; ParA, on the other hand, mainly localizes as subpolar patches [57] (see result section). The dynamic coordination of ParA and ParB localization suggests that during segregation, ParA clouds extend between the new cell pole and the segregating ParB/*parS* complex and get shortened as the ParB/*parS* complexes moves towards the poles, thereby directing the partitioning process [57] (Figure 1.7).

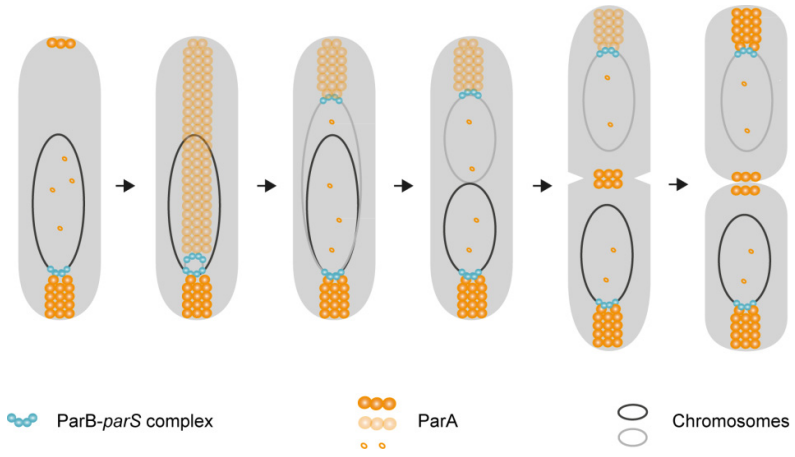

Figure 1.7: Schematic representation of ParAB/*parS*-mediated chromosome segregation in *M. xanthus*. See Introduction for more details. Modified from [57].

1.3.3 Proper subcellular positioning of ParAB

The positioning of ParA and ParB within the cell has been shown to be important for their function in chromosome segregation. Interestingly, the polar anchoring mechanism is likely not conserved among species. For example, in *C. crescentus*, the polar landmark PopZ is responsible for the polar tethering of ParB (see 1.1.3). PopZ shows a dynamic cell cycle-regulated localization pattern: in swarmer cells, PopZ localizes to the old cell pole; after the initiation of chromosome replication, PopZ additionally accumulates at the new pole to capture the segregating ParB/*parS* comple, leading to bipolar localization [10, 36]. The transition from unipolar to bipolar localization of PopZ depends on the local concentration of ParA: during the late stage of chromosome segregation, the increased concentration of ParA at the new cell pole promotes the local accumulation of PopZ, thereby raising its concentration above the threshold required for oligomerization [85]. Moreover, in *C. crescentus*, ParA was shown to interact with TipN, a polarity factor that serves as a landmark at the new pole [122]. TipN has been suggested to ensure the proper localization of new pole proteins or structures [86]. In the absence of TipN, ParA dynamics are impaired, and ParA often fails to accumulate at the new cell pole, which impairs the proper directionality of DNA segregation towards new cell poles [112].

In *V. cholerae*, by contrast, a polar anchoring protein, HubP, has been identified to be responsible for anchoring at least three ParA-like proteins to the cell pole, including $ParA_I$ [154]. Consequently, in the absence of HubP, $oriC_I$ is not tethered to the cell pole due to the mislocalization of $ParA_I$ [154]. Therefore, HubP appears to ensure the polar anchoring of multiple proteins, functionally similar to PopZ and TipN in *C. crescentus* [154]. However, HubP always localizes at both cell poles, lacking significant dynamics during cell cycle; this suggests the possible presence of additional factors that are used to mark the two different poles [154].

In Gram-positive bacteria, DivIVA was found to be widely conserved as a polar scaffolding factor in several species (see 1.1.3). Although DivIVA and PopZ share no similarity on the sequence level, they possess some common features: (1) both of them are able to self-assemble into a matrix-like structure at the cell pole; (2) both of them are multifunctional, meaning that they serve as landmarks to recruit various cell pole proteins involved in several distinct processes [10, 33, 36, 38, 132].

1.4 Scope

Bactofilins are widely conserved in the bacterial phylum; however, the function of this class of cytoskeletal elements remains unknown in most species. This work aims to investigate the function of bactofilin homologs in the Gram-negative, rod-shaped bacterium *M. xanthus*. *M. xanthus* is a soiled-adapted bacterium that is able to develop fruiting bodies upon nutrient starvation [79]. This developmental process is tightly coordinated with cell cycle progression [119, 136]. Moreover, development requires cells to move in oscillating patterns, by means of gliding motility (A-motility) and type IV pili-dependent motility (S-motility) [156]. In this work, we aim to address the following issues: (i) Multification of bactofilins has been observed

in a variety of bacterial species, including *M. xanthus*. What is the function of different bactofilin homologs in *M. xanthus*? (ii) Previous work suggested that fluorescently-labeled BacN-P localize as filamentous structures along the medial part of the cell [82]. However, this localization pattern needs to be verified. How do bactofilins localize within *M. xanthus* cells? (iii) Cytoskeletal proteins exhibit distinct dynamic patterns corresponding to their functions. For instance, FtsZ and MreB both appear to be very dynamic [1, 18, 125, 127]. In contrast, crescentin, an intermediate filament-like protein in *C. crescentus*, was shown to be stable with no obvious turnover *in vivo*, consistent with its mechanical role in maintaining cell curvature [22, 39]. Are bactofilin structures dynamic in *M. xanthus* cells? The understanding on the dynamics of bactofilins will provide more insights of their functions.

2 RESULTS

2.1 *M. xanthus* contains four bactofilin homologs.

There are in total four bactofilin homologs encoded in the *M. xanthus* genome, which are denoted *bacP*, *bacO*, *bacN* and *bacM*, respectively (Figure 2.1A) [78, 82]. *bacN-P* are located sequentially in the genome, whereas *bacM* lies in an operon with *parAB*. *bacN*, *bacO* and *bacP* encode proteins with molecular mass of 11.5 kDa, 13.5 kDa, and 24.6 kDa, respectively. Analysis of their domain organization revealed that each of the bactofilin homologs possesses a central bactofilin (DUF583) domain flanked with short non-conserved N- and C- terminal regions, with the exception of BacP, which has a long unstructured C-terminal extention. Moreover, at the C-terminal end of BacP, there is an unusual amino acid repeat (KKKVVVKKK), which may be involved in protein-protein interaction. In addition, secondary structure prediction suggested that bactofilin domains are enriched in β-strands (Figure 2.1B).

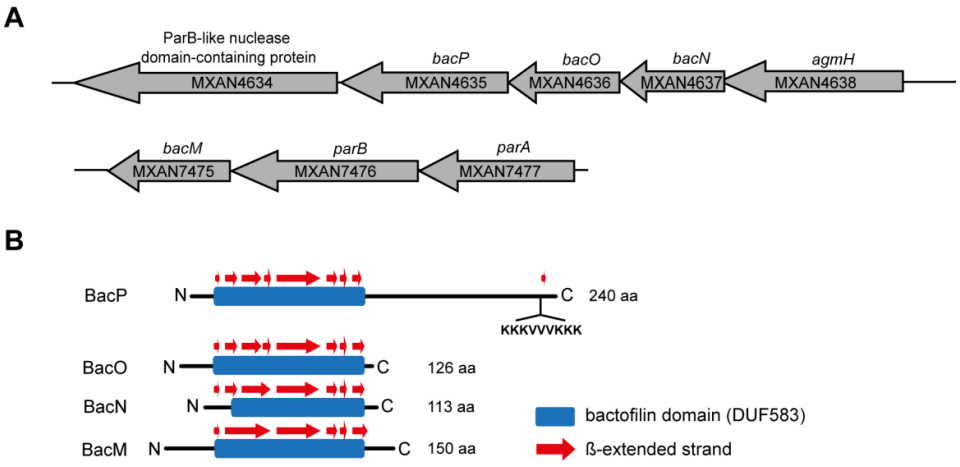

Figure 2.1: Schematic representation of bactofilin homologs in *M. xanthus*. (A) Genomic context of bactofilin homologs in the *M. xanthus* DK1622 genome. Arrows indicate the direction of transcription. (B) Domain organization and secondary structures of bactofilins. Bactofilin domains are indicated in blue; while red arrows show ß strands as revealed by the secondary structure prediction. The positions of the bactofilin domain were determined with the NCBI domain prediction tool. Secondary structures were predicted by the PSIPRED server [13, 70].

2.2 ParA and ParB dynamically localize in *M. xanthus* cells.

In the *M. xanthus* genome, *parAB* are encoded at the some operon and cotranscribed with *bacM* [78]. It has also been revealed that both ParA and ParB are essential for *M. xanthus* viability [57]. The removal of ParB in the cell leads to severe impairment of growth with prolonged doubling time, and a severe chromosome segregation defect [57]. Notably, filamentous cells

were not observed [57]. This chromosome segregation defect results in the production of a number of anucleate cells, cells with little DNA, as well as cells with an uneven distribution of chromosomal DNA during cell division [57]. Moreover, the overexpression of *parA* leads to a similar phenotype as *parB* depletion (Figure 2.2A). When *parA* was expressed under the control of the vanillate-inducible promoter in addition to the native copy, its expression level could be increased in a regulated manner. In the absence of inducer, ParA was produced at wild-type levels (Figure 2.2B). However, after addition of vanillate, it accumulated to high levels (Figure 2.2B). As a consequence, cells exhibited severe growth and chromosome segregation defects: (i) there were ~17% of anucleate cells or cells with very little DNA present in the population, while this phenomenon was barely observed in the wild type; (ii) ~11% of cells were predivisional cells with a very asymmetric distribution of DNA to the two future daughter cells due to division over the nucleoid, which later probably yielded anucleate cells and cells with excess DNA; (iii) chaining cells were observed (1-2% of the population), in which missegregated DNA appeared to block the division site (Figure 2.2A).

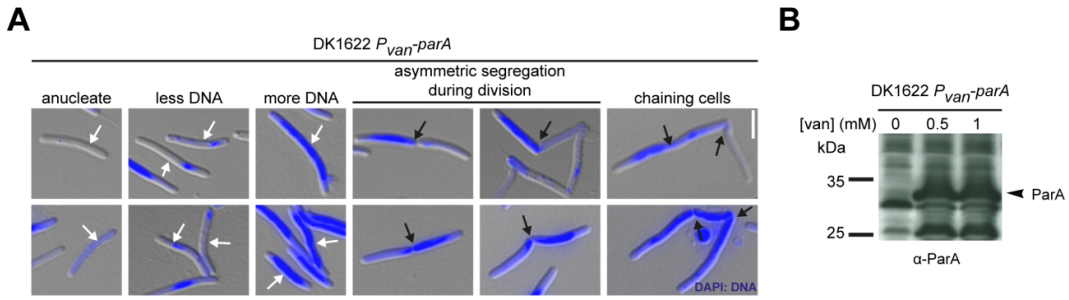

Figure 2.2: The ovexpression of *parA* leads to severe chromosome segregation defect. (A) The overproduction of ParA leads to cells with abnormal DNA distribution, including anucleate cells, cells with less DNA, and cells with excess DNA (indicated by white arrows). There is also a significant amount of predivisional cells or chaining cells with division taking place over nucleoids (indicated by black arrows). Exponentially growing cells of the strain LL196 (DK1622 P_{van}-*parA*) were diluted to an OD_{550} of ~0.1, and *parA* expression was induced with 0.5 mM vanillic acid overnight. Cells were then stained with DAPI to visualize DNA (scale bar: 3 μm). (B) Immunoblot analysis of the level of ParA after overnight induction with 0, 0.5 mM, or 1 mM vanillic acid, using α-ParA antibodies (1:1000).

Previous studies exploring the function of ParA and ParB in chromosome segregation in *M. xanthus* have established tools to localize the two proteins in live cells [57, 133]. To verify the published localization pattern in our system, we first expressed an additional copy of *parA* fused with *mCherry* ectopically from the native *parA* promoter [57]. In the wild type, the fusion often formed short bipolar patches of varying length (Figure 2.3A). Moreover, in order to localize ParB, a *parB-eyfp* fusion was ectopically expressed under the native promoter in the presence of native ParB [57, 133]. In the wild type, the majority of cells contain two ParB-eYFP foci at subpolar positions (Figure 2.3B). Here we assume that after the completion of orgin segregation both ParB foci reach localization symmetry, meaning that they have reached the same distance from the corresponding cell poles. Thus, in wild-type cells, after the completion of chromosome segregation, there are two ParB foci both localizing at ~5-15% of the cell length from each cell pole (Figure 2.3B). Moreover, when colocalizing ParA and ParB in the cell, the subpolar ends of ParA patches were often colocalized with ParB (Figure 2.3C), indicating a close association between the two proteins. These localization patterns observed are consistent

with published results that have been verified by immunofluorescence microscopy using specific antibodies against ParA and ParB, respectively [57].

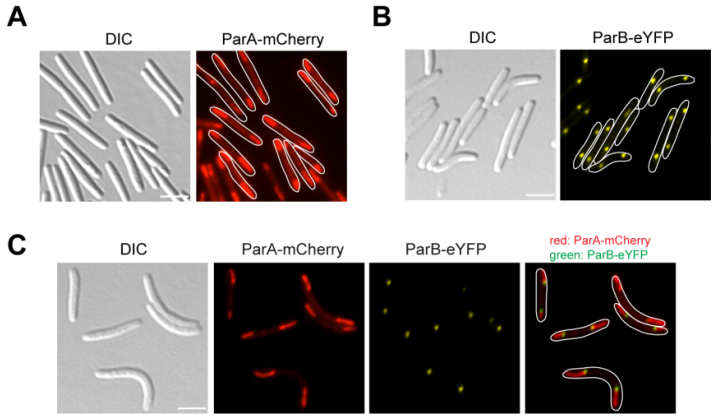

Figure 2.3: ParA and ParB localization in vegetative *M. xanthus*. (A) ParA localization in *M. xanthus* cells. Cells of strain LL145 (DK1622 P_{parA}-*parA-mCherry*) were grown in CTT medium and visualized by DIC and fluorescence microscopy. (B) ParB localization in *M. xanthus* cells. Cells of strain LL012 (DK1622 P_{parB}-*parB-eyfp*) were grown in CTT medium and visualized by DIC and fluorescence microscopy. (C) ParAB colocalization in *M. xanthus* cells. Cells of strain LL162 (DK1622 P_{parA}-*parA-mCherry* P_{cuoA}-*parB-eyfp*) were grown in CTT medium to exponential phase, diluted to an OD_{550} of ~0.1 with CTT in the presence of 100 µM $CuSO_4$, and incubated for another ~20 h. Cells were then visualized by DIC and fluorescence microscopy (bar: 3 µm).

In line with a function involved in chromosome segregation, both ParA and ParB exhibit very dynamic localization patterns, corresponding to different phases of the chromosome segregation process (Figure 2.4). For instance, ParA forms short bipolar patches in the majority of cells, while in new-born *M. xanthus* cells, there is a large cloud of ParA at one cell pole and a small accumulation of protein at the opposite cell pole. There are also cells with one subpolar ParA patch and two distinct foci at the opposite cell pole (Figure 2.4A). Interestingly, in predivisional cells, there is a short period when ParA completely disperses followed by the reappearance of ParA patches at both cell poles as well as the division plane (Figure 2.4A). Similarly, ParB also shows a dynamic localization pattern during different stages of cell cycle. In new-born cells, there is only one ParB focus. Duplication of ParB foci occurs when chromosome segregation initiates. Then one of the duplicated foci travels toward a subpolar position at the opposite cell pole (Figure 2.4B).

Notably, overexpression of *parA-eyfp* gives rise to the same phenotype as overexpression of the wild-type gene, with ~21% of cells containing none or very little DNA (Figure 2.5). When ParA is present at very high levels, it no longer localizes to the cell pole. Instead, it shows a rather irregular localization, likely corresponding to the distribution of chromosomal DNA: (i) in anucleate cells, ParA-eYFP is mostly diffuse; (ii) in cells with only very little DNA, ParA-eYFP colocalizes with this small patch of DNA; (iii) in cells containing excess DNA, ParA-eYFP is often distributed over the nucleoid; (iv) in predivisional cells and chaining cells (~9% and 1.6% of cells, respectively), ParA-eYFP often accumulates with DNA in the future daughter cell inheriting the chromosomes as well as with trapped DNA at the division plane (Figure 2.5A).

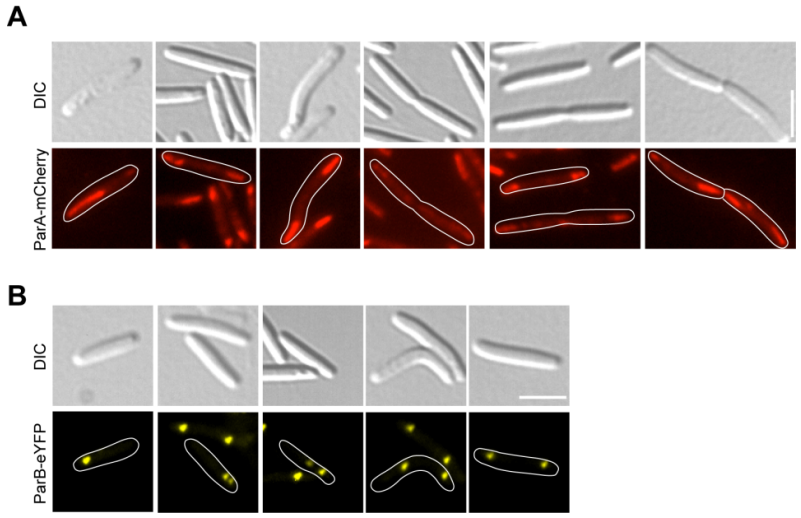

Figure 2.4: Dynamic localization of ParA and ParB of different stages of chromosome segregation in *M. xanthus*. (A) ParA localization throughout different stages of chromosome segregation. Cells of strain LL145 (DK1622 P_{parA}-*parA-mCherry*) were grown in CTT medium and visualized by DIC and fluorescence microscopy. (B) Dynamic ParB localization in *M. xanthus* cells. Cells of strain LL012 (DK1622 P_{parB}-*parB-eyfp*) were grown in CTT medium and visualized by DIC and fluorescence microscopy (bar: 3 µm).

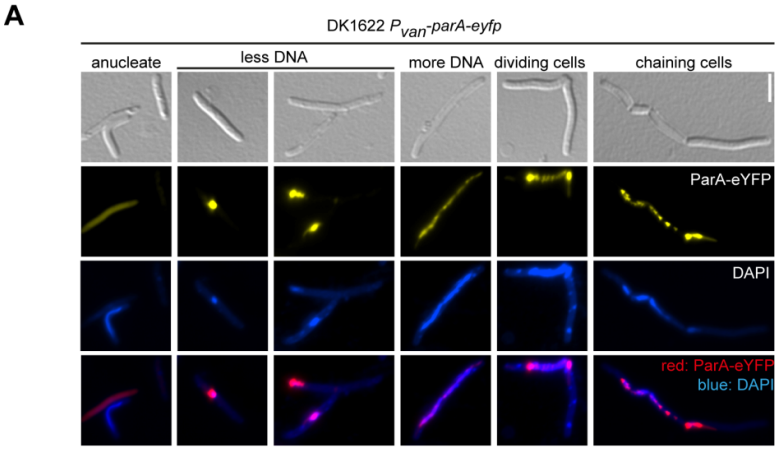

B

strains	anucleate cells/cells with less DNA %	predivional cells with asymmetric chromosome segregation %	Chaining cells %
DK1622	0	0.17±0.24	0
DK1622 P_{van}-*parA*	17.15±0.88	11.14±4.79	2.10±1.36
DK1622 P_{van}-*parA-eyfp*	21.12±3.61	9.04±4.70	1.60±0.24

Figure 2.5: The overexpression of *parA-eyfp* leads to comparable chromosome segregation defect as that of *parA*. (A) Cells of strain LL182 (DK1622 P_{van}-*parA-eyfp*) was grown to exponential phase and diluted into an OD_{550} ~0.1; then *parA-eyfp* expression was induced with 0.5 mM vanillic acid for overnight. Cells were then stained by DAPI to visualize DNA (scale bar: 3 µm). (B) Summary of the average percentage of cells (± standard deviation) with aberrant DNA contents. Cells of strains DK1622 (wild type), LL196 (DK1622 P_{van}-*parA*), and LL182 (DK1622 P_{van}-*parA-eyfp*) were grown to exponential phase and diluted into an OD_{550} of ~0.1. *parA* expression was induced with 0.5 mM vanillic acid for overnight. Nucleoids were visualized by DAPI staining. For quantification, 300-600 cells were analyzed for each replicate in each strain. Two replicates were performed per strain.

Collectively, both ParA and ParB localize dynamically in *M. xanthus* in the course of chromosome segregation, consistent with their important roles in this process. Moreover, the effect on chromosome segregation when the overexpression of *parA* is altered couples with its aberrant localization.

2.3 ParAB mislocalize in the absence of bactofilins in *M. xanthus*.

As described above, the genomic context of the bactofilin genes suggested their involvement in chromosome segregation. To explore the possibility, we first investigated the localization of both ParA and ParB in the absence of bactofilins. To this end, in-frame deletions were generated in each of the bactofilin homologs. In the wild type, ParA mostly formed short bipolar patches, whose ends often colocalized with ParB (Figure 2.3). However, in the absence of BacN-P, ParA was not able to form bipolar patches, with most ParA molecules dispersed within the cell (Figure 2.6A). However, BacM, whose corresponding gene is cotranscribed with *parAB* [78], appeared not to be involved in ParA localization (Figure 2.6A). Furthermore, among BacN-P, the absence of BacP alone led to the most striking effect, while the *ΔbacO* mutation caused less ParA localization defect. BacN, on the other hand, only had a minor contribution to ParA positioning (Figure 2.6A). Complementation of the *ΔbacP* mutation with an ectopic copy of *bacP* could restore the bipolar pattern of ParA, excluding the possibility of a polar effect (Figure 2.6B).

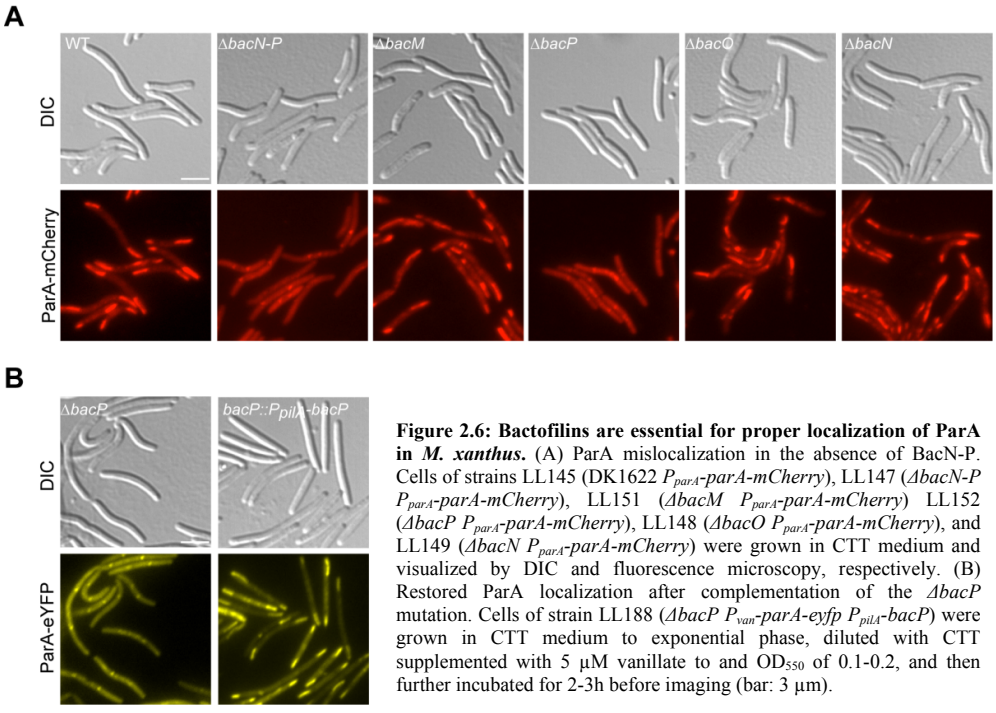

Figure 2.6: Bactofilins are essential for proper localization of ParA in *M. xanthus*. (A) ParA mislocalization in the absence of BacN-P. Cells of strains LL145 (DK1622 P_{parA}-*parA-mCherry*), LL147 (*ΔbacN-P* P_{parA}-*parA-mCherry*), LL151 (*ΔbacM* P_{parA}-*parA-mCherry*) LL152 (*ΔbacP* P_{parA}-*parA-mCherry*), LL148 (*ΔbacO* P_{parA}-*parA-mCherry*), and LL149 (*ΔbacN* P_{parA}-*parA-mCherry*) were grown in CTT medium and visualized by DIC and fluorescence microscopy, respectively. (B) Restored ParA localization after complementation of the *ΔbacP* mutation. Cells of strain LL188 (*ΔbacP* P_{van}-*parA-eyfp* P_{pilA}-*bacP*) were grown in CTT medium to exponential phase, diluted with CTT supplemented with 5 µM vanillate to and OD_{550} of 0.1-0.2, and then further incubated for 2-3h before imaging (bar: 3 µm).

Similarly, we also examined ParB localization in the absence of different bactofilins. Here we assume that reaching localization symmetry of both ParB foci indicates a complete round of chromosome segregation, meaning that both foci have reached the same distance from corresponding cell poles. Under this assumption, in an exponentially growing population of the *M. xanthus* wild type, a majority of cells have accomplished chromosome segregation (Figures 2.7A and 2.7C). However, ParB significantly mislocalizes in the absence of *bacN-P* (Figures 2.7A and 2.7B). In general, lacking *bacN-P* has two consequences on ParB: (1) the majority of cells in the population show only partially segregated ParB foci, as indicated by a much higher number of cells with a lower segregation symmetry value; (2) for cells reaching segregation symmetry, the distance between the two ParB foci is significantly smaller than that in wild-type cells, meaning that ParB foci are further away from the nearby cell pole (20%-40% of the total cell length in comparison to 5%-15% in wild type) in cells with nearly 100% segregation symmetry (Figure 2.7C). Furthermore, ParB localization was also monitored and quantified in the absence of individual bactofilins (Figure 2.7C). Deletion of either *bacP* or *bacO* resulted in the most significant defects in ParB localization, while the *ΔbacN* mutation only had a minor effect (Figure 2.7C). On the other hand, consistent with the observation made for ParA positioning, the absence of *bacM* had no effect on ParB (Figures 2.7A and 2.7C).

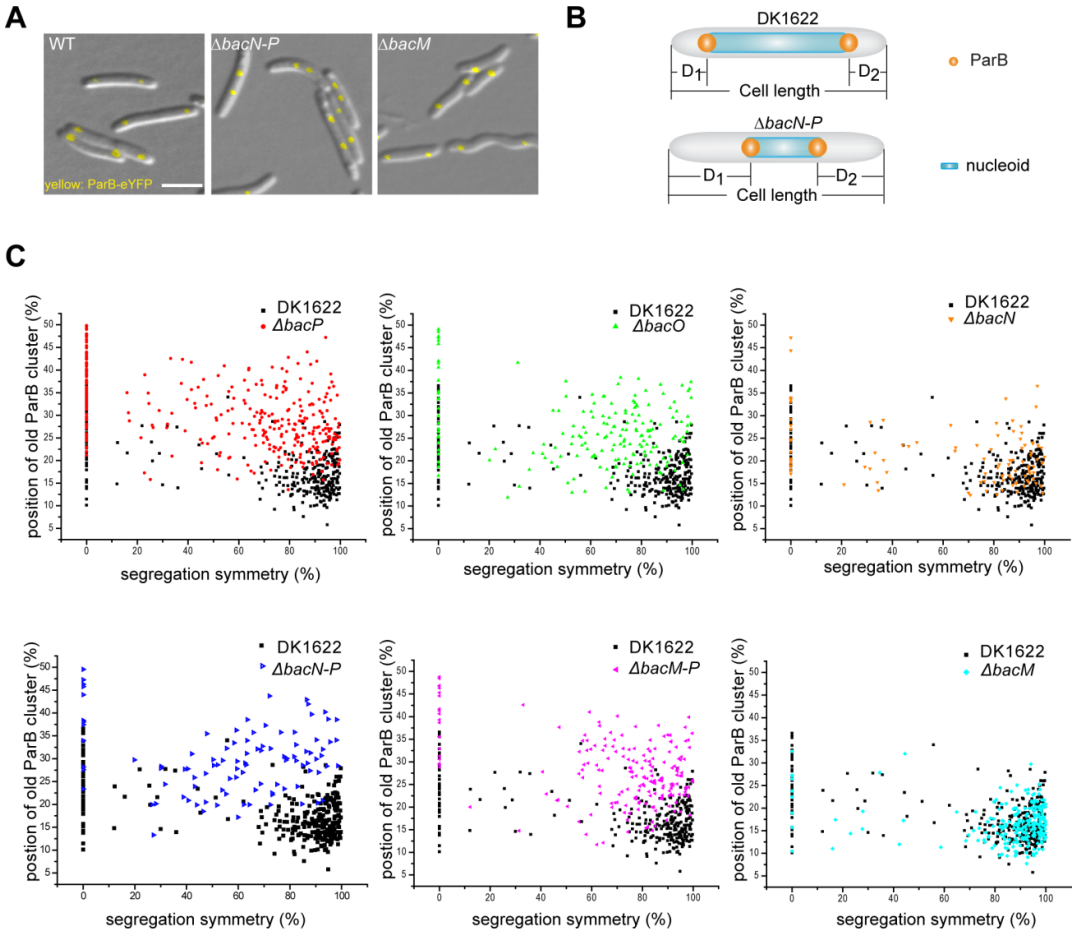

Notably, despite the severe defect on the spatial positioning of chromosome segregation components, the absence of bactofilins does not affect the cell length (Figure 2.8A) and the growth rate (data not shown); however, the average distance between two ParB foci during chromosome segregation is significantly lower in the absence of *bacO, bacP,* or *bacN-P* (Figure 2.8B).

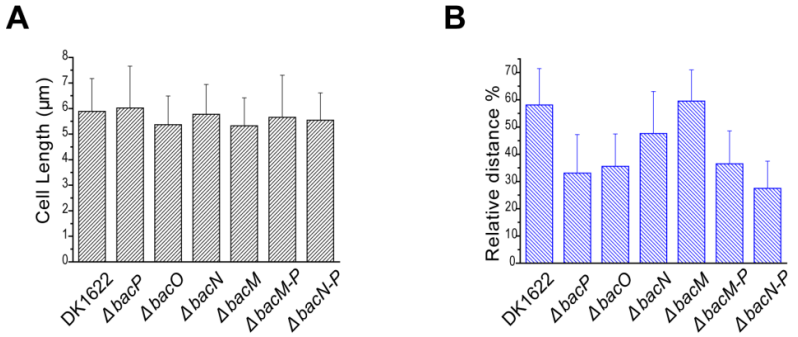

Figure 2.8: The absence of bactofilins has no effect on cell length. (A) The absence of BacN-P does not affect the overall cell length of different strains. (B) The absence of BacN-P leads to significant reduction of the distance between ParB foci within the cell. For both panels, quantifications are based on same datasets as Figure 2.7C.

2.4 BacN-P form bipolar filaments and colocalize with ParB.

To examine the localization patterns of bactofilins in *M. xanthus*, immunofluorescence microscopic analyses were performed using antibodies against BacO and BacP. Western blots verified the specific detection of BacO and BacP by the antibodies, and showed that the expression of *bacO* or *bacP* was not significantly affected by the absence of other individual bactofilins (Figure 2.9A). To visualize BacN, a strain carrying a C-terminal HA-tagged derivative of BacN was analyzed by immunolabeling using an anti-HA antibody (Figure 2.9A). Consistent with published results [16], BacP forms bipolar filamentous structures (Figure 2.9B). The other two bactofilins, BacO and BacN, was also found to form short filament-like structures at both cell poles in the majority of cells, In addition, longer cells also displayed some cloud-like structure along the medial parts, in particular at mid cell (Figure 2.9B). The length of filaments varied. The identical localization patterns of BacN-P are likely the result of copolymerization, as further supported by co-immunoprecipitation analysis: BacP was found to be co-isolated with BacN-HA from *M. xanthus* cell extracts in affinity purification experiments (Figure 2.9C). Therefore, BacN-P copolymerize into bipolar filaments in *M. xanthus*.

Figure 2.7: Bactofilins are required for the precise localization of ParB in *M. xanthus*. (A) ParB mislocalization in the absence of BacN-P. Cells of strains LL012 (DK1622 P_{parB}-*parB-eyfp*), LL019 (Δ*bacN-P* P_{parB}-*parB-eyfp*), and LL013 (Δ*bacM* P_{parB}-*parB-eyfp*) were grown in CTT medium and visualized by DIC and fluorescence microscopy. (B) Schematic representation of ParB localization in the presence (upper) or absence (lower) of BacN-P. Scale bar: 3 μm. (C) Significant difference of ParB distribution in the absence of BacN-P. Cells were grown in CTT medium to exponential phase. Cell lengths and distances of ParB-eYFP from cell poles (as indicated in panel B) were measured in Metamorph. The X-axis represents the symmetry of two ParB foci within the cell calculated by the following formula: ((cell length-D_1-D_2)/ (cell length-2×min (D_1, D_2))) ×100%. The Y-axis represents the relative position of old ParB foci within the cell, calculated by min (D_1, D_2)/cell length×100%, assuming that the ParB focus with smaller distance from the nearest cell pole was the old one. The total of 299, 340, 188, 99, 277, 99, and 200 cells were analyzed for LL012 (DK1622 P_{parB}-*parB-eyfp*), LL015 (Δ*bacP* P_{parB}-*parB-eyfp*), LL018 (Δ*bacO* P_{parB}-*parB-eyfp*), LL014 (Δ*bacN* P_{parB}-*parB-eyfp*), LL013 (Δ*bacM* P_{parB}-*parB-eyfp*), LL019 (Δ*bacN-P* P_{parB}-*parB-eyfp*), and LL016 (Δ*bacN-P* Δ*bacM* P_{parB}-*parB-eyfp*), respectively.

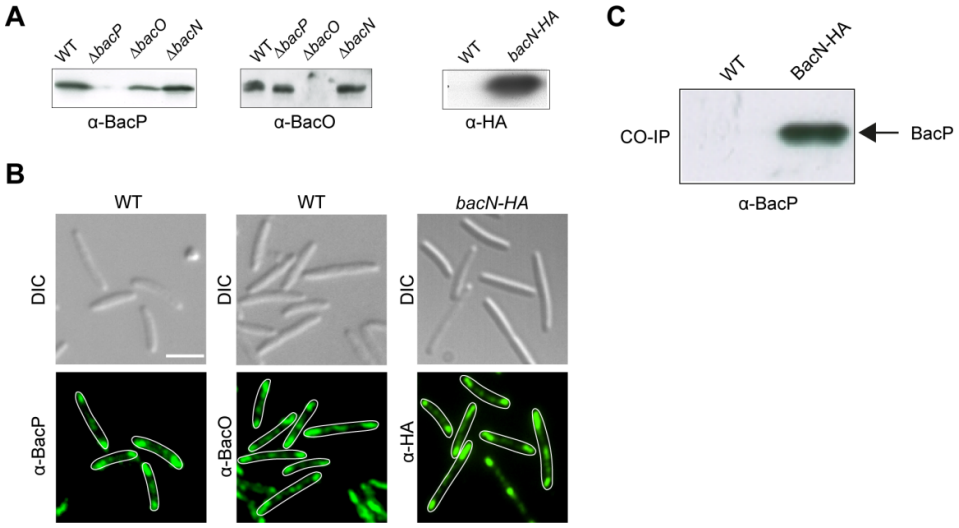

Figure 2.9: BacN-P form bipolar filaments in *M. xanthus*. (A) Immunoblot analyses of BacP, BacO, and BacN-HA accumulations using α-BacP, α-BacO and α-HA antibodies in different strains, respectively. Total cell lysates were collected from exponentially growing cells of strains DK1622, LL001 (Δ*bacP*), LL002 (Δ*bacO*), LL003 (Δ*bacN*), and LL033 (*bacN-HA*). (B) Localization of BacP, BacO, and BacN-HA by immunofluorescence. Cells of the wild type (DK1622) were grown in CTT medium to an OD_{550} of ~ 0.7, fixed, then probed with α-BacP and α-BacO antibodies, respectively. For BacN, cells of LL033 (*bacN-HA*) were grown in CTT, fixed, and then probed with α-HA antibodies. Alexa-Fluor 488-conjugated secondary antibody (Invitrogen) was then used to detect the immunocomplexes. Scale bar: 3 µm. (C) Interaction of BacP and BacN in *M. xanthus*. Co-immunoprecipitation analysis was conducted by using α-HA affinity beads to precipitate BacN-HA from cell lysates of strain LL033 (*bacN-HA*). Proteins co-precipitated with BacN-HA were eluted and probed with α-BacP (1:1000) by immunobloting. As a control, the same analysis was conducted with cell lysates of the wild-type strain (DK1622).

Interestingly, it appears that both the N- and C-termini are critical for proper localization. For instance, fusing mCherry, a fluorescent protein with a molecular mass of 28.8 kDa, to either the N- or the C-terminus resulted in a dramatic change of localization patterns. Instead of bipolar filaments, BacN-P forms a filament-like structure along the medial part of cells (Figure 2.10A), consistent with published results [82]. As a consequence, the function of BacN-P was disrupted, as indicated by the mislocalization of ParB (data not shown). Interestingly, although the localization pattern was altered by fusion to mCherry, bactofilins were still able to interact with each other: (i) BacO was co-isolated with BacP-mCherry from *M. xanthus* cell extracts by affinity purification; (ii) and both BacP and BacO were found to interact with BacN-mCherry in *M. xanthus* in co-immunoprecipitation experiments (Figure 2.10B).

An advantage for fluorescent fusion proteins is to easily monitor the protein dynamics *in vivo*. Although the function of BacN-P is impaired when fusing to mCherry, BacN-P are still able to polymerize in *M. xanthus*. Therefore, we performed fluorescence recovery after photobleaching (FRAP) analysis on BacP-mCherry, BacO-mCherry, and BacN-mCherry fusions. In all three cases, after photobleaching with laser, the fluorescene signal was restored within 100 s (Figure 2.11). By quantitative measurements, we showed that BacP-mCherry, BacO-mCherry, and BacN-mCherry proteins have the recovery half time ($t_{1/2}$) of 44.7 s (±17.3 s; n=11), 31.2 s (±12.4 s; n=10), and 35.1 s (±13.6 s; n=10), respectively. Therefore, we concluded that the mCherry-tagged BacN-P appears to be highly dynamic *in vivo*.

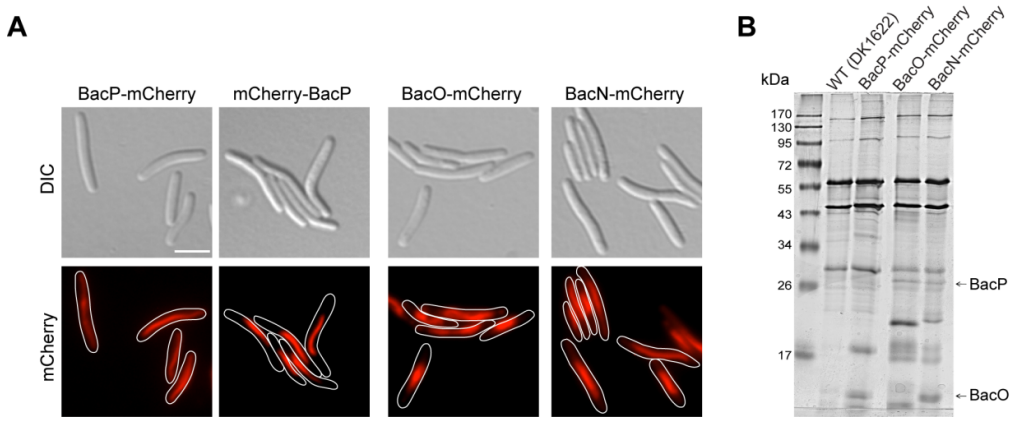

Figure 2.10: Tagging with mCherry alters the localization of BacN-P, but not their copolymerization. (A) Localizations of mCherry-tagged bactofilins in *M. xanthus*. Cells of strains LL061 (*bacP::mCherry-bacP*), MT296 (*bacP::bacP-mCherry*), MT297 (*bacO::bacO-mCherry*), and MT298 (*bacN::bacN-mCherry*) were grown in CTT medium and visualized by DIC and fluorescence microscopy. (B) Interaction of mCherry-tagged bactofilins. BacP-mCherry, BacO-mCherry, and BacN-mCherry were immunoprecipitated using α-RFP antibodies from cell lysates of MT296 (*bacP::bacP-mCherry*), MT297 (*bacO::bacO-mCherry*), and MT298 (*bacN::bacN-mCherry*), respectively. As a control, the same procedure was also applied to cell lysates of the wild type (DK1622). The precipitates were separated in an 11% SDS–polyacrylamide gel and visualized by silver staining. Bands specific to MT296, MT297, or MT298 in comparison to the wild type were further analyzed by mass spectrometry.

To facilitate the analysis of BacN-P function, we attempted to construct functional bactofilin fluorescent protein fusions using different fluorescent tags or expression under different promoters. However, so far, all constructs exhibit localization patterns that were different from that observed by immunofluorescence microscopy from wild type. However, it was noticed that the localization of fluorescently-tagged bactofilins is affected by their expression levels as well as the presence of their native copies. For instance, when expressed under the control of the copper-inducible promoter in the absence of the native gene, BacP-mCherry is produced at much lower levels than when expressed from the native promoter (data not shown). In this condition, the majority of BacP-mCherry molecules accumulate at one cell pole, with much less accumulation at the other pole (Figure 2.12A). In contrast, under the same expression conditions, BacP-mCherry accumulates along the medial part of cells in the presence of the native gene (Figure 2.12A). On the other hand, expression of *mCherry-bacP* under the control of the strong *pilA* promoter leads to the formation of filament-like structures along the medial part of cells, which is similar to the pattern observed when expressed under the native promoter (Figure 2.12B). On the other hand, in the absence of native gene, BacO-mCherry forms polar and subpolar patches when expressed at low levels, while mCherry-BacO form unipolar filament-like structures with some accumulation at the other cell pole when expressed at high levels (Figure 2.12). However, when mCherry-tagged BacO is produced in the presence of native copy, fusion proteins always form filaments along the medial part of cells regardless of the expression level (Figure 2.12). For BacN, when BacN-mCherry is produced at low levels (under the control of copper promoter) in the presence of the native gene, bipolar accumulation of proteins is observed (Figure 2.12A). However, when mCherry-tagged BacN is produced at high levels in addition to wild-type BacN, fusion proteins form irregular-shaped filaments at medial part of cells (Figure 2.12B).

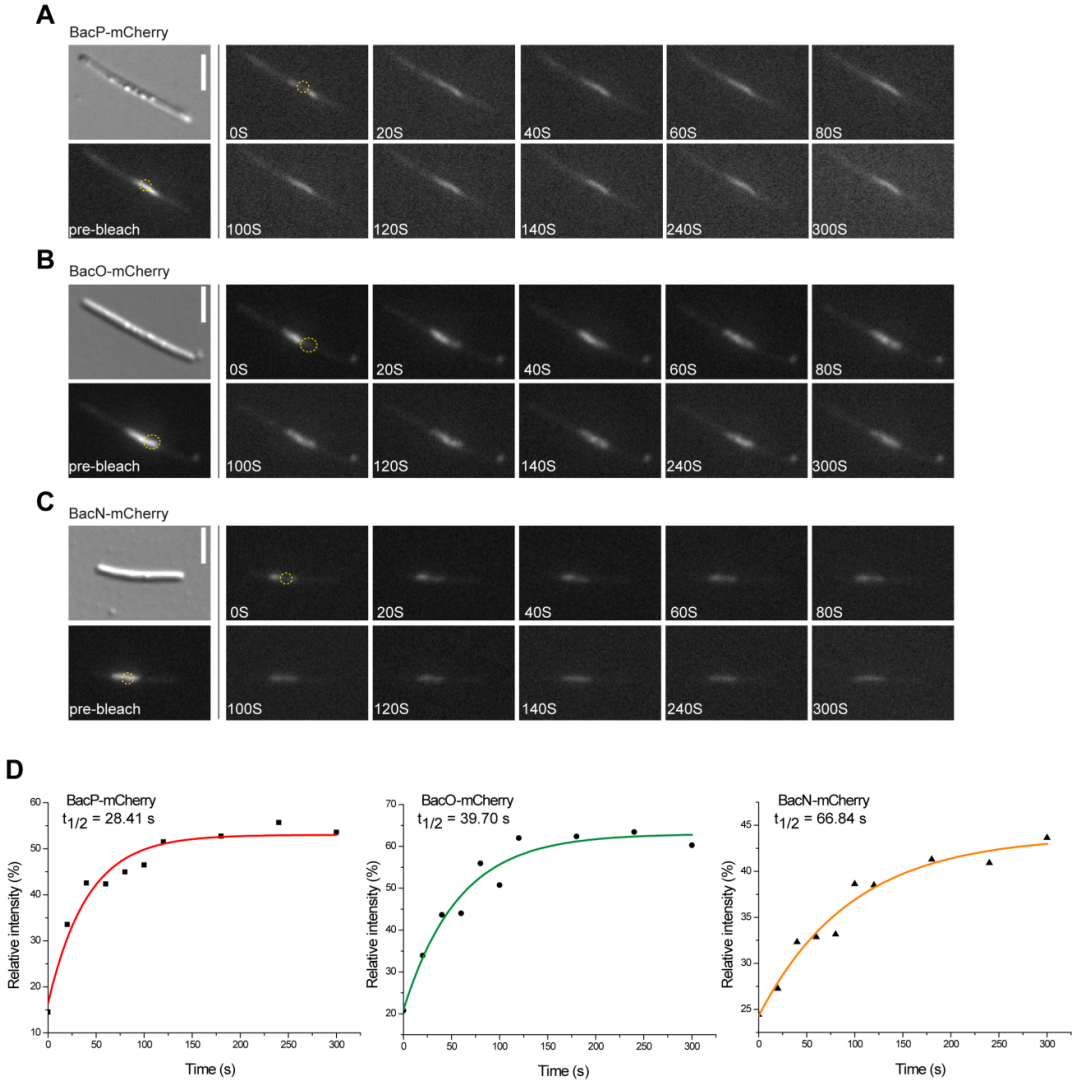

Figure 2.11: mCherry-tagged BacN-P are highly dynamic in *M. xanthus*. (A-C) Time-lapse fluorescence images of cells with BacP-mCherry, BacO-mCherry, and BacN-mCherry after bleaching of a small region of filaments, respectively. Cells of strain MT296 (*bacP::bacP-mCherry*), MT297 (*bacO::bacO-mCherry*), and MT298 (*bacN::bacN-mCherry*) were grown in CTT medium and treated with chloramphenicol for 1 h to stop protein synthesis before applying onto glass slides for imaging. Scale bar: 3 µm. (D) Quantification of recovery of fluorescence signals of the bleached regions as shown in panel A-C. The X-axis represents the time, while the Y-axis represents the relative intensity after bleaching normalized to the fluorescence decay in unbleached regions.

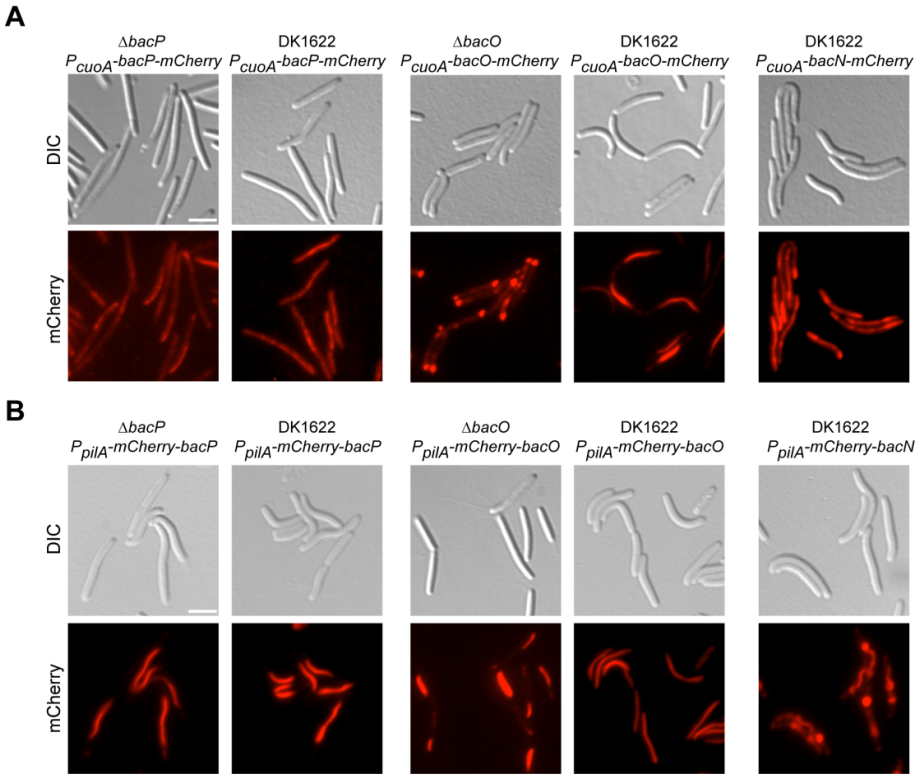

Figure 2.12: The localization of fluorescently-tagged BacN-P is influenced by the expression levels and the presence of the native gene. (A) Localization of mCherry-tagged BacN-P when expressed under the control of copper-inducible promoter. Cells of strains LL028 (Δ*bacP* P_{cuoA}-*bacP-mCherry*), LL034 (DK1622 P_{cuoA}-*bacP-mCherry*), LL037 (Δ*bacO* P_{cuoA}-*bacO-mCherry*), LL038 (DK1622 P_{cuoA}-*bacO-mCherry*), and LL035 (DK1622 P_{cuoA}-*bacN-mCherry*) were grown in CTT medium to exponential phase and diluted to an OD_{550} of 0.1, then induced with 400 µM $CuSO_4$ for 20 h before imaging. (B) Localization of mCherry-tagged BacN-P when highly expressed under the control of *pilA* promoter. Cells of strains LL080 (Δ*bacP* P_{pilA}-*mCherry-bacP*), LL084 (DK1622 P_{pilA}-*mCherry-bacP*), LL074 (Δ*bacO* P_{pilA}-*mCherry-bacO*), LL085 (DK1622 P_{pilA}-*mCherry-bacO*), and LL086 (DK1622 P_{pilA}-*mCherry-bacN*) were grown in CTT medium to exponential phase before imaging. Scale bar: 3 µm.

As shown, mCherry-tagging dramatically altered the localization and function of BacN-P. Therefore, we alternatively constructed a derivative of BacP ($BacP_{TC}$) in which a tetracysteine tag (FLNCCPGCCMEP) was inserted internally shortly after the bactofilin domain (Figure 2.13C). However, the staining with the fluorescent dyes FlAsH that specifically binds to this tag revealed localization pattern that was significantly different from that of the wild type. Overally, $BacP_{TC}$ appears to form long filaments within the cell, while higher accumulation at the cell pole was only observed for some cells (Figure 2.13A). A derivative of BacN ($BacN_{TC}$) that contains a C-terminal tetracysteine tag exhibits a similar localization pattern (Figure 2.13A). Tagging affects the function of BacN-P, since ParA exhibits partially aberrant localization pattern in the presence of tetracysteine-tagged bactofilins (Figure 2.13B). Therefore, based on this aberrant localization patterns and their adverse effects on ParA, we conclude that these derivatives are not fully functional.

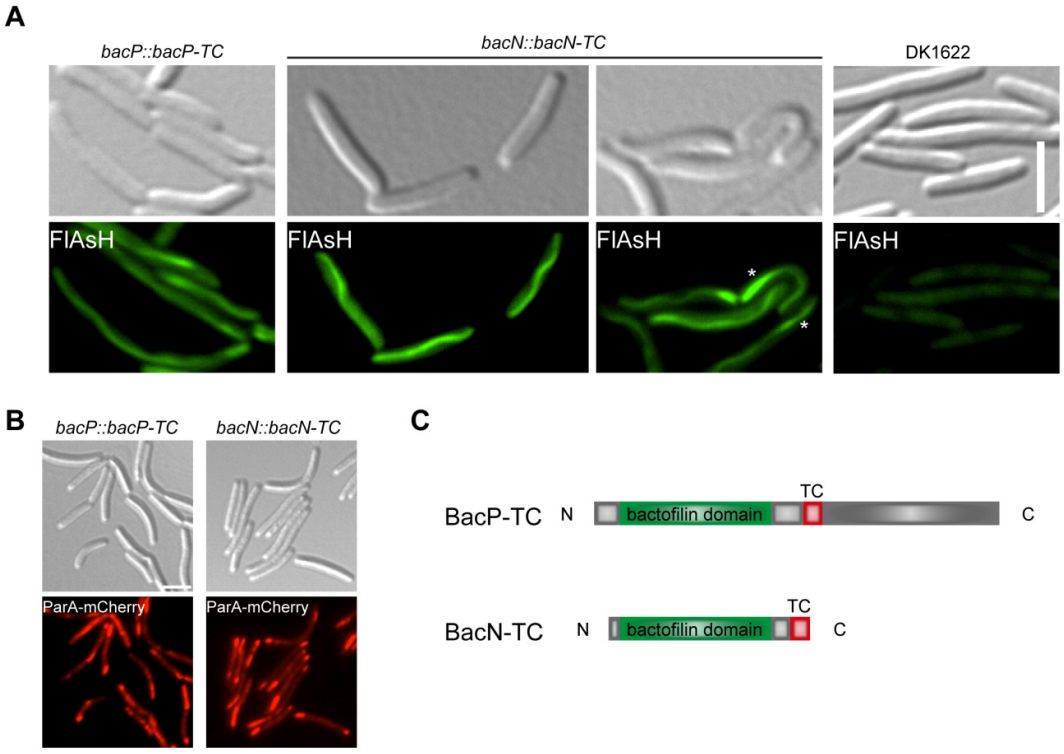

Figure 2.13: Tagging with tetracysteine alters the localization of BacN-P. (A) Localization of tetracysteine-tagged BacP and BacN. Cells of strains LL104 (*bacP::bacP*$_{TC}$) and LL146 (*bacN::bacN-TC*) were grown in CTT medium and treated with FlAsH before imaging. (B) Localiatzion of ParA in the presence of tetracysteine-tagged BacP or BacN. Cells of strains LL158 (*bacP::bacP*$_{TC}$ *P*$_{parA}$*-parA-mCherry*) and LL159 (*bacN::bacN*$_{TC}$ *P*$_{parA}$*-parA-mCherry*) were grown in CTT meidium before imaging. Scale bar: 3 µm. (C) Schematic representation of the construction of tetracysteine-tagged BacP and BacN derivatives.

As shown, BacN-P form short filamentous structures at both cell poles, which may correlate with ParB clusters. To test this hypothesis, we colocalized bactofilins and ParB. Immunofluorescence microscopy was applied to strains in which ParB was fused to eYFP. This analysis showed that ParB localized at the subpolar end of bactofilin filaments near the cell pole (Figure 2.14A). This was even true in filamentous cells generated by cephalexin treatment, in which the majority of ParB complexes still remained anchored to BacN-HA filaments (Figure 2.14B). This result strongly suggests a close association between ParB and BacN-P bipolar filaments *in vivo*. Notably, ParB-YFP also dynamically localized to the ends of the mCherry-BacP filaments, although the filaments mislocalized to the middle of the cell (Figure 2.15A). Time-lapse experiments showed that during origin segregation one ParB focus was immobile at one end of the mCherry-BacP, while second ParB focus was moving towards the other end of the filament (Figure 2.15B). This finding further supports the hypothesis that ParB interacts with BacN-P in *M. xanthus*.

Although functional fluorescently-tagged derivatives of BacN-P are not available so far, our immunofluorescence data suggests that ParB associates with bipolar BacN-P filaments. The interaction between BacN-P and ParB is further supported by the association between ParB and aberrantly localized mCherry-BacP filaments.

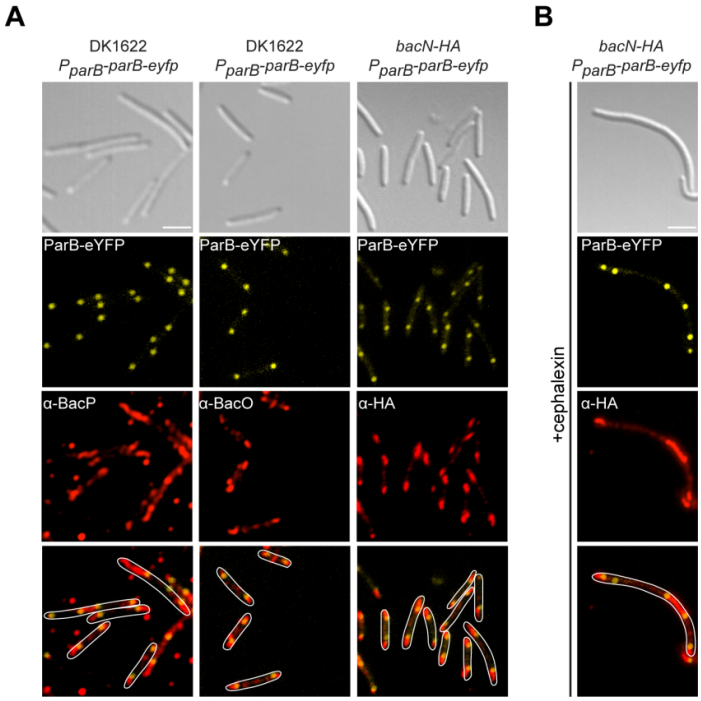

Figure 2.14: Colocalization of ParB and BacN-P in *M. xanthus*. (A) Colocalization of ParB with BacN-P filaments in *M. xanthus*. To colocalize ParB and BacP, cells of LL012 (DK1622 P_{parB}-*parB-eyfp*) were grown in CTT medium, fixed, and then probed with α-BacP antibody. Alexa-Fluor 594-conjugated secondary antibody (Invitrogen) was then used to detect the immunocomplexes. Alternatively, to colocalize ParB and BacO, the same procedure was performed with cells of LL012 (DK1622 P_{parB}-*parB-eyfp*), but using the α-BacO antibody. On the other hand, LL040 *(bacN::bacN-HA* P_{parB}-*parB-eyfp*) were also used for immunofluorescence analysis using the α-HA antibody. (B) Colocalization of BacN-HA and ParB in filamentous cells. *M. xanthus* strain LL040 (*bacN::bacN-HA* P_{parB}-*parB-eyfp*) was treated with 100 µM cephalexin for 8 hours to induce the filamentation of cells. Afterwards, cells were subjected to immunofluorescence analysis using the α-HA antibody. Scale bar: 3 µm.

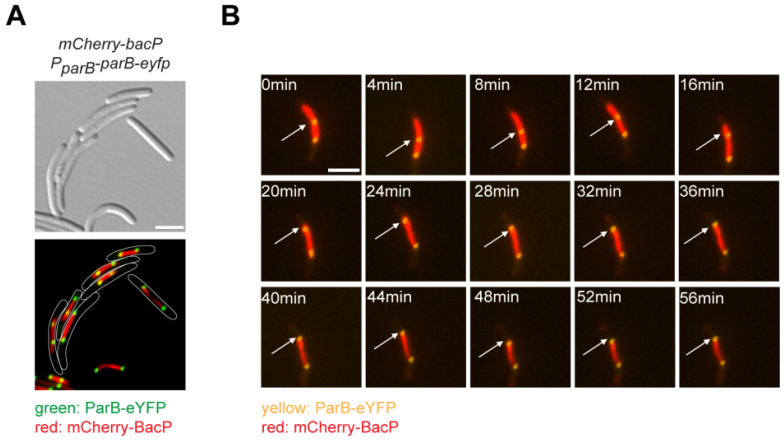

Figure 2.15: Association between ParB and mCherry-BacP filaments. (A) Colocalization of ParB with mCherry-BacP filaments in *M. xanthus*. Cells of strain LL067 (*bacP::mCherry-bacP* P_{parB}-*parB-eyfp*) were grown in CTT medium and visualized by DIC and fluorescence microscopy. (B) Dynamic localization of ParB on mCherry-BacP filaments during chromosome segregation. Cells of strain LL067 (*bacP::mCherry-bacP* P_{parB}-*parB-eyfp*) were grown in CTT medium and visualized by DIC and fluorescence microscopy at 4-min intervals. Scale bar: 3 µm.

2.5 A dominant-negative mutation of BacP leads to severe chromosome segregation defects and growth arrest.

As shown, the deletion or the fluorescence tagging of BacN-P has a great impact on the localization of ParA and ParB, while cell growth is not significantly affected. Interestingly, a dominant-negative variant of BacP obtained by fusing its C-terminus with a small HA tag forms long unipolar filaments (Figure 2.16A). Its synthesis leads to a severe growth defect (Figure 2.16B), which probably results from a defect in chromosome segregation.

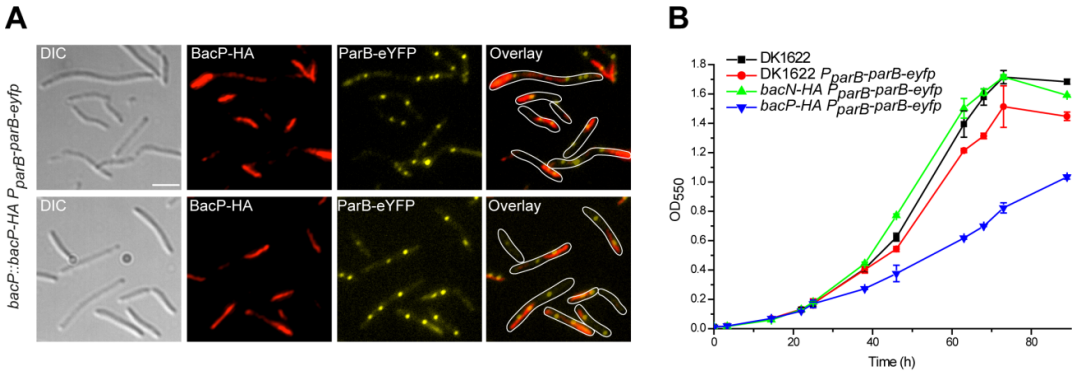

Figure 2.16: BacP-HA severely impairs chromosome segregation and cell growth in *M. xanthus*. (A) BacP-HA forms unipolar filaments and severely disrupts ParB localization and segregation. Cells of LL046 (*bacP::bacP-HA* P_{parB}-*parB-eyfp*) were grown in CTT medium, fixed, and then probed with α-HA antibody. An Alexa-Fluor 594-conjugated secondary antibody was then used to detect the immunocomplexes. Scale bar: 3 µm. (B) Growth defect in the presence of BacP-HA. Cells of strains DK1622, LL012 (DK1622 P_{parB}-*parB-eyfp*), LL040 (*bacN::bacN-HA* P_{parB}-*parB-eyfp*), and LL046 (*bacP::bacP-HA* P_{parB}-*parB-eyfp*) were grown in CTT to exponential phase, and then diluted to an OD_{550} of 0.01. OD_{550} were then measured at different time points for 89 hours. Two replicates were performed per strain.

Indeed, in the presence of BacP-HA, more than 20% of cells showed an abnormal number of ParB foci (either more than 2 foci or no foci), compared with less than 3% in the wild type and ~8% in the Δ*bacP* mutant (Figures 2.17A and 2.17B). In many predivisional cells, ParB foci were distributed unequally, with one of the future daughter cells having two or even more foci, while the other one had none and was anucleate (Figure 2.17A). In addition, ParA also mislocalized into unipolar patches (Figure 2.17C).

Similarly, the expression of *bacO-HA* also led to dysfunction of BacN-P, with many cells showing only unipolar BacO filaments (Figure 2.17D) and ParA mislocalization (data not shown). In contrast, BacN-HA shows normal bipolar localization, with no effect on ParA positioning (data not shown). Although the molecular mechanism by which the HA-tagged derivative of BacP disturbs chromosome segregation is still unclear, these findings further support the importance of BacN-P for chromosome segregation.

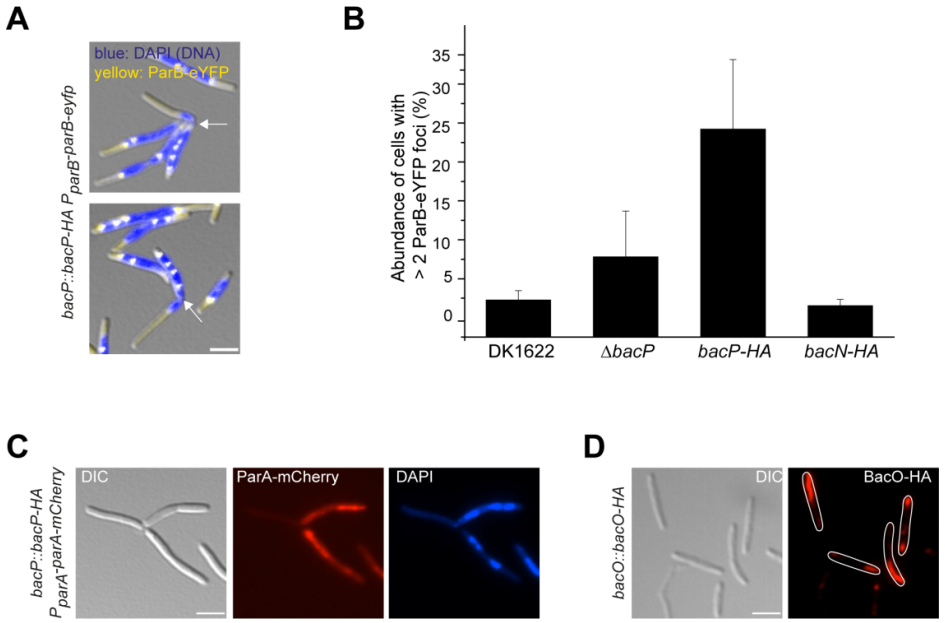

Figure 2.17: BacP-HA severely impairs ParAB localization in *M. xanthus*. (A) BacP-HA leads to unequal distribution of chromosomes and ParB in predivisional cells. Cells of LL046 (*bacP::bacP-HA* P_{parB}*-parB-eyfp*) were grown in CTT medium, stained with 4', 6-diamidino-2-phenylindole (DAPI), and visualized by DIC and fluorescence microscopy. (B) Higher abundance of cells with abnormal numbers of ParB foci in the presence of BacP-HA. Strains LL012 (DK1622 P_{parB}*-parB-eyfp*), LL015 (Δ*bacP* P_{parB}*-parB-eyfp*), LL040 (*bacN::bacN-HA* P_{parB}*-parB-eyfp*), and LL046 (*bacP::bacP-HA* P_{parB}*-parB-eyfp*) were grown to exponential phase. Quantification was conducted for 3 independent repeats for each strain with more than 500 cells counted each time. The abundance of cells with more than two ParB-eYFP foci was normalized to the total number of cells analyzed. (C) ParA mislocalization in the presence of BacP-HA. Cells of strain LL150 (*bacP::bacP-HA* P_{parA}*-parA-mCherry*) were grown in CTT medium and stained with DAPI before imaging. (D) BacO-HA forms unipolar filaments in many cells. Cells of strain LL048 (*bacO::bacO-HA*) were analyzed by immunofluorescence microscopy using an α-HA antibody. Scale bar: 3 µm.

2.6 BadA, a ParB-like protein, is involved in bactofilin-mediated ParAB positioning.

The phenotypic analysis and the localization pattern of BacN-P indicated that BacN-P are indeed crucial for the precise localization of ParA and ParB, which are key components of chromosome segregation. To further explore the bactofilin-mediated positioning of chromosome segregation, we set out to identify more components of this system. In bacteria, genes lying adjacent to each other have often been shown to be involved in the same cellular process. Therefore, we first generated an in-frame deletion in the downstream gene, MXAN4634, henceforth referred to as *badA* (bactofilin-associated DNA binding protein A). BadA is annotated as a ParB-like nuclease domain-containing protein. It has a predicted molecular mass of 50.7 kDa, with a large unstructured N-terminal region and potential helix-turn-helix (HTH) motif in the C-terminal region (Figure 2.18A). Moreover, in species closed related to *M. xanthus*, its genomic context is conserved (Figure 2.18B), indicating a possible functional relation to bactofilins.

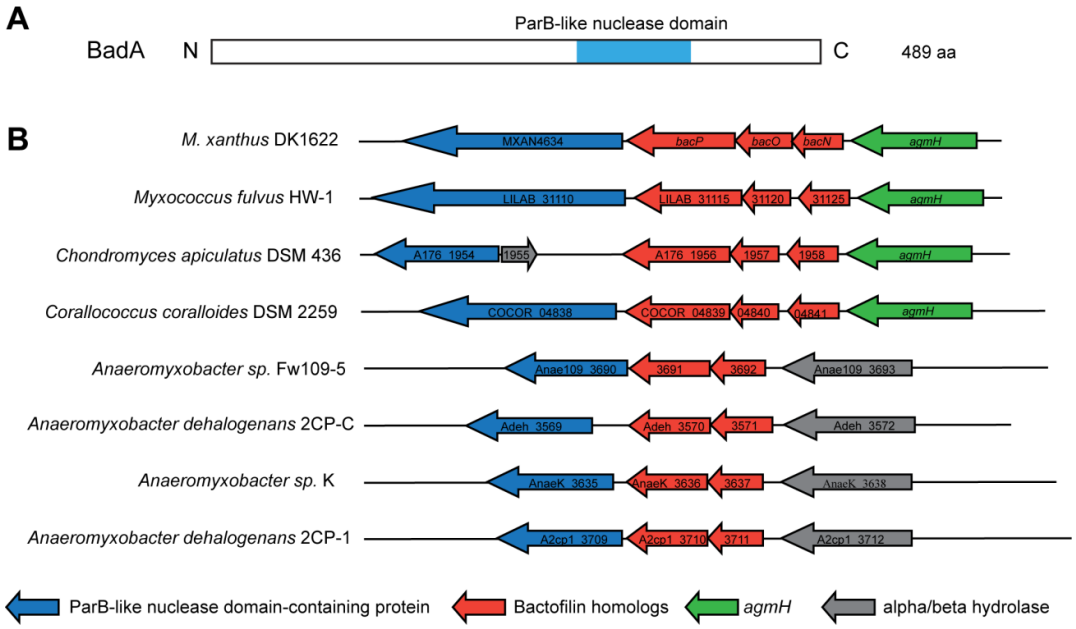

Figure 2.18: Schematic representation of BadA (MXAN4634). (A) Domain organization of BadA. The position of the ParB-like nuclease domain is indicated in blue. (B) Conservation of genomic context of *badA* in other *Myxococcales*. Homologs of *badA* are indicated in blue; bactofilin homologs are shown in red; green arrows represent *agmH*. A gene of putative alpha/beta hydrolase is shown in grey. The direction of the arrows indicates the direction of transcription.

We first examined the localization of ParA and ParB in the absence of BadA. It was observed that deletion of *badA* resulted in the mislocalization of ParA (Figure 2.19). To test whether this defect could be complemented by the ectopic expression of *badA*, we constructed a strain in which native *badA* was deleted, while an ectopic copy was expressed under the control of a vanillate-inducible promoter. Without induction, we observed severe mislocalization of ParA. However, upon induction with vanillate, the production of BadA led to the reappearance of bipolar ParA patches (Figure 2.19).

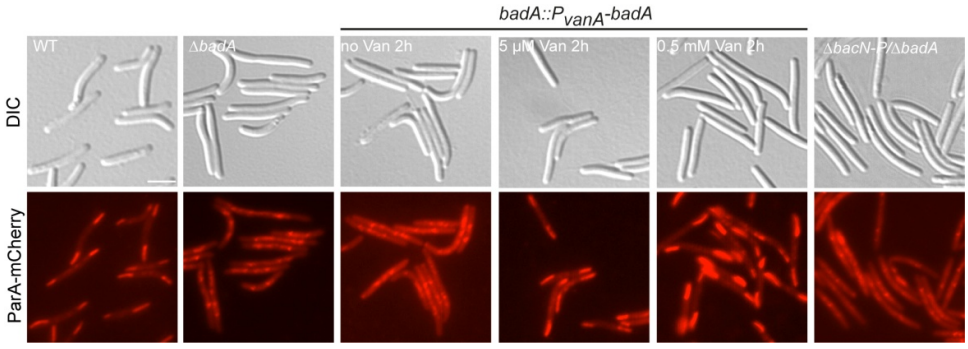

Figure 2.19: The mislocalization of ParA and ParB in the absence of BadA. ParA mislocalization in the absence of BadA. Cells of strains of LL145 (DK1622 P_{parA}-*parA-mCherry*), LL154 (*ΔbadA* P_{parA}-*parA-mCherry*), and LL175 (*ΔbacN-P ΔbadA* P_{parA}-*parA-mCherry*) were grown in CTT medium and analyzed by microscopy. For complementation, cells of strain LL192 (*ΔbadA* P_{parA}-*parA-mCherry* P_{van}-*badA*) were grown to exponential phase and diluted to an OD_{550} of 0.1-0.2 in CTT medium in the presence of 0 µM, 5 µM or 500 µM of vanillate, respectively. After 2 h induction, cells were visualized by DIC and fluorescence microscopy. Scale bar: 3 µm.

Similarly, ParB localization was significantly affected in the absence of BadA, with ParB showing distribution pattern similar to that of a *ΔbacN-P* mutant (Figure 2.20). In addition, we also confirmed that the deletion of the entire MXAN4634-7 cluster *(*Δ*bacN-P* Δ*badA*) resulted in a phenotype identical to that observed in the absence of BacN-P or BadA alone (Figures 2.19 and 2.20).

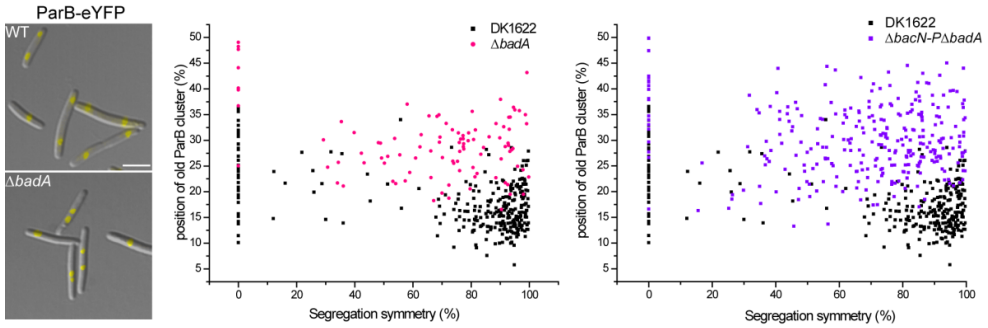

Figure 2.20: ParB mislocalization in the absence of BadA. Cells of strains LL012 (DK1622 P_{parB}-*parB-eyfp*), LL102 (*ΔbadA* P_{parB}-*parB-eyfp*), LL176 (*ΔbacN-P ΔbadA* P_{parB}-*parB-eyfp*) were grown in CTT medium for imaging. Distribution analysis was conducted as described in Figure 2.7. A total of 299, 100, and 300 cells were analyzed for LL012 (DK1622 P_{parB}-*parB-eyfp*), LL102 (*ΔbadA* P_{parB}-*parB-eyfp*), and LL176 (*ΔbacN-P ΔbadA* P_{parB}-*parB-eyfp*), respectively. Scale bar: 3 µm.

The wild-type expression level of *badA* as well as the recovery of BadA production induced by vanillate was analyzed by immunoblot analysis using α-BadA antibodies (Figure 2.21A). It was apparent that the expression of *badA* was not affected by deletion of *bacN-P* (Figure 2.21B). Moreover, the expression of the adjacent genes, *bacP* and *bacO*, was not affected by the deletion of *badA* (Figures 2.21C and 2.21D).

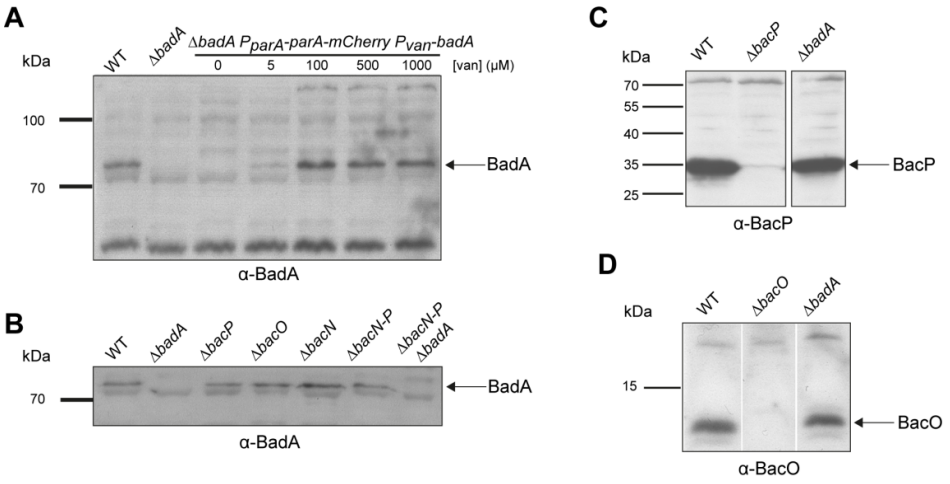

Figure 2.21: BadA or BacN-P do not affect the protein levels of each other. (A) Detection of BadA using α-BadA antibody (1:2500) in cell lysates of DK1622 (WT), LL101 (*ΔbadA*) and LL192 (*ΔbadA* P_{parA}-*parA-mCherry* P_{van}-*badA*) upon induction by vanillate. (B) Detection of BadA using α-BadA antibody (1:2500) in cell lysates of DK1622 (WT), LL101 (*ΔbadA*), LL001 (*ΔbacP*), LL002 (*ΔbacO*), LL003 (*ΔbacN*), MT295 (*ΔbacN-P*), and LL174 (*ΔbacN-P ΔbadA*). (C) Detection of BacP using α-BacP antibody (1:1000) in cell lysates of DK1622 (WT), LL001 (*ΔbacP*) and LL101 (*ΔbadA*). (D) Detection of BacO using α-BacO antibody (1:10000) in cell lysates of DK1622 (WT), LL002 (*ΔbacO*), and LL101 (*ΔbadA*).

Taken together, the absence of BadA leads to defects in the localization of ParA and ParB similar to those observed when BacN-P is absent. Moreover, the expression levels of *badA* and *bacN-P* are independent of each other, indicating that the effect of BadA on ParAB positioning is not a consequence of an effect on the expression level of *bacN-P*. This is further supported by the observation that the normal localization of ParA can be fully restored by expression of an ectopic copy of *badA*. Therefore, it is likely that BadA and BacN-P acts at the same mechanism that is responsible for proper positioning of ParA and ParB.

2.7 BadA colocalizes with BacN-P and ParA in a bactofilin-dependent manner.

Our phenotypic analysis of Δ*badA* mutant demonstrated that BadA is indeed involved in the positioning of ParA and ParB. To further verify the role of BadA, we first applied immunofluoresence microscopy to localize a BacN-HA fusion in the absence of BadA. BacN-HA formed multiple foci in the cell, but failed to form the typical bipolar filaments, indicating a potential role of BadA in BacN-P polymerization (Figure 2.22A).

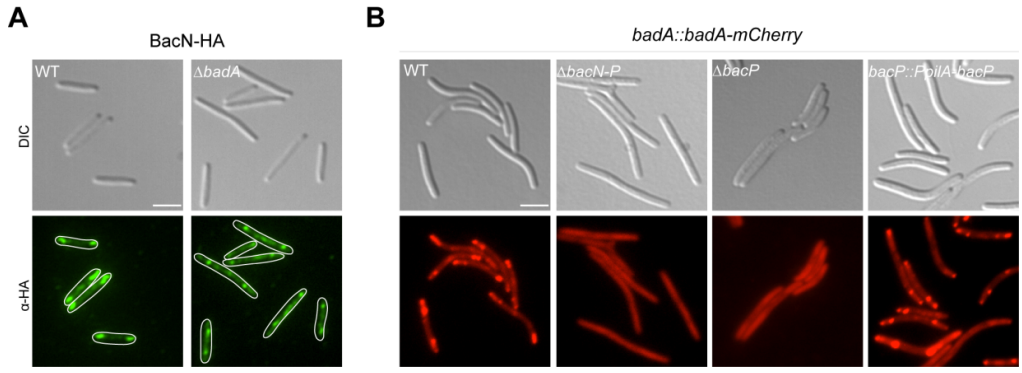

Figure 2.22: BacN-P and BadA affect the localization of each other. (A) Mislocalization of BacN-HA in the absence of BadA. Cells of strain LL110 (*bacN::bacN-HA ΔbadA*) were grown in CTT medium and analyzed by immunofluorescence using an α-HA antibody and an Alexa-Fluor 488-conjugated secondary antibody. (B) BacN-P is essential for BadA localization. Cells of strains LL116 (*badA::badA-mCherry*), LL117 (*ΔbacN-P badA::badA-mCherry*), LL130 (*ΔbacP badA::badA-mCherry*) and LL135 (*ΔbacP badA::badA-mCherry* P_{pilA}*-bacP*) were grown in CTT medium and visualized by DIC and fluorescence microscopy. Scale bar: 3 µm.

In order to explore the subcellular localization of BadA, we first constructed a strain in which the native *badA* gene was replaced with a *badA-mCherry* fusion. In this strain, BadA-mCherry was able to localize to the subpolar regions, exhibiting either a filament-like pattern or forming one subpolar and one polar focus (Figure 2.22B). In the absence of BacN-P, BadA-mCherry was produced at the same level as in a wild-type background (data not shown). However, the lack of BacN-P led to the complete abolishment of BadA localization, and the protein was dispersed throughout the cell (Figure 2.22B). Consistent with previous observation, the deletion of *bacP* alone caused the most pronounced effect (Figure 2.22B). The inactivation of BacO had a less severe effect whereas a strain lacking BacN showed the wild-type BadA localization

pattern (data not shown). The defect caused by the absence of BacP could be complemented by ectopically expressing *bacP* (Figure 2.22B). These observations demonstrated that BacN-P, and in particular, BacP are essential for BadA localization.

However, the replacement of the wild-type *badA* gene with a *badA-mCherry* fusion led to a defect in the localization of ParAB as well as bactofilins, indicating the partial loss of BadA function (Figure 2.23A). Notably, ParA still associated with BadA-mCherry, indicating that the association between BadA and ParA was not impaired (Figure 2.23A). Moreover, we were also able to restore ParA polar localization by ectopically expressing a *badA-mCherry* fusion, suggesting that Bad-mCherry fusion maintains its association with ParA and is still able to recruit ParA to cell poles (Figure 2.23B). The localization of ParA in this strain is slightly aberrant, which is probably due to the partial loss of BadA function. In addition, the expression levels under the control of a vanillate-inducible promoter in our experiment may be slightly different from those obtained with the native promoter.

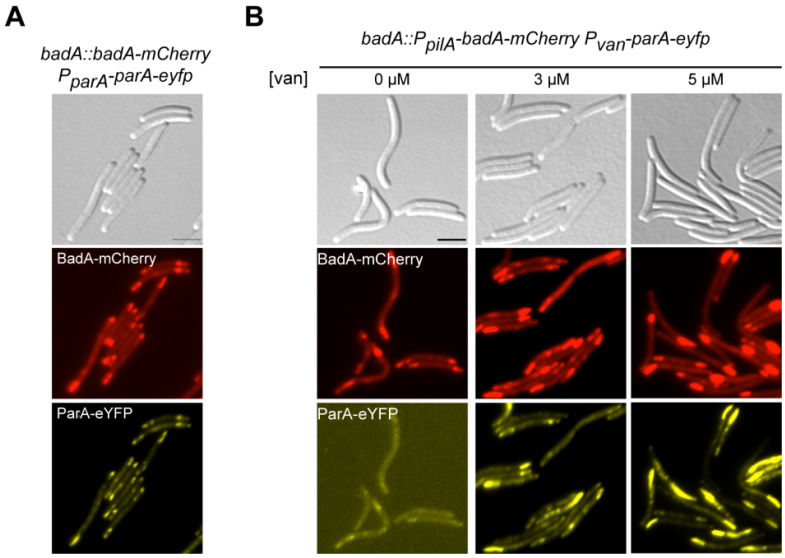

Figure 2.23: BadA-mCherry is able to recruit ParA to cell poles. (A) ParA forms subpolar and polar foci with *bad-mCherry* expressed from its native promoter. Cells of strain LL172 (*badA::badA-mCherry* P_{parA}*-parA-eyfp*) were grown in CTT medium and visualized by DIC and fluorescence microscopy. (B) ParA localization can be largely restored by complemented with BadA-mCherry. Cells of strain LL195 (*ΔbadA* P_{pilA}*-badA-mCherry* P_{van}*-parA-eyfp*) were grown to exponential phase and diluted to an OD_{550} of 0.1-0.2 with CTT medium in the presence of 0 µM, 3 µM or 5 µM of vanillate, respectively. After 2-3h induction, cells were visualized by microscopy. Scale bar: 3 µm.

To further characterize BadA localization, *badA-mCherry* was ectopically expressed under a copper-inducible promoter in the presence of the native *badA* gene. At a very low level of induction, BadA-mCherry was already able to form foci in the subpolar regions or at the cell poles; upon increasing the expression level, BadA-mCherry mostly formed bipolar filaments, similar to the pattern observed for BacN-P and ParA (Figure 2.24A). To further test if BadA-mCherry colocalizes with BacN-P, we expressed *bad-mCherry* ectopically in a strain producing BacN-HA fusion and then applied immunofluorescence microscopy using an α-HA antibody. This analysis showed that Bad-mCherry patches clearly colocalize with BacN (Figure 2.24B).

Notably, when ectopically expressing *badA-eyfp* in the presence of mCherry-BacP, most of the BadA protein associated with mCherry-BacP, which shows a change in its localization to the mid-cell (Figure 2.24C), further indicating a close association of BadA with the BacN-P filaments. Taken together, BadA probably interacts with both BacN-P and ParA in *M. xanthus*.

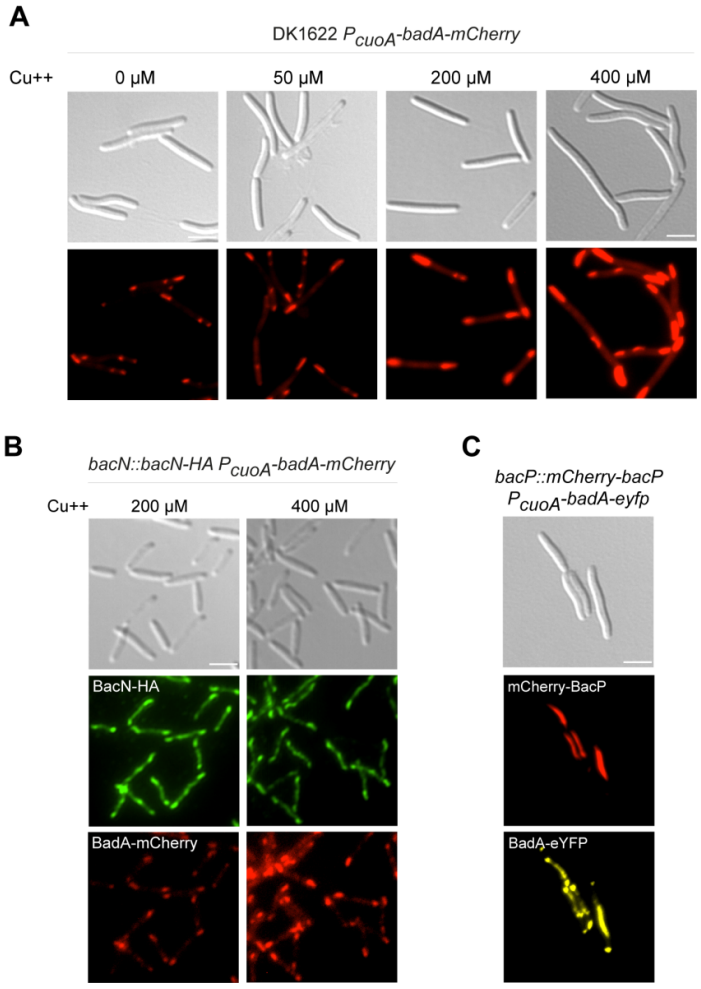

Figure 2.24: BadA colocalizes with both BacN-P and ParA in *M. xanthus*. (A) Expression of *badA-mCherry* under the control of the copper-inducible promoter in presence of native *badA*. Cells of strain LL134 (DK1622 P_{cuoA}-*badA-mCherry*) were grown in CTT medium with no copper to exponential phase, 1:10 diluted in CTT medium supplemented with a series of $CuSO_4$ concentrations: 0 µM, 50 µM, 200 µM, and 400 µM, respectively, then incubated at 32 ˚C overnight. (B) Copper-induced expression of *badA-mCherry* in the presence of wild-type BadA reveals colocalization with BacN-HA. Cells of Strain LL140 (*bacN-HA* P_{cuoA}-*badA-mCherry*) were grown and induced by $CuSO_4$ as described in panel A. Afterwards, cells were subjected to immunofluorescence microscopy, using an α-HA antibody and an Alexa-Fluor 488-conjugated secondary antibody. (C) BadA changes its localization in the presence of mCherry-BacP filaments. Cells of strain LL167 (*bacP::mCherry-bacP* P_{cuoA}-*badA-eyfp*) were grown in CTT medium and dilute to an OD_{550} of 0.1-0.2 in CTT medium supplemented with 100 µM $CuSO_4$ and grown overnight before imaging. Scale bar: 3 µm.

2.8 BadA delocalize in predivisional cells.

Whereas most cells exhibited bipolar ParA patches, a small population of predivisional cells showed an even distribution of ParA within the cell (Figure 2.4A). A similar pattern was observed for BadA in a subset of predivisional cells (50% of all predivisonal cells; Figure 2.25A). Time-lapse analysis for these predivisional cells showed that BadA delocalizes for a short period before cell division takes place (Figure 2.25B). After this period, BadA re-accumulates close to ParB (Figure 2.25B). However, how and why this delocalization of BadA occurs remains unknown. However, it is possible that the delocalization of ParA or BadA is a consequence of the coordination of chromosome segregation and cell division during cytokinesis.

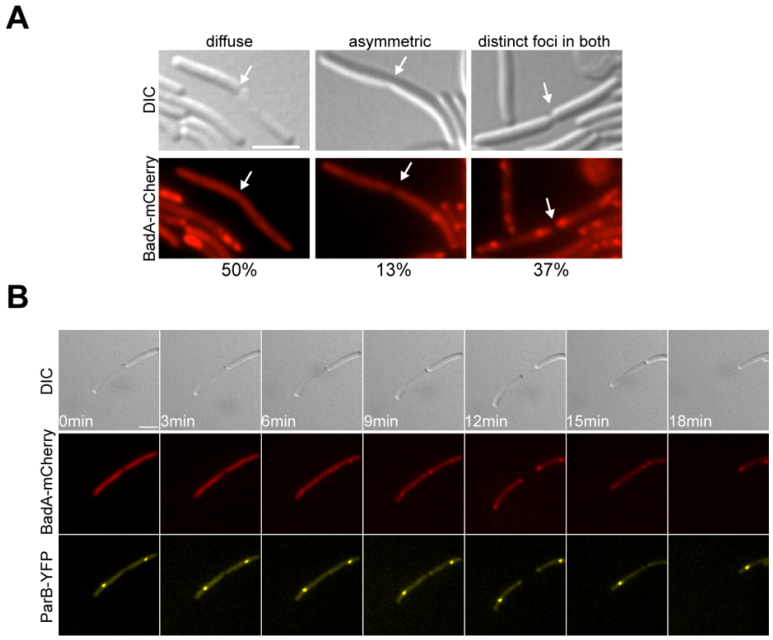

Figure 2.25: Dynamic localization of BadA during cell division. (A) Localization patterns of BadA-mCherry in predivisional cells. Cells of strain LL116 (*badA::badA-mCherry*) was grown in CTT medium. For quantification, in total 54 predivisional cells were analyzed. (B) Time-lapse analysis of BadA and ParB localization in predivisional cells. Cells of strain LL118 (*badA::badA-mCherry* P_{parB}*-parB-yfp*) was grown in CTT and visualized by DIC and fluorescence microscopy in 3-min time intervals. Scale bar: 3 µm.

2.9 BacP associates with ParB in *E. coli*.

The *in-vivo* localization analysis suggested that BacN-P, BadA and ParAB probably interact with each other either directly or indirectly. To further resolve the interaction network among them, we heterologously expressed these proteins in *E. coli* tagged with different fluorescent proteins to investigate their direct interactions, since bactofilins, ParAB, and BadA are absent from *E. coli*. As mentioned above, despite its aberrant localization, mCherry-BacP is not impaired in its association with its interaction partners. Taking advantage of this fact, we

examined the localization dependence of candidate proteins with mCherry-BacP. To do so, *mCherry-bacP* and *cfp-bacO* were co-expressed under the control of the T7 promoter, while the expression of *eyfp*-fused candidate genes was either driven by the T7 promoter or a tetracycline (tet)-inducible promoter. mCherry-BacP alone formed filament-like structures that extended throughout the cell body, causing a chaining phenotype and growth defects (data not shown). However, when expressing both *mCherry-bacP* and *cfp-bacO*, they colocalize to form patches and short filaments, mostly at cell poles or the mid cell (Figure 2.26A). The patch- or filament-like localization of bactofilins in *E. coli* provided a great advantage to directly examine the interaction with other proteins. Thus, we first synthetically expressed *eyfp* under the control of the tet-inducible promoter, to exclude the possibility of a non-specific association. Indeed, eYFP remained diffuse in the presence of BacP and BacO (Figure 2.26A). In contrast, the additional expression of *eyfp-bacN* led the colocalization of all three proteins (Figure 2.26B). These data suggest that BacP acts as the core of the BacN-P complex, which agrees with its most dominant phenotypes in the previous experiments.

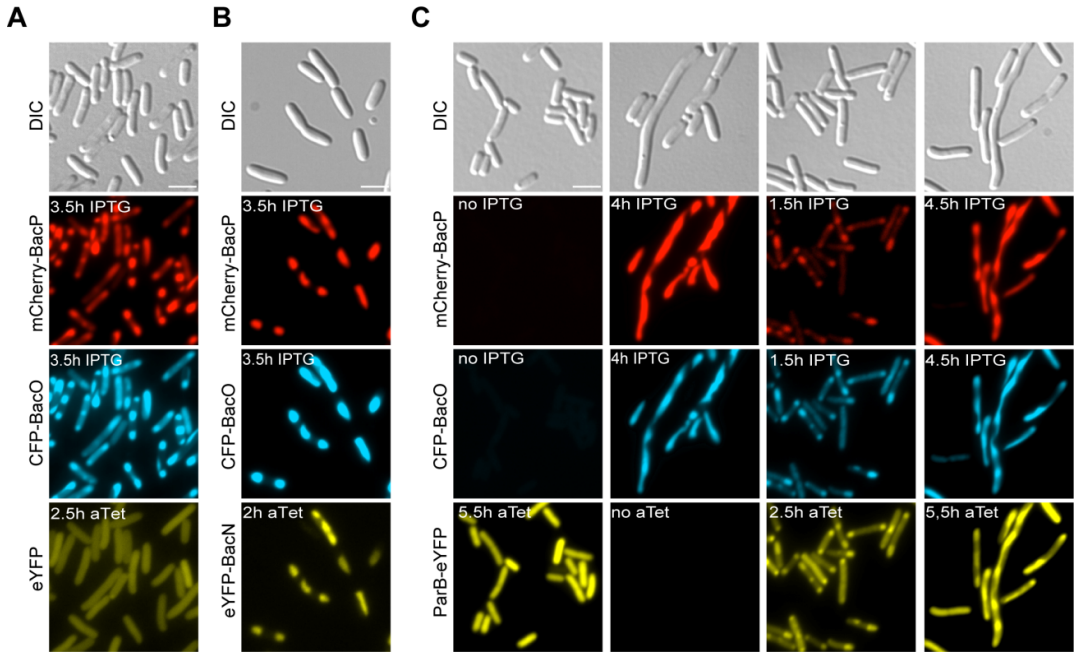

Figure 2.26: Bactofilins colocalize with ParB when heterologously expressed in *E. coli*. (A) Diffuse localization of eYFP in the presence of mCherry-BacP and CFP-BacO in *E. coli*. Cells of *E. coli* Rosetta™(DE3)pLysS bearing both plasmid pLL54 (P_{T7}-*mCherry-bacP* P_{T7}-*cfp-bacO*) and plasmid pLL61 (P_{tet}-*eyfp*) were grown in LB medium to exponential phase. Expression of *mCherry-bacP* and *cfp-bacO* was induced with 0.5 mM IPTG, while the production of eYFP was induced with 0.2 µg/ml anhydrotetracycline. Induction time was indicated in individual panels. (B) Colocalization of mCherry-BacP, CFP-BacO and eYFP-BacN in *E. coli*. Cells of *E. coli* Rosetta™(DE3)pLysS bearing both plasmid pLL54 (P_{T7}-*mCherry-bacP* P_{T7}-*cfp-bacO*) and plasmid pPS20 (P_{tet}-*eyfp-bacN*) were grown in LB medium to exponential phase. Expression of the target genes under the T7 or tet-inducible promoters was induced as described in panel A. (C) Colocalization of mCherry-BacP, CFP-BacO and ParB-eYFP in *E. coli*. Cells of *E. coli* Rosetta™(DE3)pLysS bearing both plasmid pLL54 (P_{T7}-*mCherry-bacP* P_{T7}-*cfp-bacO*) and plasmid pLL52 (P_{tet}-*parB-eyfp*) were grown in LB medium to exponential phase. Expression of target genes under the T7 or tet-inducible promoters was induced as described in panel A. Scale bar: 3 µm.

Using the same co-expression strategy, we expressed *parB-eyfp* under the control of the tet-inducible promoter together with *mCherry-bacP* and *cfp-bacO* expressed from the T7

promoter. In the absence of the two bactofilins, ParB-eYFP fluorescence filled the entire *E. coli* cells. In the presence of mCherry-BacP and CFP-BacO, by contrast, it colocalized with the bactofilin patches (Figure 2.26C).

We further asked if the non-structural C-terminal region of BacP was crucial for the interaction between ParB and BacP. To address this question, we co-expressed ParB-eYFP with a mCherry-tagged truncated form of BacP lacking the long C-terminal region extention ($BacP_{\Delta aa123\text{-}240}$) heterologously in *E. coli*. mCherry-$BacP_{\Delta aa123\text{-}240}$ was still able to form filaments; however, it failed to extend the filament-like structure to the cell poles (Figure 2.27A). At the same time, ParB was no longer able to interact with BacP although full-length BacP alone is able to recruit ParB (Figure 2.27A). The association between ParB and BacP turned out to be species-specific. eYFP fused *Caulobacter* ParB (ccParB-eYFP) was excluded from the bactofilin filaments when co-expressed with both *mCherry-bacP* and *cfp-bacO* (Figure 2.27B). Since the chromosomes were excluded by bactofilin filaments, ccParB probably associated with nucleoids, therefore were exclude from bactofilins (Figure 2.27B).

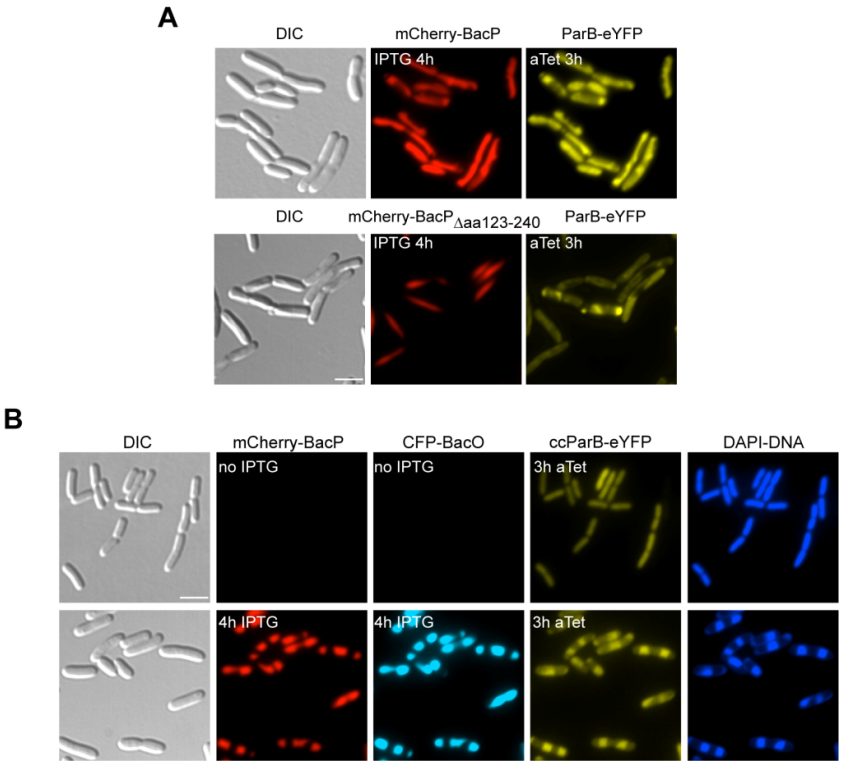

Figure 2.27: Specificity of the BacP-ParB interaction. (A) BacP lacking its C-terminal extension no longer associates with ParB in *E. coli*. Cells of *E. coli* Rosetta™(DE3)pLysS bearing plasmid pLL52 (P_{tet}-*parB-eyfp*) along with either pLL48 (P_{T7}-*mCherry-bacP*) or pLL60 (P_{T7}-*mCherry-bacP*$_{\Delta aa123\text{-}240}$) were grown in LB medium to exponential phase. Expression of *mCherry-bacP* or *mCherry-BacP*$_{\Delta aa123\text{-}240}$ was induced with 0.5 mM IPTG, whereas the production of ParB-eYFP was induced by 0.2-1 µg/ml anhydrotetracycline. (B) BacP and BacO does not colocalize with ccParB in *E. coli*. Cells of *E. coli* Rosetta™(DE3)pLysS bearing both plasmid pLL54 (P_{T7}-*mCherry-bacP* P_{T7}-*cfp-bacO*) and plasmid pLL65 (P_{tet}-*ccparB-eyfp*) were grown in LB medium to exponential phase. Expression of mCherry-BacP and CFP-BacO was induced with 0.5 mM IPTG, while the production of ccParB-eYFP was induced by 0.2 µg/ml anhydrotetracycline. Nucleoids were visualized by DAPI staining. Scale bar: 3 µm.

2.10 Bactofilins associate with BadA, but not ParA directly.

In *M. xanthus*, we observed that BacN-P, ParA and BadA exhibit very similar localization pattern, and the altered localization of BacN-P always leads to effects on the localization of ParA and BadA. To test if BacN-P interacts with ParA, we also co-expressed *parA-eyfp* with *mCherry-bacP* and *cfp-bacO*, and observed no colocalization. Instead, ParA-eYFP was excluded from the bactofilin patches, possibly due to non-specific binding to chromosomal DNA (Figure 2.28A). However, when BadA-eYFP was produced in the presence of mCherry-BacP and CFP-BacO, it colocalized with the two proteins, indicating that BadA may directly interact with BacN-P (Figure 2.28B). This interaction is also observed in the absence of the unstructured N-terminal region of BadA (Figure 2.28B).

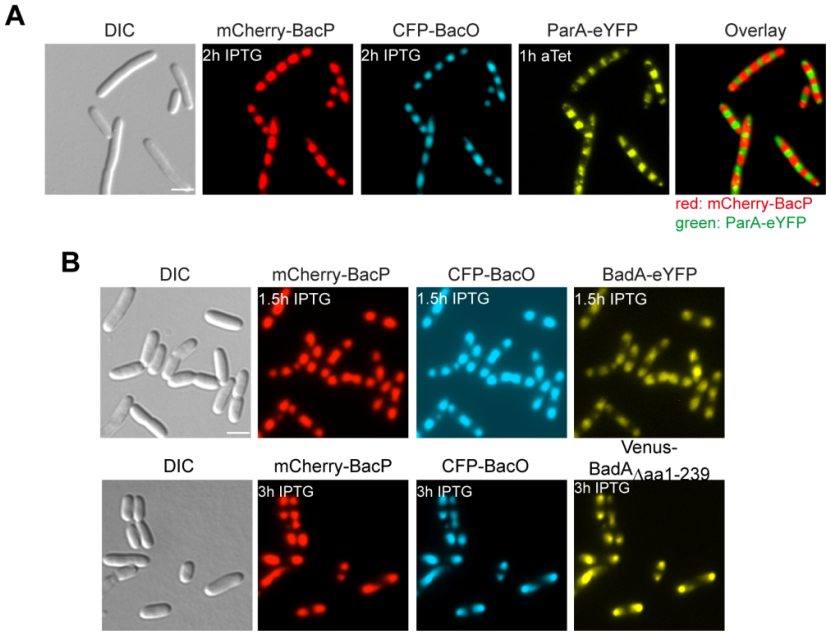

Figure 2.28: Bactofilins colocalize with BadA, but not ParA when heterologously expressed in *E. coli*. (A) ParA is excluded from bactofilins in *E. coli*. Cells of *E. coli* Rosetta™(DE3)pLysS bearing both plasmid pLL54 (P_{T7}-*mCherry-bacP* P_{T7}-*cfp-bacO*) and plasmid pLL86 (P_{tet}-*parA-eyfp*) were grown in LB medium to exponential phase. Expression of the target genes under T7 or tet-inducible promoters was induced as described in Figure 2.27A. (B) Colocalization of mCherry-BacP, CFP-BacO and BadA-eYFP in *E. coli*. Upper panel: Cells of *E. coli* BL21(DE3) bearing both plasmid pLL54 (P_{T7}-*mCherry-bacP* P_{T7}-*cfp-bacO*) and plasmid pLL101 (P_{T7}-*badA-eyfp*) were grown in LB medium to exponential phase. Expression was induced with 0.5 mM IPTG. Lower panel: Cells of *E. coli* BL21(DE3) bearing both plasmid pLL54 (P_{T7}-*mCherry-bacP* P_{T7}-*cfp-bacO*) and plasmid pLL120 (P_{T7}-*venus-badA*$_{\Delta aa1-239}$) were grown in LB medium to exponential phase. Expression was induced with 0.5 mM IPTG. Scale bar: 3 µm.

These observations raised the possibility that ParA was indirectly recruited to the bipolar BacN-P bipolar filaments by BadA during chromosome segregation in *M. xanthus*. To test this hypothesis, we co-expressed *badA-eyfp* under the control of the T7 promoter and *parA-mCherry*, which was under the tet-inducible promoter. As shown, BadA-eYFP colocalized with condensed nucleoid structures (Figure 2.29A). Upon induction, ParA-mCherry was able to colocalize with BadA-eYFP on the nucleoids (Figure 2.29B). However, it was not clear if this

association was due to direct protein-protein interaction or indirectly through the known non-specific DNA binding activity of ParA. To differentiate between these two possibilities, we expressed mCherry-tagged ParA varients (ParA^{R209A} or ParA^{R238E}) whose DNA binding activity was largely abolished due to the mutation of two conserved arginine residues [60]. To induce cell filamentation, cells were pre-treated with cephalexin to inhibit cell division. Nucleoids became condensed after treatment of chloramphenicol before imaging. Control experiments showed that wild-type ParA has non-specific DNA binding, as indicated by the association of ParA-mCherry with condensed nucleoids in filamentous cells; by contrast, both of the two mutant derivatives showed the diffuse distribution despite the condensation of nucleoid structure (Figure 2.29C). However, the colocalization between these two ParA variants and BadA was retained (Figure 2.29B), indicating a possible direct contact between ParA and BadA.

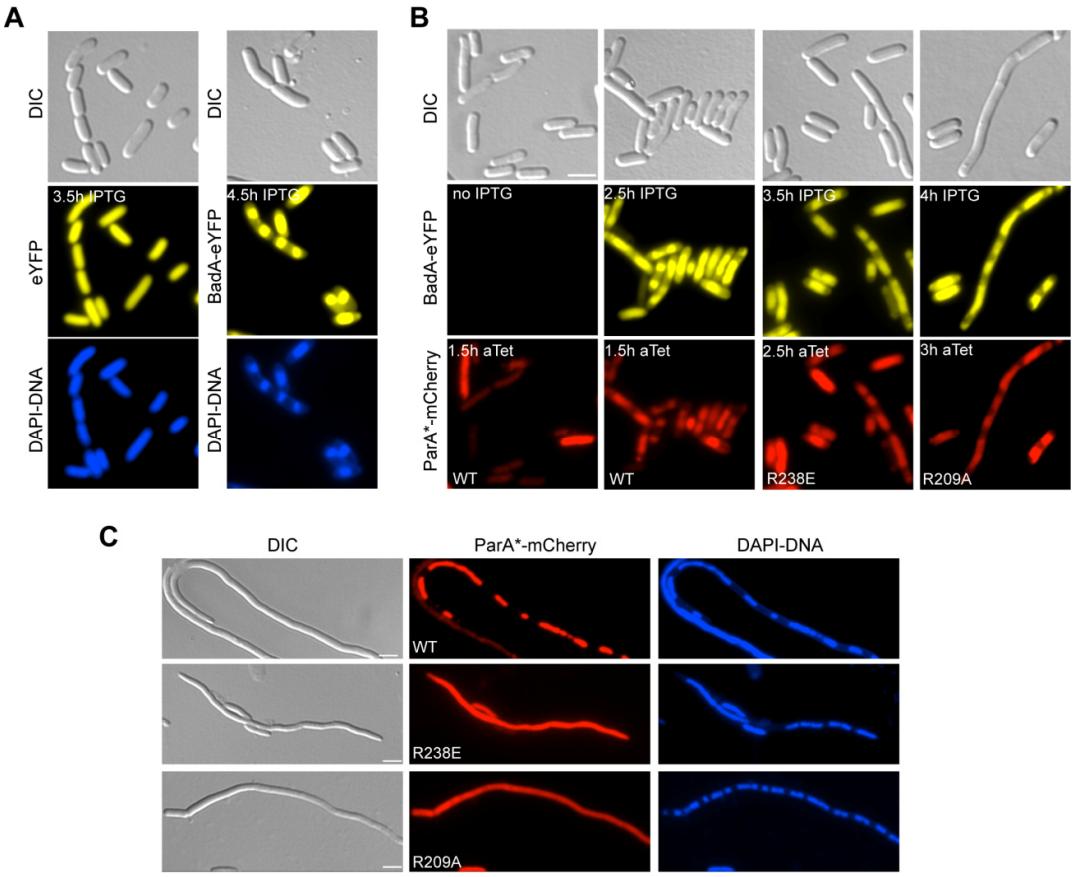

Figure 2.29: Direct interaction between BadA and ParA in *E. coli*. (A) Colocalization of BadA-eYFP and condensed nucleoids in *E. coli*. Cells of *E. coli* BL21(DE3) bearing plasmid pLL137 (P_{T7}-*eyfp*), or alternatively, pLL101(P_{T7}-*badA-eyfp*) were grown in LB medium to exponential phase. Expression was induced with 0.5 mM IPTG. DNA was stained by DAPI. (B) Colocalization of BadA-eYFP and ParA-mCherry in *E. coli*. Cells of *E. coli* BL21(DE3) bearing plasmid pLL101 (P_{T7}-*badA-eyfp*), along with plasmid pLL100 (P_{tet}-*parA-mCherry*), pLL122 (P_{tet}-*parA*$_{R238E}$-*mCherry*), or pLL124 (P_{tet}-*parA*$_{R209A}$-*mCherry*) were grown in LB medium to exponential phase. Expression of the target genes under the T7 or tet-inducible promoters was induced as described in Figure 2.26A. (C) Point mutations of two conserved arginine residues in ParA abolish its DNA binding activity. Cells of *E. coli* BL21 (DE3) bearing plasmid pLL100 (P_{tet}-*parA-mCherry*), pLL122 (P_{tet}-*parA*$_{R238E}$-*mCherry*) or pLL124 (P_{tet}-*parA*$_{R209A}$-*mCherry*) were grown in LB medium and treated with cephalexin for 3h to induce cell filamentation. Protein production was induced with 0.2 µg/ml anhydrotetracycline. Before visualization, cells were incubated for 20 min with 20 µg/ml chloramphenicol to achieve chromosome condensation. Nucleoids were stained by DAPI for visualization. Scale bar: 3 µm.

2.11 BacP closely associates with ParB in *M. xanthus*.

Th interaction between BacN-P and ParB have been strongly suggested by the colocalization either in *M. xanthus* or in *E. coli*. To further verify the interaction between BacP and ParB, we performed pull-down assays on mixtures of *M. xanthus* DK1622 lysates and purified StrepII-ParB. StrepII-ParB along with associated proteins was affinity-purified from the lysates. Immunoblot analysis using an α-BacP antibody showed that BacP attached to StrepII-ParB (Figure 2.30), suggesting a close association between BacP and ParB in *M. xanthus*. Together, the pull-down assay, the colocalization in the heterologous *E. coli* system, and the colocalization in the native *M. xanthus* environment, strongly suggest that BacP is closely associated with the chromosome partitioning protein ParB in *M. xanthus*.

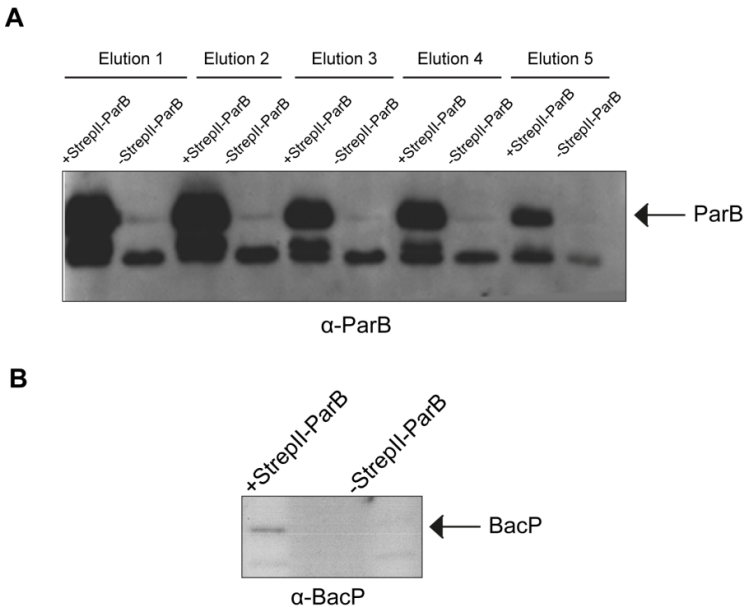

Figure 2.30: Biochemical interaction between ParB and BacP. (A) Co-immunoprecipitation of BacP with ParB in pull-down assays. Cell lysates from strain DK1622 were mixed with purified StrepII-ParB. Cell lysates not containing StrepII-ParB were used as a control. StrepII-ParB and interacting proteins were precipitated using Strep-Tactin® Superflow Plus resin. Eluted proteins were probed with an α-ParB antibody (1:5000) by immunoblot analysis. (B) BacP co-elutes with StrepII-ParB. The eluted proteins shown in panel A were first concentrated with trichloroacetic acid and then probed with an α-BacP antibody (1:1000).

2.12 BadA interacts with both BacP and BacO in *M. xanthus*.

The *in-vivo* analysis indicated that BadA probably interacts with BacN-P. To further test this hypothesis, we performed pull-down assays using BadA as the 'bait'. We first attempted to purify the full-length BadA fused to either His_6 tag or a larger tag like MBP. However, the full-length BadA protein appeared to be unstable (data not shown). Therefore, we alternatively purified the ParB-like domain followed by the C-terminal region, fused with the His_6-tag. This truncated version of BadA was still able to colocalize with BacP and BacO when heterologously expressed in *E. coli* (Figure 2.28B). Thus, we used purified His_6-$BadA_{\Delta aa1-239}$ mixed with a cell

extract from DK1622 for affinity purification experiments (Figure 2.31). Proteins specifically bound to His_6-$BadA_{\Delta aa1-239}$ were isolated using Ni-NTA affinity beads. Immunoblots analysis of the elutions showed that both BacP and BacO co-eluted with His_6-$BadA_{\Delta aa1-239}$ (Figure 2.31), demonstrating a close association between BadA, BacP and BacO. The interaction of BadA with BacP and BacO was also confirmed by MALDI-MS analysis of the eluted proteins (data not shown).

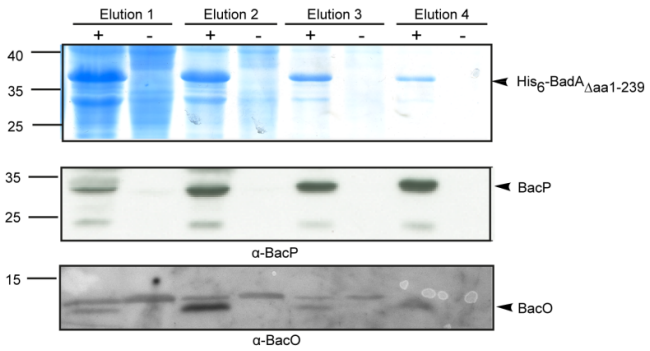

Figure 2.31: Co-immunoprecipitation of BacP and BacO with BadA in pull-down assays. Cell lysates from strain DK1622 were mixed with purified His_6-$BadA_{\Delta aa1-239}$. The protein complexes were precipitated using Ni-NTA resin. Elution fractions were subjected for SDS-PAGE, and analyzed by immunoblots using the α-BacP (1:1000) and α-BacO (1:10000) antibodies, respectively. Cell lysates not mixed with His_6-$BadA_{\Delta aa1-239}$ were used as control.

2.13 BadA may be a DNA-binding protein.

BadA is predicted to have a ParB-like nuclease containing a putative helix-turn-helix DNA binding motif; moreover, in *E. coli*, it was shown to colocalize with the nucleoid. These indicate that BadA may exhibit DNA-binding activity. To test this possibility, we performed the electrophoretic mobility shift assay (EMSA) analyzing the interaction of the nuclease-like domain (His_6-$BadA_{\Delta aa1-239}$) with non-specific plasmid DNA (pMCS-2). In this assay, a significant shift was observed at relatively high protein concentrations (≥20 µM) of His_6-$BadA_{\Delta aa1-239}$ protein; this effect was not observed when BSA was used as a control at the same concentration (Figure 2.32).

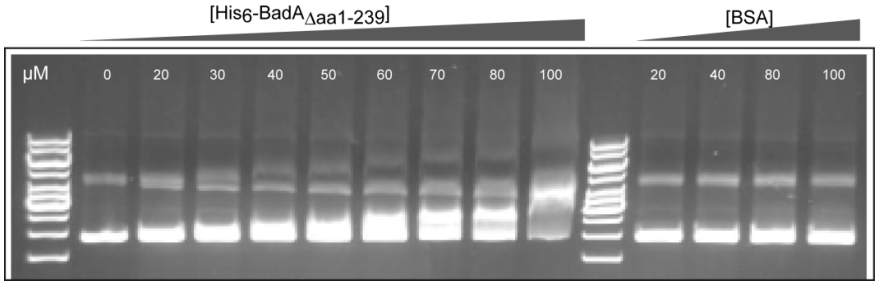

Figure 2.32: $BadA_{\Delta aa1-239}$ shows weak non-specific DNA binding activity. Interaction with DNA was detected by EMSA. Plasmid DNA (pMCS-2, 20 nM) was incubated with 0, 10, 20, 40, 60, 80, and 100 µM of purified His_6-$BadA_{\Delta aa1-239}$, or, alternatively, with 20, 40, 80, and 100 µM of BSA as negative control. Complexes were resolved in a 1% agarose gel and visualized by ethidium bromide staining.

Therefore, it appears that this truncated BadA protein has the ability to interact non-specifically with DNA. However, it remains unclear whether specific binding sites exist on the *M. xanthus* chromosome.

2.14 The absence of BacN-P and BadA leads to shorter nucleoid lengths.

Our results have shown that BacN-P/BadA system is crucial for the proper localization of ParA and ParB. However, in the absence of BacN-P and BadA, chromosomes were still able to segregate, despite the mislocalization of ParA and ParB; however, the nucleoid often appeared to be significantly shorter in the mutants, compared with wild-type cells (Figure 2.33A). In the wild type (DK1622), the average length of the nucleoids was 51% of the cell length, while in the absence of *bacN-P* or *badA* there was a 10% and 5% decrease, respectively (Figure 2.33B). The combined deletion of both *bacN-P* and *badA* led to the most significant decrease in nucleoid length. All of the mutants exhibited significant differences in nucleoid lengths (*t*-test, $p<0.001$), with the exception that there was no significant difference between the Δ*bacP* and Δ*bacN-P* mutants (*t*-test, $p=0.927$). This confirmed again that BacP plays a central role in the function of BacN-P filaments.

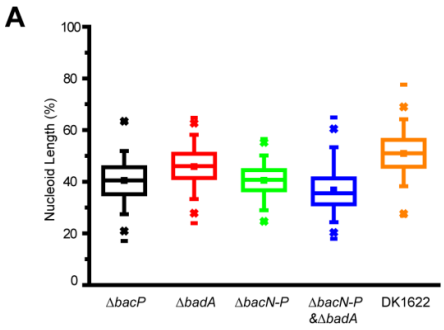

B

Strains	nucleoid length/cell length (%)
DK1622 (WT)	50.929±8.079
ΔbacP	40.470±7.807
ΔbadA	45.867±7.365
ΔbacN-P	40.538±6.074
ΔbacN-PΔbadA	36.741±8.416

Figure 2.33: Nucleoids are shorter in the absence of BacN-P. (A) Significantly shorter length of nucleoids in the absence of BacN-P and BadA. Cells carrying the indicated mutations were grown in CTT medium to exponential phase and stained with DAPI to visualize the nucleoids. Cell lengths and nucleoid lengths were measured in Metamorph. In Y-axis, nucleoid lengths were normalized to cell lengths. The total of 173, 150, 180, 201, and 258 cells were analyzed for strains LL001 (*ΔbacP*), LL101 (*ΔbadA*), MT295 (*ΔbacN-P*), LL174 (*ΔbacN-P ΔbadA*), and DK1622, respectively. (B) Summary of the average of the relative nucleoid length in different strains shown in panel A.

2.15 Bactofilins are involved in diverse cellular processes.

Our data imply that BacN-P build a scaffolding structure at the cell pole for the positioning of polar proteins, such as ParA and ParB. However, phenotypic analysis of mutant cells also revealed the involvement of bactofilins in other cellular processes. First of all, we examined the behavior of cell movement in the absence of individual bactofilins by performing motility assays. On 1.5% agar plates, cells prefer to move by means of A-motility, while on 0.5% agar plates, S-motility is more dominant [61]. On 1.5% agar plates, we observed no difference in the

shape of the colony edges between the wild type and bactofilin mutants, indicating that bactofilins are not involved in A-motility (data not shown). On 0.5% agar, wild-type cells formed colonies with flare-like protrusions after incubation for 24 h, while cells of S-motility-defective control strains formed smooth edges with no flares (Figure 2.34). The absence of BacP led to a dramatic impairment of S-motility, as indicated by much shorter flares compared to the wild type after 24 h incubation (Figure 2.34). When lacking BacO, BacN or BacM, by contrast, cells exhibit normal S-motility (Figure 2.34). Therefore, BacP is important for S-motility. Bulyha *et. al.* further revealed that the bipolar filamentous structure of BacP is required for the subpolar localization of SofG, which is an important cell polarity regulator [16] (see introduction 1.2.3).

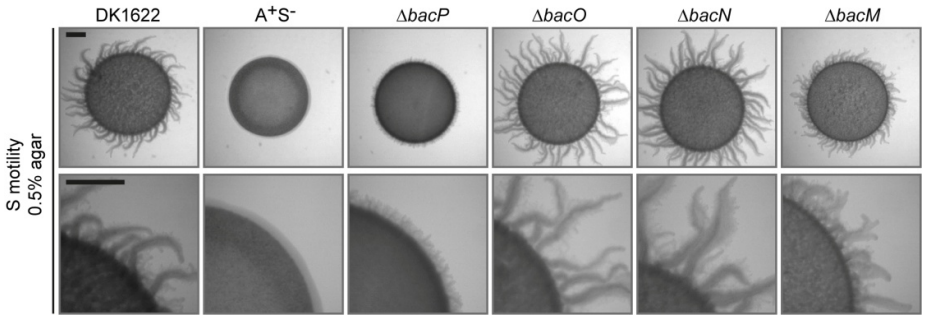

Figure 2.34: S-motility is impaired in the absence of BacP. Cells of strains DK1622 (wild type), DK1300 (*ΔsglG*; A^+S^-), LL001 (*ΔbacP*), LL002 (*ΔbacO*), and LL003 (*ΔbacN*) and MT300 (*ΔbacM*) were grown in CTT medium, spotted onto 0.5% CTT agar plates and incubated for 24 h. The flare-like structure reflects the movement by means of social gliding. Scale bar: 1 mm.

Interestingly, the *ΔbacP* mutant exhibits a striking developmental phenotype. When starving on TPM agar, wild-type cells typically start aggregating into fruiting bodies within 24 h, which darkened when incubated longer (Figure 2.35). A *csgA* mutant in which the signaling pathway for the induction of fruiting body development is disrupted was served as the negative control, and was unable to form fruiting bodies [76, 77, 93]. In the absence of BacP, cells completely failed to aggregate to fruiting bodies, while lacking either of the other bactofilins had no obvious effect on development (Figure 2.35). However, it remains unclear if the effect of BacP on development is related to its function on the positioning of SofG.

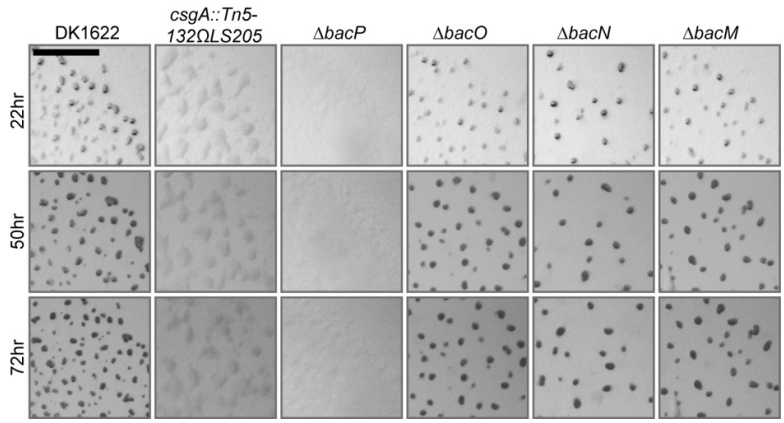

Figure 2.35: Cells lacking BacP are not able to aggregate and form fruiting bodies during nutrient starvation. Cells of strains DK1622, DK5208 (*csgA*::Tn5-132ΩLS205), LL001 (*ΔbacP*), LL002 (*ΔbacO*), and LL003 (*ΔbacN*) and MT300 (*ΔbacM*) were grown in CTT medium and incubated on TPM agar for starvation at 32 ºC for 22 h, 50 h, and 72 h. Scale bar: 1 mm.

Unlike BacN-P, BacM is not involved in chromosome segregation, motility or development. Instead, it plays a role in cell morphogenesis in *M. xanthus*. In the absence of BacM, cells often formed irregular kinks or curls, which appeared to be more pronounced in filamentous cells (Figure 2.36). To achieve cell filamentation, exponentially growing cells were incubated in the presence of the cell division inhibitor cephalexin and spotted onto a hard surface (glass slides) for observation. Wild-type cells were straight and filamentous, while a number of cells lacking BacM formed kinks or curls. Strikingly, some filamentous cells even exhibited helical 'telephone cable'-like shapes (Figure 2.36). The Δ*bacMNOP* mutant exhibited a similar phenotype as the Δ*bacM* mutant. In contrast, cells lacking BacN-P show no obvious defect in cell shape (Figure 2.36). These data are consistent with a previously published study [78]. However, the mechanism underlying it requires further investigation.

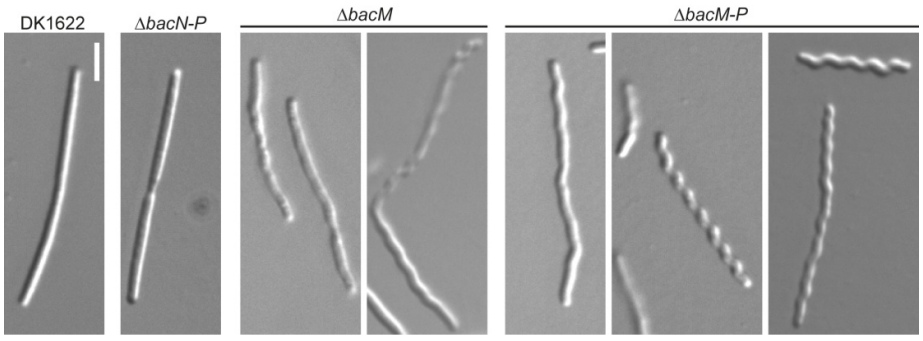

Figure 2.36: BacM is required for proper cell shape maintenance. Cells of strains DK1622, MT295 (Δ*bacN-P*), MT300 (Δ*bacM*) and JK328 (Δ*bacM-P*) were grown in CTT medium to exponential phase and treated with 100 µM cephalexin for 8 hrs before imaging. Scale bar: 3 µm.

Taken together, bactofilins are involved in several distinct processes in *M. xanthus*, including chromosome segregation, cell movement, and cell morphogenesis during vegetative growth, as well as fruiting body formation during nutrient starvation. These results underscore the high degree of functional diversification of this class of cytoskeletal proteins in bacteria.

3 DISCUSSION

3.1 BacN-P: polar scaffolds for the chromosome segregation machinery

Bactofilins are a group of bacteria-specific cytoskeletal proteins that are widely distributed among the bacterial phylum, with potentially high diversity of functionality across species. In this work, we focused on the functional analysis of bactofilin homologs in *M. xanthus*. The genomic context of bactofilins revealed a possible link with the DNA partitioning components ParA and ParB, whose genes are encoded upstream of *bacM*. In wild-type cells, ParA normally forms bipolar patch-like structures, with ParB localizing to the subpolar ends of these patches. Surprisingly, in this work, we demonstrated that BacM is not involved in either the localization or function of these two proteins. Instead, we found that ParA and ParB both mislocalize in the absence of BacN-P. ParA is largely diffuse without BacN-P. In addition, the loss of BacN-P leads to a significantly larger distance of ParB foci from the nearest cell pole in a majority of the cells in a population. Investigating the contribution of each single bactofilin to ParAB localization, we identified the leading role of BacP in this process. BacO also has a significant, albeit lower impact, whereas BacN only shows a minor contribution. The aberrant localization of ParA and ParB influences chromosome segregation, which leads to a significantly shorter nucleoid length. However, despite the significant impact on ParAB localization, cell growth is not obviously affected and chromosome segregation can still take place. Another line of evidence supporting the link between BacN-P and chromosome segregation comes from the analysis a dominant-negative form of BacP. When cells express *bacP-HA*, cell growth was greatly arrested, due to the severe chromosome replication and segregation defect, providing more evidence for the importance of BacN-P in ParAB function. The mechanism underlying this severe defect requires further investigation. However, one can speculate that the unipolar long filaments formed by BacP may retain ParA at one cell pole and block ParB segregation.

Collectively, this work demonstrates that BacN-P is essential for the precise subcellular localization of chromosome segregation components, with the mislocalization of ParAB probably leading to chromosome organization or segregation defects. However, the absence of bactofilins does not completely abolish chromosome segregation. Therefore, we hypothesize that there may be other bactofilin-independent mechanisms, which together with bactofilins, ensure the robustness of chromosome segregation.

In this work we also showed that BacP, BacO, and BacN all form short bipolar filamentous structures in *M. xanthus*. We also observed a direct interaction between the different bactofilin paralogs both *in vivo* and *in vitro*. It is therefore highly possible that BacN-P copolymerize into these bipolar structures. Moreover, each protein contributes to the formation of filaments to different extents. For instance, in the absence of BacO, the localization of BacP was affected, but BacP was still able to form polar structures; in contrast, there was no significant on BacP in the absence of BacN (data not shown). On the other hand, the localization of BacO was strongly affected by the disruption of BacP (data not shown). These results are consistent with the

functional dominance of different bactofilins. Furthermore, consistent with the function on ParAB positioning, we showed that ParB mostly localizes to the subpolar end of bactofilin structures, indicating a tight association between ParB and BacN-P. It is technically not possible to colocalize ParA and BacN-P by far; however, they show strikingly similar localization pattern *in vivo*, suggesting a correlation of their subcellular localization.

The dynamics of BacN-P bipolar structures remain unclear. However, it was observed that the length of the filament varies; moreover, in longer cells, there is often an accumulation near the mid-cell position. In addition, as ParB normally localizes to the end of a BacN-P structure, one can speculate that the length of the filament may correlate to the dynamic movement of ParB. Moreover, despite the loss of function, mCherry-tagged BacN-P nevertheless are highly dynamic, supported by the fast recovery after photobleaching. However, behavior of the wild-type proteins still needs to be clarified.

3.2 BadA: a key player in BacN-P mediated ParAB localization

In this work, a bactofilin-associated protein, BadA, was revealed to participate in ParA and ParB localization. This protein contains a ParB-like nuclease domain, with low homology to ParB. The loss of BadA leads to similar ParA and ParB mislocalization as that of BacN-P. BadA is often found to colocalize with BacN-P, as well as with ParA. When BacN-P dramatically relocalize as an extended filaments along mid-cell after fusion with fluorescent proteins, the majority of BadA still associates with BacN-P, with additional accumulation at the cell pole. Importantly, in the absence of BadA, BacN-P mislocalize and fail to form filament-like structures, suggesting a role of BadA in BacN-P polymerization. However, it is not conclusive if this regulation is an effect on the assembly or dynamics of BacN-P. More strikingly, we also showed that BacN-P, in particular BacP, turns out to be essential for BadA localization.

Interestingly, at the C-terminal region of BadA, there is a potential HTH motif, which is usually an indication of DNA-binding activity. When expressed heterologously in *E. coli*, BadA was shown to colocalize with condensed nucleoids. Furthermore, the purified His_6-$BadA_{\Delta aa1-239}$ protein showed a weak non-specific DNA binding activity *in vitro*. However, it is possible that BadA binds to specific sequences on the *M. xanthus* chromosome, which requires further clarification. So far, the precise function of BadA and the underlying mechanisms are still unclear.

Interestingly, the delocalization of BadA shortly before cell division taking place suggested a possibility that BadA may play a role in the coordination of chromosome segregation and cytokinesis. Close coordination of these processes has been shown to be essential in many bacteria. For example, in *B. subtilis*, a nucleoid occlusion protein, Noc, originally identified as a ParB-like protein, associates with chromosomes to prevent cell division taking place over the nucleoid [124, 150, 151]. Noc specifically binds to a concensus sequence named NBS (Noc-binding sequence), which is scattered over the chromosome, except near the terminal region [151]. It was proposed that at the end of the chromosome replication, Noc is absent from

mid-cell where the *ter* region is located; once DNA replication and segregation are accomplished, Z-ring assembly occurs at this region [150, 151]. The precise function of BadA is still under investigation; however, our data suggest that it is likely to have some affinity for the nucleoid.

3.3 The interaction network: BacN-P, BadA with ParAB

In *M. xanthus*, we showed that BacN-P all exhibit bipolar localization. ParB localizes to the subpolar ends of BacN-P filaments, while BadA and ParA exhibit similar bipolar localization pattern as BacN-P, which suggested a possible interaction among these proteins. However, if ParAB and BadA directly interact with BacN-P remain unclear. Therefore, we extensively explored the interaction network among BacN-P, ParAB and BadA using the heterologous expression system in *E. coli* as well as biochemical approaches. First of all, the interaction between BacN and BacP was supported by co-immunoprecipitation experiments. Furthermore, BacN-P associate with each other when expressed in *E. coli*. Therefore, BacN-P most likely copolymerize into a complex. The direct interaction between BacN-P and ParB was also observed. ParB always colocalizes with fluorescence-tagged BacP and BacO patches when heterologously expressed in *E. coli*. In particular, the C-terminal extension of BacP seems to be crucial for the interaction in *E. coli*. The close association between ParB and BacP was also supported by pull-down assays in *M. xanthus*. Similarly, we have also shown that BadA interacts with BacN-P directly. In *E. coli*, BadA always colocalizes with bactofilin patches, even in the absence of the N-terminal region. The interaction between BadA and BacP was further verified by performing pull-down assays with His_6-$BadA_{\Delta aa1\text{-}239}$ as bait proteins. In contrast, the direct contact was never observed between BacP and ParA by either means of *E. coli* colocalization or the biochemical approaches. However, when coexpressed in *E. coli*, ParA associates with BadA in a DNA-binding-independent manner. Therefore, rather than interacting directly, ParA is more likely to connect with BacN-P filaments via BadA. Taken together, we concluded that both BadA and ParB directly associates with BacP. We also speculated that BadA is the possible link between BacN-P and ParA.

3.4 BacN-P: polar landmarks in *M. xanthus*

As mentioned, it has been shown that BacP also mediates the localization of other polar proteins such as SofG, which is a small GTPase important for cell polarity in *M. xanthus* [16]. The involvement of BacP in cell polarity results in a significant decrease of S-motility. Here, we further demonstrated that BacN-P filaments are crucial for the precise localization of a set of proteins that are key components for another distinct cellular event, chromosome segregation. Therefore, the bipolar filaments by BacN-P probably serve as general scaffolding structures at the cell pole for recruiting multiple proteins and as a result participate in various cellular processes. Despite the lack of sequence similarity, BacN-P share many features with other polar landmark proteins shown to be important for bacterial cell pole organization in other species, such as PopZ: (i) both of them form polymeric or multimeric structures at the cell pole and

anchor polar proteins; (ii) both of them can polymerize or multimerize *in vitro*; (iii) it was shown that the region where accumulation of PopZ takes place is a ribosome/DNA free zone; in *M. xanthus*, chromosomal DNA does not extend to the very cell pole; instead, after chromosome segregation, there is a region at each cell pole that ranging from 5-15% of the cell length that is DNA-free. This region seems to overlay with BacN-P filaments. Moreover, ParB is usually the indicator where the origins of replication are located. The fact that ParB usually localizes at the tip of BacN-P filaments strongly suggests that the DNA-free space in *M. xanthus* cells is covered by BacN-P filaments. These observations indicate a potential connection between BacN-P and the distribution of DNA contents. Therefore, we proposed that in *M. xanthus*, BacN-P forms scaffolding structures at the cell poles and plays important roles in cell pole organization by anchoring different proteins such as SofG, ParB and BadA, similar to PopZ in *C. crescentus* (Figure 3.1). In the absence of BacN-P, ParB can no longer be anchored to the proper subcellular position, while BadA completely diffuses in the cell, which leads to ParA mislocalization (Figure 3.1).

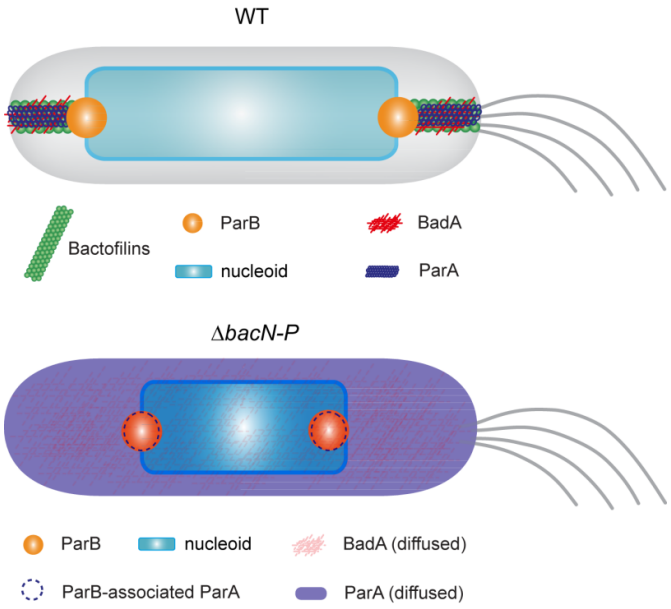

Figure 3.1: Schematic model of BacN-P filaments and stabilization of chromosome segregation in *M. xanthus*. In this model, BacN-P build bipolar scaffolding structure by polymerization, and recruit polar proteins such as ParB and BadA to the precise localization at subpolar regions. BadA then recruits ParA to cell poles. In the absence of BacN-P, ParB mislocalizes; while BadA completely diffuses in the cells. As a result, ParA fails to be recruited to the cell pole. Furthermore, nucleoid space is significantly smaller than that in wild type. However, the underlying mechanism is not known.

3.5 Conclusions and remarks

In this work we describe a polar landmark complex consisting of three bactofilin homologs, BacN, BacO and BacP, in *M. xanthus*. We showed that BacN-P formed bipolar filaments to directly or indirectly recruit proteins such as ParA and ParB. Our results imply a direct association between ParB and BacP both *in vivo* and *in vitro*; however, this direct contact has never been observed between BacP and ParA. Instead, it seems that it requires a bactofilin-

associated protein BadA to mediate ParA localization. We discovered that BadA acts in the same mechanism with BacN-P for stabilizing chromosome segregation. We further showed that BacN-P and BadA are required for the proper localization of each other. BadA and BacN-P also closely interact in *M. xanthus*. We hypothesized that ParA is more likely to connect with BacN-P filaments via BadA. Taken all together, BacN-P together with BadA is responsible for the precise subcellular positioning of chromosome segregation components. BacN-P, with BacP as the core of the complex, build the bipolar scaffolding structure and recruit different sets of protein such as ParAB for chromosome segregation as well as SofG for cell polarity, thereby widely involved in diverse cellular processes in *M. xanthus*.

The mechanism how *M. xanthus* coordinates three bactofilin homologs to accomplish the polar polymerization remains unclear. Our results show that BacP is likely the center of this complex. First of all, we showed that the absence of BacP exhibited the most pronounced defect. Secondly, BacO mislocalizes when BacP is absent (data not shown). In addition, our *E. coli* colocalization studies suggest that BacP directly recruits ParB into bactofilin filaments, while BacO and BacN alone do not (data not shown). Moreover, the unique extended C-terminal region of BacP seems to be crucial for BacP functions. This C-terminal region appears to be essential for the interaction with ParB. However, whether C-terminal region of BacP is indeed directly responsible for these interactions and how BacO and BacN contribute to the mechanism still need to be clarified. Interestingly, in *C. crescentus*, it was proposed that the increase of local concentration of ParA could trigger PopZ accumulation and localization, to ensure proper spatial and temporal regulation of this process [85]. However, how BacN-P polymerization and localization are regulated in *M. xanthus* remains unknown.

Unlike many other cytoskeletal proteins in bacteria, bactofilins exhibit a high degree of conservation as well as frequent gene duplication events, suggesting they are likely playing significant roles in different species. However, as described above, bactofilin homologs often show significant diversity in terms of sequence, localization as well as function among species [58, 78, 82, 113, 129]. Furthermore, this diversity is even apparent within species. For instance, in this work, three bactofilin homologs (BacN-P) were shown to be crucial for proper positioning of ParAB, the two chromosome segregation proteins in *M. xanthus*. Moreover, BacP is also essential for the function of a small GTPase, SofG, which is a polarity factor involved in social motility [16]. BacM, on the other hand, was found to be important for proper *M. xanthus* cell shape maintenance [78]. Collectively, four bactofilin homologs indeed show highly diverse functions in *M. xanthus*. This functional diversity is reflected by the distinct localization patterns. BacN-P is accumulating at both cell poles as filaments, while BacM assembles into helical cable-like structure throughout the cell [78]. However, the molecular determinants responsible for the differences in the functionality of bactofilins remain unclear.

The high diversity of bactofilins, as a class of widespread bacteria-specific cytoskeletal elements, is probably the result of the adaptation of different bacterial species to distinct environments. However, it appears the ability to build scaffolding structures at specific subcellular locations is the general basis why bactofilins are involved in so many distinct cellular processes. For example, this work revealed a new mechanism of stabilizing the chromosome segregation machinery in bacteria by bipolar bactofilin scaffolds. Although there is a large subset of bactofilin family proteins are not characterized, based on knowledge collected about bactofilins in several different species so far, it is reasonable to hypothesize that

most bactofilins have evolved from a common ancestor, with a function in cell shape. Later during evolution, they then divided into distinct subgroups with different subcellular localization patterns and functions. This functional diversity is probably determined by different domain architectures, such as long N- or C- terminal extensions. The conservation but high divergence in sequence of bactofilins underscores the significance of this large group of non-canonical cytoskeletal elements in bacteria.

4 MATERIALS AND METHODS

4.1 Materials

4.1.1 General usage of chemicals and enzymes

Unless indicated otherwise, all reagents and enzymes were obtained from Carl-Roth (Germany), Invitrogen (Germany), SIGMA-Aldrich (Germany), GE-Healthcare (Germany), Bioline (Germany), Merck (Germany), Millipore (Germany), Perkin Elmer (Germany), Becton Dickinson (USA), Peqlab (USA), Thermo Scientific (USA), Qiagen (Germany), Expedeon (United Kingdom), Fisher Scientific (Germany), Kobe (Germany), New England Biolabs (NEB, USA), or Fermentas (Canada).

4.1.2 Buffers and solutions

Standard buffers and solutions were prepared as described by [3, 52].

Buffers and solutions used in specific experiments were described in the respective protocols. If needed, buffers and solutions were sterilized by filtration (pore size 0.2 µm or 0.45 µm; Sarstedt, Germany) or by autoclaving at 121 °C for 20 min.

4.1.3 Media

All media were sterilized by autoclaving at 121 °C for 20 min. For solid media, 1.5% (w/v) agar was added to medium prior to autoclaving, while for soft CTT agar, 0.75% (w/v) agar was added to CTT medium. Antibiotics and carbohydrates were filter-sterilized (pore size 0.2 µm or 0.45 µm; Sarstedt, Germany) and added to medium (at ~60 °C). The concentrations of respective antibiotics and carbohydrates are listed in Table 1 and Table 2.

CTT	1% (w/v) Casitone
	10 mM Tris/HCl (pH 7.6)
	1 mM potassium phosphate (pH 7.6)
	8 mM $MgSO_4$
Luria-Bertani (LB)	1% (w/v) Tryptone
	0.5% (w/v) yeast extract
	1% (w/v) NaCl

Super Broth (SB)	3.5% (w/v) Tryptone
	2% (w/v) yeast extract
	0.5% (w/v) NaCl

Table 1. Antibiotics used for *E. coli* and *M. xanthus* in this work.

antibiotic	stock concentration (mg/ml)	Final concentration (µg/ml)			
		E. coli liquid media	*E. coli* solid media	*M. xanthus* liquid media	*M. xanthus* solid media
Ampicilin	100	50	200	-	-
Cephalexin	5	5	-	100 µM	-
Chloramphenicol (in 70% ethanol)	10	20	30	-	-
Gentamicin	10	15	20	-	-
Kanamycin	20	30	50	50	50
Tetracycline	25	15	15	-	-
Oxytetracycline	10	-	-	10	10
Spectinomycin	20	50	100	-	-
Streptomycin	10	30	30	-	-

Table 2. Carbohydrates used for *E. coli* and *M. xanthus* in this work.

carbohydrates	stock concentration (% w/v)	final concentration (% w/v)
glucose	20	0.2
galactose	20	2.5

4.1.4 Oligonucleotides

Oligonucleotides for molecular cloning were designed using Vector NTI Advance™ 11 (Invitrogen, Germany) and synthesized by either Eurofins MWG Operon (Germany) or SIGMA-Aldrich (Germany). The oligonucleotides used in this work are listed in the appendix (Table 7).

4.1.5 *In-silico* plasmid construction

Plasmid design was conducted using Vector NTI Advance™ 11 (Invitrogen, Germany). A complete list of plasmids used in this work can be found in appendix (Table 8).

4.2 Microbiological Methods

4.2.1 Bacterial growth conditions

M. xanthus was grown at 32 ˚C in CTT broth with shaking at 220 rpm, or on CTT agar plates. Antibiotics were added when necessary (Table 1). All *M. xanthus* strains used in this work were derived from the wild-type strain *M. xanthus* DK1622 [74]. Expression of genes under the control of copper-inducible promoter was induced with different concentrations of $CuSO_4$ (≤ 400 μM); while the vanillate-inducible promoter was induced with different concentrations of vanillic acid (≤ 1 mM).

E. coli was grown at 37 ˚C in LB or SB broth with shaking at 220 rpm or on LB-agar plates. Antibiotics were supplemented to the final concentrations listed in Table 2. *E. coli* TOP10 (Invitrogen) chemically competent cells were used for general cloning purposes. For protein overproduction, Rosetta™(DE3)pLysS competent cells (Novagen) or BL21(DE3) (Novagen) were used. Expression of genes under the control of T7 promoter was induced with 0.5 mM isopropyl β-D-1-thiogalactopyranoside (IPTG), while the tet-inducible promoter was induced by 0.2-1 μg/ml anhydrotetracycline.

4.2.2 Strain storage

Overnight bacterial cultures were stored supplemented with 15% (v/v) DMSO (dimethyl sulfoxide) at -80 °C.

4.2.3 Growth curves

M. xanthus strains were grown in CTT to exponential phase, and then diluted with CTT media to an OD_{550} of 0.01. Growth was then monitored by measuring the OD_{550} at different time points for ~90 h with two replicates per strain.

4.2.4 Social motility assay of *M. xanthus*

M. xanthus cells from different strains were grown in CTT medium to an OD_{550} of 0.4-0.9, harvested at 4700 rpm for 10 min, and concentrated to OD_{550} of 7 with CTT medium. 5μl of aliquots were spotted onto CTT plates containing 0.5% agar [61]. Colonies were examined using Leica MZ8 stereomicroscope after 24 h incubation at 32 ºC. Images were acquired using Leica DFC280 camera and analyzed in Leica IM50 software (Leica, Germany).

4.2.5 Development assay of *M. xanthus*

For developing assay, *M. xanthus* cells from different strains were grown in CTT medium to an OD_{550} of 0.4-0.9, harvested at 4700 rpm for 10 min, and concentrated to OD_{550} of 7 with TPM buffer (10 mM Tris/HCl, pH 7.6, 1 mM KH_2PO_4, pH 7.6, 8 mM $MgSO_4$). 20 µl aliquots were spotted onto TPM starvation plates supplemented with 1.5% agar [83]. Fruiting body formation was visualized after 22, 50 or 72 h using the Leica MZ8 stereomicroscope and analyzed as described for S-motility assay.

4.3 Microscopic methods

Microscopic analyses were conducted using a Zeiss Axio Imager.M1 microscope, a Zeiss Plan Apochromat 100x/1.40 Oil DIC objective and a Photometrics Cascade: 1K CCD camera; alternatively, a Zeiss Axio Imager.Z1 microscope with a 100x/1.46 Oil DIC objective and a pco.edge sCMOS camera were used. The X-Cite®120PC metal halide light source (EXFO, Canada) and ET-DAPI, ET-CFP, ET-YFP, ET-GFP or ET-TexasRed filter cubes (Chroma, USA) were used for fluorescence detection.

In general, for live-cell microscopy, *E. coli* cells were immobilized on pads made of 1.5% agarose buffered with H_2O, while *M. xanthus* cells were immobilized on 1.5% agarose pads buffered with TPM (10 mM Tris/HCl, pH 7.6, 1 mM potassium phosphate, pH 7.6, 8 mM $MgSO_4$).

Images were processed using Metamorph 7.7 (Molecular Devices). The quantification of imaging data was conducted as described in the results.

4.3.1 Nucleoid staining

E. coli and *M. xanthus* cells were incubated with 0.5 µg/ml 4',6-diamidino-2-phenylindole (DAPI) for 15 min in the dark with shaking at 37 °C or 32 °C, respectively. Stained samples were then processed for further imaging.

4.3.2 Immunofluorescence microscopy

Immunofluorescence microscopic analysis was performed as described before [15]. Briefly, cells were grown to exponential phase and fixed with 1.6-2.6% (w/v) paraformaldehyde and 0.008% (w/v) glutaraldehyde for 20 min on poly-L-Lysine coated 8-well slides (Thermo Scientific, USA). Fixed cells were then permeabilized with GTE buffer (50 mM glucose, 20 mM Tris/HCl, pH 7.6, 10 mM EDTA) for 5-30 min. Afterwards, the cells were incubated overnight at 4 °C with α-HA, α-BacP, or α-BacO antibodies at dilutions of 1:200, 1:400, and 1:1000, respectively. Immunocomplexes were then labeled by incubation of the cells with Alexa-Fluor 594 Goat Anti-Rabbit or Alexa-Fluor 488 Goat Anti-Rabbit (Molecular Probes) at a dilution of 1:200 for 1-3 h at RT in the dark. All antibodies were diluted in PBS buffer (137 mM NaCl, 2.7 mM KCl, 10 mM Na_2HPO_4, 2 mM KH_2PO_4) supplemented with 2% (w/v)

bovine serum albumin (BSA). Before imaging, SlowFade® Antifade (Invitrogen, Germany) was applied to each well.

4.3.3 FlAsH staining

Tetracysteine tags were detected using the TC-FlAsH™ II In-Cell Tetracysteine Tag Detection Kit (Invitrogen, Germany). Briefly, cells at exponential phase were stained with 2.5 µM FlAsH-EDT_2 labeling reagent in the dark at 32 ºC for 30-45 min, followed by washing twice with BAL buffer. Stained cells were then grown in the reagent-free medium for another 30-45 min to reduce the background staining. Cells were then subjected for imaging, with staining detected by green fluorescence channel.

4.3.4 FRAP (Fluorescence Recovery After Photobleaching)

Image acquisition and FRAP experiments were performed on Axio Imager M1 microscope (Zeiss), with a 561-nm-solid-state laser and a multi-point FRAP module (2D-VisiFRAP Galvo System, Visitron Systems, Germany). Cells were grown to exponential phase in CTT medium, pre-treated with 50 µg/ml chloramphenicol for at least 1 h to stop protein synthesis, and transferred to a glass slide. Slides were then covered with sealed coverslips and processed to microscopic observation. A small region of fluorescent signals was photobleached using the laser, and the recovery was monitored for the following 300 s, with time intervals of 20 s. Measurement of fluorescence intensity was obtained at each time point using region measurement tool in Metamorph (Molecular Devices). Background intensity was first subtracted for each bleaching region. The intensity was then normalized with the fluorescence decay in unbleached regions during image acquisition. Finally, the normalized pre-bleached intensity was set as 100%, then intensities at all time points were divided by the pre-bleached intensity. The half time was calculated by the formula $t_{1/2} = \ln(0.5)/(-B)$, where B was derived from formula $F(t) = A\,(1-e^{-B*t})+C$ with F(t) as the fluorescence intensity at time t. 11, 10, and 10 cells were analyzed for strain MT296 (*bacP::bacP-mCherry*), MT297 (*bacO::bacO-mCherry*), and MT298 (*bacN::bacN-mCherry*), respectively.

4.4 Molecular cloning

4.4.1 Isolation of chromosomal DNA

M. xanthus chromosomal DNA was prepared as follows: *M. xanthus* cells from cultures with an OD_{550} of more than 1 were harvested and resuspended in TE buffer (10 mM Tris/HCl, pH 8, 1 mM EDTA), and incubated with rapid lysis mix (5% SDS, 125 mM EDTA, 0.5 M Tris/HCl, pH 9.4) containing pronase (Fluka, Germany) at 37 °C for 1 h. The solution was then mixed with 1 vol. of phenol and centrifuged to seperate the aqueous phases and phenol. The aqueous phase was then mixed with ¾ vol. of phenol and ¼ vol. of $CHCl_3$. After centrifugation, the aqueous phase was isolated and mixed with 1 vol. of $CHCl_3$. Centrifugation was performed to separate the aqueous phase, which was then mixed with 2 vol. of 96% ethanol. The precipitated

DNA was washed with 70% ethanol and resuspended in TE buffer. Chromosomal DNA was stored at -20 °C. Alternatively, *M. xanthus* chromosomal DNA was purified as follows: after harvest, *M. xanthus* cells were resuspended in TE buffer and mixed with 0.5% SDS, 100 µg/ml proteainase K (SIGMA-Aldrich, Germany), and 50 µg/ml RNase A (Fluka, Germany). The mixture was incubated at 37 °C for 1 h. Subsequently, 1/6 vol. of 5 M NaCl and 0.114 vol. of CTAB/NaCl solution were added. The mixture was incubated at 65 °C for 10 min. Equal vol. of 24:1 chloroform:isoamyl alcohol was then added. After centrifugation to separate the different phases, the aqueous layer was then mixed with equal vol. of 25:24:1 phenol:chloroform:isoamyl alcohol. After another centrifugation step, the aqueous phase was mixed gently with 0.6 vol. of isopropanol until genomic DNA became precipitated. Genomic DNA pellet was washed by 70% ethanol and then resuspended in EB buffer (10 mM Tris/HCl, pH 8). *C. crescentus* chromosomal DNA used in this work was purified using the illustra™ bacteria genomicPrep Mini Spin Kit (GE Healthcare, Germany).

4.4.2 Plasmid DNA isolation

Plasmid DNA was isolated using the GenElute™ Plasmid Kit (SIGMA-Aldrich, Germany) according to the instruction provided by the manufacturer. The concentration of DNA was determined using Nanodrop ND-1000 spectrophotometer (Nanodrop, USA).

4.4.3 Polymerase chain reaction (PCR)

The specific amplification of DNA fragments was conducted using KOD Hot Start DNA Polymerase (Merck, Germany). The reaction mixtures and programs are listed in Table 3. Amplification was verified by agarose gel electrophoresis. The reaction products were purified using either the GeneElute™ PCR Clean-Up Kit (SIGMA-Aldrich, Germany) or the GeneElute™ Gel Extraction Kit (SIGMA-Aldrich, Germany).

Table 3. Standard KOD PCR reaction.

100 µl KOD PCR reactions (filled with H_2O to a final vol.)		Standard cycling			
reagent	concentration				
DNA template	50-200 ng				
Reaction buffer	1×	Initial denaturation	94 °C	2 min	
$MgSO_4$	1 mM	Denaturation	94 °C	30s	30 cycles
		Annealing	60-70 °C	30s	
dNTP	0.2 mM	Elongation	72 °C	30s per kb	
DMSO	5-10%	Final elongation	72 °C	4-10 min	
oligonucleotides	0.5 µM each				
KOD polymerase	2 units				

Colony PCR was performed using BioMix™ Red (Bioline, Germany). The reaction mixtures and programs are listed in Table 4. For colony PCR with *M. xanthus* cells, crude genomic DNA was obtained by boiling cells in the Lyse-N-Go PCR reagent (Thermo Scientific, Germany) at 96 °C for 10 min. Amplification was verified by agarose gel electrophoresis.

Table 4. Standard colony PCR reaction.

10 µl colony PCR reactions (filled with H_2O to a final vol.)		**Standard cycling**			
reagent	**concentration**				
DNA template	crude genomic DNA or purified DNA	Initial denaturation	94 °C	2 min	
		Denaturation	94 °C	30s	30 cycles
BioMix™ Red	1×	Annealing	60-70 °C	30s	
DMSO	5%	Elongation	72 °C	30s per kb	
		Final elongation	72 °C	4-10 min	
oligonucleotides	0.5 µM each				

4.4.4 Restriction digestion

DNA digestion was performed by incubating 1-5 µg of DNA with selected restriction endonucleases (NEB, Germany; Fermentas, Canada) for 1-12 h at 37 °C. 0.1 mg/ml bovine serum albumin (BSA; NEB, Germany) was supplemented if necessary. To generate plasmid backbones for cloning purpose, Shrimp Akaline Phosphatase (SAP or fastAP; Fermentas, Canada) was added to the reactions to dephosphorylate 5' ends. Digested products were further purified using either the GeneElute™ PCR Clean-Up Kit (SIGMA-Aldrich, Germany) or the GeneElute™ Gel Extraction Kit (SIGMA-Aldrich, Germany).

4.4.5 Blunting reaction

The generation of blunt ends was carried out using T4 DNA polymerase (Fermentas, Canada). Digested DNA fragments were mixed with T4 DNA polymerase and 0.2 mM dNTPs. The reaction was performed at RT for 10 min, and the products were purified using the GeneElute™ PCR Clean-Up Kit (SIGMA-Aldrich, Germany).

4.4.6 Ligation

DNA ligation was performed using T4 DNA ligase (Fermentas, Canada). In general, a mixture of inserted DNA and recipient vector with a molar ratio of 3 was incubated with T4 DNA ligase in rapid-lysis buffer (Fermentas, Canada) for 5-30 min at RT.

4.4.7 Detection of DNA by agarose gel electrophoresis

DNA products were mixed with 10× DNA loading buffer (50 % glycerol, 0.2 % bromphenol blue, 0.2 % xylene cyanol, 0.2 M EDTA) and separated in 1% agarose gels. The agarose gel was prepared in 0.5× TAE buffer (20 mM Tris/HCl, pH 8, 0.175 % acetic acid, 0.5 mM EDTA, pH 8) and supplemented with 0.005% ethidium bromide for visualization. A UV-transilluminator (UVP-BioDoc-IT™ Imaging System, UniEquip, Germany) was used to detect DNA exposed to UV light. If necessary, DNA products of interest were excised from the gels for further purification.

4.4.8 Transformation of *E. coli*

The preparation of chemically competent *E. coli* was performed as described [52]. In brief, overnight cultures of *E. coli* cells were diluted 1: 100 in 500 ml LB medium. Cells were grown to an OD_{600} of 0.6-0.8 and then incubated on ice for 10 min. Cells were then harvested at 4 °C, resuspended in ice-cold 0.1 M $CaCl_2$, and incubated on ice for 30 min. After centrifugation, the cells were resuspended in 8 ml of ice-cold 0.1 M $CaCl_2$ supplemented with 15% (v/v) glycerol. Aliquots of competent cells (150 µl each) were snap-frozen in liquid nitrogen and stored at -80 °C for further use.

The transformation of chemically competent *E. coli* cells was performed as follows: competent cells were mixed with ligation mixtures or ~ 10 ng of plasmid DNA and incubated on ice for 30 min. A heat-shock was then applied for 45-90 s at 42 °C. Cells were then incubated again on ice for 5 min before mixing with 500 µl of LB or SOC medium. The cell suspension was then incubated at 37 °C for 30-90 min with shaking and spread on LB agar plates supplemented with appropriate antibiotics. Plates were incubated at 37 °C until single colonies were visible.

4.4.9 DNA sequencing

DNA sequencing was performed by Eurofins MWG Operon (Germany). In general, 50-100 ng of DNA products were provided along with suitable oligonucleotides. Sequencing results were analyzed using Vector NTI Advance™ 11 (Invitrogen, Germany).

4.4.10 Plasmid construction

Plasmids for in-frame deletions. To construct plasmid **pLL1**, a fragment (from 5815725 bp to 5816327 bp) containing 567 bp of the *bacP* downstream region and the last 36 bp of *bacP* was amplified with primers MXAN4635-down-for and MXAN4635-down-rev and digested with HindIII and BamHI. In addition, a fragment (from 5816979 bp to 5817616 bp) containing 602 bp of the *bacP* upstream region and the first 36 bp of *bacP* was amplified with primers MXAN4635-up-for and MXAN4635-up-rev, and digested with BamHI and EcoRI. The two fragments were ligated into HindIII/EcoRI treated pBJ114.

To construct plasmid **pLL2**, a fragment (from 5816427 bp to 5817053 bp) containing 591 bp of the *bacO* downstream region and the last 36 bp of *bacO* was amplified with primers MXAN4636-down-for and MXAN4636-down-rev and digested with HindIII and BamHI. In addition, a fragment (from 5817364 bp to 5817980 bp) containing 581 bp of the *bacO* upstream region and the first 36 bp of *bacO* was amplified with primers MXAN4636-up-for and MXAN4636-up-rev, and digested with BamHI and EcoRI. The two fragments were ligated into HindIII/EcoRI treated pBJ114.

To construct plasmid **pLL3**, a fragment (from 5816806 bp to 5817430 bp) containing 589 bp of the *bacN* downstream region and the last 36 bp of *bacN* was amplified with primers MXAN4637-down-for and MXAN4637-down-rev and digested with HindIII and BamHI. In addition, a fragment (from 5817701 bp to 5818332 bp) containing 596 bp of the *bacN* upstream region and the first 36 bp of *bacN* was amplified with primers MXAN4637-up-for and MXAN4637-up-rev, and digested with BamHI and EcoRI. The two fragments were ligated into HindIII/EcoRI treated pBJ114.

To construct plasmid **pLL38**, a fragment (from 5814000 bp to 5814826 bp) containing 791 bp of the *badA* downstream region and the last 36 bp of *badA* was amplified with primers MXAN4634-down-for and MXAN4634-down-rev and digested with BamHI and EcoRI. In addition, a fragment (from 5816225 bp to 5817061 bp) containing 801 bp of the *badA* upstream region and the first 36 bp of *badA* was amplified with primers MXAN4634-up-for and MXAN4634-up-rev, and digested with BamHI and HindIII. The two fragments were ligated into HindIII/EcoRI treated pBJ114.

To construct plasmid **pLL104**, a fragment (from 5814091 bp to 5814826 bp) containing 700 bp of the *badA* downstream region and the last 36 bp of *badA* was amplified with primers MXAN4634down-1-HindIII and MXAN4634down-2-BamHI then digested with HindIII and BamHI. In addition, a fragment (from 5817701 bp to 5818436 bp) containing 736 bp of the *bacN* upstream region and the first 36 bp of *bacN* was amplified with primers BacN-up-BamHI and BacN-up-2-EcoRI, and digested with BamHI and EcoRI. The two fragments were ligated into HindIII/EcoRI digested pBJ114.

Plasmids for fusing genes with fluorescence fusions. To construct plasmid **pLL17**, a fragment encoding *bacP* was amplified with primers MXAN4635-For and MXAN4635-Rev and digested with BglII and NheI. The digested fragment was then ligated into BglII/NheI treated pXCHYN-2.

To construct **pLL18**, a fragment encoding *bacO* was amplified with primers MXAN4636-For and MXAN4636-Rev and digested with BglII and NheI. The digested fragment was then ligated into BglII/NheI treated pXCHYN-2.

To construct **pLL19**, a fragment encoding *bacN* and *bacO* was amplified with primers MXAN4637-For and MXAN4636-Rev and digested with BglII and NheI. The digested fragment was then ligated into BglII/NheI treated pXCHYN-2.

To construct **pLL47**, a fragment encoding *bacO* was amplified with primers MXAN4636-For and MXAN4636-Rev and digested with BglII and NheI. The digested fragment was then ligated into BglII/NheI treated pVCFPN-4.

To construct plasmid **pLL53**, a fragment encoding the C-terminal region of *bacP* (nt 333-723) was amplified with primers MXAN4635$C_{111-240}$-For and MXAN4635-Rev and digested with BglII and NheI. The digested fragment was then ligated into BglII/NheI treated pXCHYN-2.

To construct **pLL64**, a fragment encoding *badA* was amplified with primers MXAN4634-new-For-NdeI and MXAN4634-new-Rev-EcoRI, and digested with NdeI and EcoRI. The digested fragment was then ligated into NdeI/EcoRI treated pXCHYC-1.

To construct **pLL65**, a fragment encoding *parB* (*C. crescentus*) was amplified with primers ccParB-for and ccParB-rev, and digested with NdeI and EcoRI. The digested fragment was then ligated into NdeI/EcoRI treated pXYFPC-2.

To construct **pPS17**, a fragment encoding *bacN* was amplified with primers MXAN4637-for-2 and MXAN4637-rev-2, and digested with EcoRI and BamHI. The digested fragment was then ligated into equally treated pXYFPN-2.

To construct **pLL85**, a fragment encoding *parA* was amplified with primers ParA-for-NdeI and ParA-rev-EcoRI, and digested with NdeI and EcoRI. The digested fragment was then ligated into equally treated pXYFPC-2.

To construct **pLL87**, a fragment encoding *badA* was amplified with primers MXAN4634-For-new-NdeI and MXAN4634-Rev-new-EcoRI, and digested with NdeI and EcoRI. The digested fragment was then ligated into equally treated pXYFPC-2.

To construct **pLL118**, a fragment encoding $badA_{\Delta aa1-239}$ was amplified with primers MXAN4634c-for and mxan4634c-rev, and digested with BglII and EcoRI. The digested fragment was then ligated into equally digested pXVENN-2.

Plasmids for site-directed mutagenesis. Plasmid **pLL117** was constructed by site-directed mutagenesis of pLL85 using primers parA(R238E)-for and parA(R238E)-rev. To construct plasmid **pLL121**, the $parA^{R238E}$ gene was released from pLL117 by digestion with NdeI and EcoRI and then ligated into equally treated pXCHYC-1.

Plasmid **pLL119** was constructed by site-directed mutagenesis of pLL85 using primers parA(R209A)-for and parA(R209A)-rev. To construct plasmid **pLL123**, the $parA^{R209A}$ gene was released from pLL119 by digestion with NdeI and EcoRI and then ligated into equally treated pXCHYC-1.

Plasmids for gene replacement. To construct **pLL9**, a fragment encoding *bacP*-HA was amplified with primers MXAN4635-HA-1 and MXAN4635-HA-2 and digested with HindIII and BamHI; it should be noted that oligo MXAN4635-HA-2 includes the nucleotide sequence of the HA affinity tag. In parallel, a fragment (from 5816291 bp to 5816566 bp) containing 746 bp of the *bacP* downstream was amplified with primers MXAN4635HA-down-for and MXAN4635HA-down-rev, and digested with BamHI and EcoRI. The two fragments were ligated into HindIII/EcoRI-treated pBJ114.

To construct **pLL10**, a fragment encoding a fragment (from 5817021 bp to 5817736 bp) fused with the HA tag was amplified with primers MXAN4636-HA-1 and MXAN4636-HA-2 and digested with HindIII and BamHI; it should be noted that oligo MXAN4636-HA-2 includes the nucleotide sequence of the HA affinity tag. In parallel, a fragment (from 5816028 bp to 5817039 bp) containing 1012 bp of the *bacO* downstream was amplified with primers

MXAN4636HA-down-for and MXAN4636HA-down-rev, and digested with BamHI and EcoRI. The two fragments were ligated into HindIII/EcoRI-treated pBJ114.

To construct **pLL11**, a fragment encoding 275 bp of the *bacN* upstream region and *bacN*-HA (from 5817398 bp to 5818011 bp) was amplified with primers MXAN4637-HA-1 and MXAN4637-HA-2 and digested with HindIII and BamHI; it should be noted that primer MXAN4637-HA-2 includes the nucleotide sequence of the HA affinity tag. In parallel, a fragment (from 5816404 bp to 5817394 bp) containing 991 bp of the *bacN* downstream was amplified with primers MXAN4637HA-down-for and MXAN4637HA-down-rev, and digested with BamHI and EcoRI. The two fragments were ligated into HindIII/EcoRI-treated pBJ114.

To construct **pLL23**, a fragment encoding 751 bp (from 58177015 bp to 5817765 bp) of the upstream region of *bacP* was amplified using primers MXAN4635up-for-2 and MXAN4635up-rev-2, and then digested with NdeI and NotI. The digested fragment was then ligated into NdeI/NotI-treated pLL17, giving the resulting plasmid **pLL20**. Afterwards, a fragment containing the 751 bp upstream region along with *mCherry-bacP* sequence was amplified using primers MXAN4635upFor-EcoRI and MXAN4635Rev-HindIII. The PCR product was then digested with EcoRI and HindIII then ligated into equally treated pBJ114.

To construct plasmid **pLL42**, a fragment encoding 275 bp of the *bacN* upstream region and *bacN* (from 5817398 bp to 5818011 bp) fused with a tetracysteine tag was amplified with primers MXAN4637-HA-1 and MXAN4637TC-rev, and digested with HindIII and BamHI. In parallel, a fragment (from 5816404 bp to 5817394 bp) containing 991 bp of the *bacN* downstream was amplified with primers MXAN4637HA-down-for and MXAN4637HA-down-rev, and digested with BamHI and EcoRI. The two fragments were ligated into HindIII/EcoRI-treated pBJ114.

To construct plasmid **pLL45**, a fragment (from 5816625 bp to 5817014) containing 390 bp of the *bacP* gene fused with a tetracysteine tag was amplified using primers MXAN4635TC2-for and MXAN4635TC2-rev, and digested with HindIII and XmaI. In parallel, a fragment (from 5816091 bp to 5816624 bp) containing the last 333 bp of the *bacP* gene and 201 bp of the *bacP* downstream region was amplified with primers MXAN4635TC2-down-for and MXAN4635TC2-down-rev, and digested with XmaI and EcoRI. The two fragments were ligated into HindIII/EcoRI-treated pBJ114.

To construct **pLL72**, a fragment encoding 780 bp (from 5814011 bp to 5814790 bp) of the downstream region of *badA* was amplified using primers MXAN4634down-for-2 and MXAN4634down-rev-2, and then digested with NheI and EcoRI. The digested fragment was then ligated into equally treated pLL64, giving the resulting plasmid **pLL66**. Afterwards, a fragment containing *badA-mCherry* and the 780 bp downstream region was amplified from pLL66 using primers MXAN4634-For-XbaI and MXAN4634down-Rev-NheI. The PCR product was then digested with XbaI and NheI and subsequently blunted with T4 DNA polymerase. In parallel, pBJ114 was digested by XbaI and subsequently blunted with T4 DNA polymerase. The blunted PCR product and pBJ114 was then ligated to give plasmid pLL72.

Plasmids for integrating into DK1622 chromosome. To construct **pLL14**, *bacP-mCherry* was amplified from pMT978 using primers MXAN4635-for-XbaI and mCherry-rev-HindIII, and

digested with XbaI and HindIII. The digested product was then ligated into equally treated pMAT4.

To construct **pLL15**, *bacO-mCherry* was amplified from pMT979 using primers MXAN4636-for-XbaI and mCherry-rev-HindIII, and digested with XbaI and HindIII. The digested product was then ligated into equally treated pMAT4.

To construct **pLL16**, *bacN-mCherry* was amplified from pMT980 using primers MXAN4637-for-XbaI and mCherry-rev-HindIII, and digested with XbaI and HindIII. The digested product was then ligated into equally treated pMAT4.

To construct **pLL30**, *mCherry-bacP* was amplified from pLL17 using primers mCherry-for-XbaI and MXAN4635-rev-HindIII, and digested with XbaI and HindIII. The digested product was then ligated into equally treated pSW105.

To construct **pLL31**, *mCherry-bacO* was amplified from pLL18 using primers mCherry-for-XbaI and MXAN4636-rev-HindIII, and digested with XbaI and HindIII. The digested product was then ligated into equally treated pSW105.

To construct **pLL32**, *mCherry-bacN* was amplified from pLL19 using primers mCherry-for-XbaI and MXAN4637-rev-HindIII, and digested with XbaI and HindIII. The digested product was then ligated into equally treated pSW105.

To construct **pLL33**, *bacP* was amplified by primers Comp MXAN4635-for and Comp MXAN4635-rev, and then treated by XbaI and HindIII. The digested product was then ligated into equally treated pSW105.

To construct **pLL73**, *badA-mCherry* fragment was amplified from pLL72 using primers MXAN4634-For-XbaI and mCherry-Rev-NheI, and then digested by NheI. The digested product was subsequently blunted with T4 DNA polymerase. The plasmid pSW105 was digested with HindIII and treated with T4 DNA polymerase. Afterwards, both blunted *badA-mCherry* fragment and pSW105 were digested with XbaI. Then the digested products were ligated.

To construct **pLL74**, *badA-mCherry* fragment was amplified from pLL72 using primers MXAN4634-For-XbaI and mCherry-Rev-NheI, and then digested by NheI. The digested product was subsequently blunted by T4 polymerase. Meanwhile, pMAT4 was digested with HindIII then treated by T4 polymerase. Afterwards, both blunted *badA-mCherry* fragment and pMAT4 were digested with XbaI. Then digested products were ligated.

To construct **pLL89**, *eyfp* was amplified from pXYFPC-2 using primers eYFP-for-BamHI and eYFP-rev-HindIII then digested with BamHI and HindIII. pAH59 was digested equally to remove the fused *mCherry* fragment. The digested plasmid and fragment were then ligated.

To construct **pLL93**, *badA-eyfp* fragment was amplified from pLL87 using primers MXAN4634-For-XbaI and eYFP-rev-NheI, and then digested by NheI. The digested product was subsequently blunted with T4 DNA polymerase. The plasmid pMAT4 was digested with HindIII and treated with T4 DNA polymerase. Afterwards, both blunted *badA-eyfp* fragment and pMAT4 were digested with XbaI. Then the digested products were ligated.

To construct **pLL116**, *parA-eyfp* fragment was amplified from pLL85 using primers ParA-for-NdeI and eYFP-rev-NheI, and then digested with NdeI and NheI. Digested product was ligated into equally treated pMR3691.

To construct **pLL126**, *badA* fragment was amplified from DK1622 genomic DNA using primers MXAN4634-For-new-NdeI and mxan4634c-rev and digested with NdeI and EcoRI. The digested fragment was ligated into equally treated pMR3690.

To construct **pLL132**, *parA* fragment was amplified from pLL116 DNA using primers ParA-for-NdeI and ParA-rev-EcoRI-2, followed with digestion with NdeI and EcoRI. The digested product was ligated into equally treated pMR3691.

Plasmids for expression in *E. coli*. To construct **pLL48**, *mCherry-bacP* fragment was amplified from pLL17 using primers mCherry-For-NdeI and mCherry-MXAN4635-Rev-XhoI and digested with NdeI and XhoI. The digested fragment was then ligated into equally digested pETDuet-1.

To construct **pLL51**, *cfp-bacO* fragment was amplified from pLL47 using primers NcoI-CFP-For and CFP-MXAN4636-Rev-EcoRI and digested with NcoI and EcoRI. The digested fragment was then ligated into equally digested pETDuet-1.

To construct **pLL52**, *parB-eyfp* fragment was amplified from pAH7 using primers parB-yfp-for-XbaI and parB-yfp-Rev-XmaI and digested with XbaI and XmaI. The digested fragment was then ligated into equally digested pMT325.

To construct **pLL54**, *mCherry-bacP* fragment was amplified from pLL17 using primers mCherry-For-NdeI and mCherry-MXAN4635-Rev-MfeI and digested with NdeI and MfeI. The digested fragment was then ligated into equally digested pLL51.

To construct **pLL55**, *mCherry-bacO* fragment was amplified from pLL18 using primers mCherry-For-NdeI and mCherry-MXAN4636-Rev-MfeI and digested with NdeI and MfeI. The digested fragment was then ligated into equally digested pETDuet-1.

To construct **pLL57**, *mCherry-bacP*$_{\Delta aa1\text{-}110}$ fragment was amplified from pLL53 using primers mCherry-For-NdeI and mCherry-MXAN4635-Rev-MfeI and digested with NdeI and MfeI. The digested fragment was then ligated into equally digested pETDuet-1.

To construct **pLL60**, *mCherry-bacP*$_{\Delta aa123\text{-}240}$ fragment was amplified from pLL17 using primers mCherry-for-NdeI-2 and mCherry-MXAN4635N-rev and digested with NdeI and MfeI. The digested fragment was then ligated into equally digested pETDuet-1.

To construct **pLL61**, *eyfp* fragment was amplified from pAH7 using primers XbaI-RBS-eYFP-for and parB-yfp-Rev-XmaI and digested with XbaI and XmaI. The digested fragment was then ligated into equally digested pMT325.

To construct **pLL69**, *ccparB-eyfp* fragment was amplified from pLL65 using primers ccParB-YFP-for-xbaI and parB-yfp-Rev-XmaI and digested with XbaI and XmaI. The digested fragment was then ligated into equally digested pMT325.

To construct **pLL80**, *parB* fragment was amplified from DK1622 genomic DNA using primers ParB-for-BamHI strep and ParB-rev-NotI strep and digested with BamHI and NotI. The digested product was then ligated into equally treated pET51b+.

To construct **pPS20**, *eyfp-bacN* fragment was amplified from pPS17 using primers YFP-MXAN4637-For and YFP-MXAN4637-Rev and digested with XmaI and BamHI. The digested fragment was then ligated into equally digested pMT325.

To construct **pLL86**, *parA-eyfp* was amplified from pLL85 using primers ParA-yfp-for-XbaI and ParA-yfp-rev-XmaI and digested with XbaI and XmaI. The digested product was then ligated into equally treated pMT325.

To construct **pLL97**, *badA* fragment was amplified from DK1622 genomic DNA using primers MXAN4634-For-new-NdeI and MXAN4634-rev-new-EcoRI and digested with NdeI and EcoRI. The digested product was then ligated into equally treated pET21a+.

To construct **pLL100**, *parA-mCherry* was amplified from pAH59 using primers ParA-eyfp-for-XbaI and mCherry-rev-HindIII and digested with XbaI and HindIII. The digested product was then ligated into equally treated pMT325.

To construct **pLL101**, *badA-eyfp* was amplified using primers MXAN4634-For-new-NdeI and eYFP-rev-NheI from pLL87A and digested with NheI followed by treatment with T4 DNA polymerase. In parallel, pRSFDuet-1 was digested with KpnI and treated with T4 DNA polymerase. Afterwards, both blunted *badA-eyfp* fragment and pRSFDuet-1 were digested with NdeI. The digested products were ligated.

To construct **pLL105**, a fragment encoding $badA_{\Delta aa1-239}$ was amplified with primers mxan4634c-for and mxan4634c-rev, and digested with NdeI and EcoRI. The digested product was ligated into equally treated pET28a+.

To construct **pLL120**, *venus-*$badA_{\Delta aa1-239}$ was amplified using primers NcoI-CFP-For and mxan4634c-rev, and digested with NcoI and EcoRI. The digested product was then ligated into equally treated pRSFDuet-1.

To construct **pLL122**, $parA^{R238E}$*-mCherry* was amplifed from pLL121 using primers ParA-eyfp-for-XbaI and mCherry-rev-HindIII, and digested with XbaI and HindIII. The digested product was then ligated into equally treated pMT325.

To construct **pLL124**, $parA^{R209A}$*-mCherry* was amplifed from pLL123 using primers ParA-eyfp-for-XbaI and mCherry-rev-HindIII, and digested with XbaI and HindIII. The digested product was then ligated into equally treated pMT325.

To construct **pLL131**, a fragment encoding *badA* was amplified with primers MXAN4634-For-new-NdeI and mxan4634c-rev, and digested with NdeI and EcoRI. The digested product was then ligated into equally treated pET28a+.

To construct **pLL137**, *eyfp* was amplified using primers NcoI-CFP-For and eYFP-rev-HindIII, and digested with NcoI and HindIII. The digested product was then ligated into equally treated pRSFDuet-1.

4.4.11 Transformation of *M. xanthus*

The transfer of plasmids to *M. xanthus* was achieved by electroporation as follows: *M. xanthus* cells were grown in CTT medium overnight to exponential phase, 1.5 ml of the cultures were

harvested for 1 min at RT. The pellets were then washed twice with 1 ml of ice-cold sterile deionized H_2O and finally resuspended in 40 µl of H_2O. The competent cells were then mixed with 0.1-1 µg of plasmid DNA and transferred into a sterile electroporation cuvette (0.1 cm, Bio-Rad, Germany). The electroporation was carried out at 650 V, 400 Ω and 25 µF in GenePulser XCell™ (Bio-rad, Germany); then 1 ml CTT was added immediately to the mixture. The suspension was then incubated at 32 °C for 4-8 h with shaking (220 rpm). Different amounts of the suspension (50 µl, 200 µl, or 500 µl) were then mixed with 4 ml CTT soft agar supplemented with appropriate antibiotics. The mixture was then spread onto CTT agar plates containing appropriate antibiotics. The plates were incubated at 32 °C for 5-14 days until colonies are visible. Colonies were transferred onto fresh plates and verified by colony PCR for correct integration of plasmids. All *M. xanthus* strains were listed in the Appendix (Table 8).

4.4.12 Gene replacements in *M. xanthus*

Gene replacement was achieved by double homologous recombination [137]. In general, plasmids for gene replacement were derived from the suicide vector pBJ114 [72] and used for transforming *M. xanthus* by electroporation. Recombinant cells were first selected in the presence of kanamycin. The resistant colonies were transferred onto fresh plates with kanamycin and then grown in CTT liquid medium to exponential phase. 20 µl, 50 µl, or 200 µl of the culture were then mixed with 4 ml CTT soft agar containing 2.5% (w/v) galactose. The suspension was then spread onto CTT agar plates supplemented with 2.5% (w/v) galactose for selection. Colonies exhibiting galactose tolerance and high kanamycin sensitivity were further verified by colony PCR. All *M. xanthus* strains are listed in the Appendix (Table 8).

4.5 Biochemical methods

4.5.1 Protein detection

SDS-PAGE (SDS-Polyacrylamide gel electrophoresis) was used for the separation of proteins [84]. Protein samples of cell lysates were obtained as follows: *M. xanthus* cells were harvested at 9000 rpm and 4 °C for 10 min. The cells were then resuspended in 2× SDS (sodium dodecyl sulfate) sample buffer (125 mM Tris, 20% (w/v) glycerol, 2% (w/v) SDS, 200 mM dithiothreitol, 0.05 % bromophenol blue, pH 6.8) to a theoritical OD_{550} of 10. The suspension was then heated at 95 °C for 15 min. Protein samples from biochemical assays (protein purification, Co-IP and pull-down assays) were diluted with SDS sample buffer and heated at 95 °C for 10 min. Protein samples were then loaded to an SDS gel consisting of a 5% stacking gel and 8-11% resolving gel (Table 5), along with a molecular mass marker (PageRuler™ Prestained Protein Ladder; Fermentas, Canada). Proteins were seperated at 10-35 mA per gel in SDS running buffer (25mM Tris base, 192mM Glycine, 0.1% SDS), using The PerfectBlue™ Twin S system (Peqlab, USA).

Table 5. Composition of SDS-PAGE gels.

Component	5% stacking gel 2.5 ml	8% (80-200 kDa) resolving gel 5 ml	11% (10-200 kDa) resolving gel 5 ml	15% (3-100 kDa) resolving gel 5 ml
Deionized H_2O	1.43 ml	2.4 ml	1.9 ml	1.19 ml
4× stacking buffer (0.5 M Tris/HCl pH 6.8, 0.4 % (w/v) SDS)	625 µl	-	-	-
4× resolving buffer (1.5 M Tris/HCl pH 8.8, 0.4 % (w/v) SDS)	-	1.25 ml	1.25 ml	1.25 ml
30% Rotiphorese® NR Acrylamide/Bis-(29:1)	417 µl	1.25 ml	1.9 ml	2.5 ml
10% w/v APS (ammonium persulfat)	25 µl	40 µl	40 µl	40 µl
TEMED (N,N,N',N'-Tetramethylethylenediamine)	1.9 µl	3µl	3 µl	3 µl

After electrophoresis, the SDS gel was either stained with Coomassie blue (40 % methanol, 10 % acidic acid, 0.1 % (w/v) Brilliant Blue R 250) for 10 min followed with destaining in a solution of 20 % ethanol and 10 % acidic acid, or stained with Instant Blue (Expedeon, United Kingdom). Alternatively, the proteins were visualized by silver staining as follows: after electrophoresis, the proteins were fixed with fixation solution (10% CH_3COOH, 40% Ethanol) for more than 15 min, followed by incubation of the gel with sensitizing solution (30% ethanol, 2 g/l $Na_2S_2O_3 \cdot 5H_2O$, 68 g/l CH_3COONa) for 30-60 min. The gel was then washed with H_2O four times for 5 min each, followed by staining with 0.25% of $AgNO_3$ for 20 min in the dark. After washing with H_2O twice, the gel was developed in a solution containing 2.5% Na_2CO_3 and 400 µl/l 37% formaldehyde for 0.5-4 min, until protein bands were visible. The reaction was then stopped by incubation of the gel in 14.6 g/l EDTA$\cdot 2H_2O$ for 10 min. The gel was washed three times with H_2O for 5 min each and stored in a solution containing 1% glycerol and 30% ethanol.

4.5.2 Immunoblot analysis

For immunoblot analysis, proteins were first separated by SDS-PAGE, and then transferred onto PVDF (polyvinylidene fluoride) membranes (Millipore, USA) by a semi-dry transfer using a PerfectBlue™ Semi-Dry-Elektro Blotter (Peqlab, USA). To this end, the PVDF membrane was first soaked in 100% methanol for 15 s and then rinsed with H_2O for 2 min. The membrane was then incubated in Western blot buffer (25 mM Tris, 192 mM glycine, 10 % methanol) for at least 5 min. Proteins were transferred from the gel onto the membrane at 2 mA/cm² for 1.5-2 h. The membrane was then blocked in 1× TBST buffer (10 mM Tris/HCl, pH 7.5, 150 mM NaCl, 0.1 % w/v Tween 20) containing 2.5-5% non-fat milk for either 1-2 h at RT or overnight at 4 °C with gentle agitation. After blocking, the membrane was incubated with primary antibodies (Table 6) for 1-2 h at RT or overnight at 4 °C with gentle agitation and washed for three times

with 1× TBST buffer. A secondary anti-rabbit IgG-horseradish perioxidase (HRP) conjugate was then incubated with the membrane for 1-2 h at RT. After five washes with 1× TBST buffer, the membrane was incubated with Western Lightning™ Chemiluminescence Reagent Plus for 1 min (Perkin Elmer, USA) according to the manufacturer's instruction. The membrane was exposed to Amersham Hyperfilm™ ECL-Chemiluminenscence films (GE Healthcare, Germany) and developed with an LAS-4000 Luminescent Image Analyzer (Fujifilm, Germany).

Table 6. Antibodies used for immunoblot analysis.

Antibody*	Dilution	Reference/source
primary antibodies		
α-BacP	1:1000	[16]
α-BacO	1:10000	Generated by immunization of rabbits using purified BacO-His_6
α-HA	1:8000	Millipore, Germany
α-ParA	1:1000	[57]
α-ParB	1:5000	[57]
α-RFP	1:10000	[23]
α-GFP	1:10000	SIGMA-Aldrich, Germany
α-BadA	1:2500	Generated by immunization of rabbits using purified His_6-$BadA_{\Delta aa1-239}$
secondary antibodies		
α-rabbit-HRP	1:20000	Perkin Elmer, USA

4.5.3 Protein purification

BacO-His_6 was expressed and purified as described before [82]. Briefly, plasmid pSW17 was transferred into *E. coli* Rosetta™ (DE3)/pLysS (Invitrogen). Transformants were then grown in 750 ml of LB medium supplemented with appropriate antibiotics. The overexpression was then induced with 0.5 mM IPTG for 3 h at 37 ˚C. The culture was then harvested at 6500 rpm and 4 ˚C for 10 min followed by washing with buffer B1 (50 mM NaH_2PO_4, 300 mM NaCl, 10 mM imidazole, pH 8.0) and resuspended in 15.5 ml of buffer B2 (50 mM NaH_2PO_4, 300 mM NaCl, 10 mM imidazole and 1 mM ß-mercaptoethanol, pH 8.0) supplemented with 10 µg/ml DNase I and 100 µg/ml PMSF (phenylmethyl sulfonyl fluoride). Cells were lysed by two passages in a French press (16000 psi), and cell debris was removed by centrifugation at 30000 g for 30 min. The cleared lysates were mixed with 5 ml Ni-NTA agarose beads (Qiagen) that were equilibrated with buffer B2, and then incubated with gentle agitation for 1 h at 4 ˚C. Ni-NTA beads with bound proteins were then collected at 4000 rpm for 15 min. The beads were washed

three times with 40 ml of buffer B3 (50 mM NaH_2PO_4, 300 mM NaCl, 20 mM imidazole and 1 mM ß-mercaptoethanol, pH 8.0). Proteins were finally eluted by incubation of the beads twice in 15 ml of buffer B4 (50 mM NaH_2PO_4, 300 mM NaCl, 250 mM imidazole and 1 mM ß-mercaptoethanol, pH 8.0). After centrifugation at 4000 rpm for 10 min, the elutes (top phase) and the slurry pellet (opaque phase; diluted in B4 buffer) were collected and dialyzed against 3 L Dialysis Buffer B6 (50 mM HEPES, pH 7.2, 50 mM NaCl, 5 mM $MgCl_2$, 0.1 mM EDTA, 10% glycerol, 1 mM ß-mercaptoethanol). Purified proteins were snap-frozen and stored at -80 ˚C until further use.

In order to purify **StrepII-ParB**, plasmid pLL80 was transferred into *E. coli* Rosetta™ (DE3)/pLysS (Invitrogen). Transformants were then grown in 500 ml of LB medium to an OD_{600} of 1. Expression of *strepII-parB* was induced with 0.5 mM IPTG. After incubation for 3 h at 37 ˚C, the cells were harvested at 6500 rpm and 4 ˚C for 10 min, and washed twice with buffer B1. They were then resuspended in 7.5 ml buffer NP (50 mM NaH_2PO_4, 300 mM NaCl, pH 8.0) supplemented with 10 µg/ml DNase I and 100 µg/ml PMSF. Cells were lysed by three passages in a French press (16000 psi), and cell debris was removed by centrifugation at 30000 g for 30 min. The cleared lysates were mixed with 800 µl Strep-Tactin® Superflow Plus (Qiagen) resin and incubated with gentle agitation for 2 h at 4 ˚C. The mixtures were then transferred into a column with the bottom outlet capped and washed with 3 × 4 ml buffer NP. Proteins were finally eluted with 6 × 500 µl buffer NPD (50 mM NaH_2PO_4, 300 mM NaCl, 2.5 mM dethiobiotin, pH 8.0). The elutes were dialyzed against 2.5 l dialysis buffer (50 mM NaH_2PO_4, 150 mM NaCl, 1 mM EDTA) to remove dethiobiotin. Purified proteins were snap-frozen and stored at -80 ˚C until further use. Used Strep-Tactin® Superflow Plus was regenerated according to manufacturer's protocol.

For the purification of **His_6-$BadA_{\Delta aa1-239}$**, plasmid pLL105 was transferred into *E. coli* Rosetta™(DE3) /pLysS (Invitrogen). Transformants were then grown in 750 ml of LB medium to an OD_{600} of 0.8. Expression was induced with 0.5 mM IPTG. After incubation for 4 h at 37 ˚C, the cells were harvested at 6500 rpm and 4 ˚C for 10 min followed by washing twice with buffer B1. They were then resuspended in 16 ml buffer B2 supplemented with 10 µg/ml DNase I and 100 µg/ml PMSF. Cells were lysed by three passages in a French press (16000 psi), and cell debris was removed by centrifugation at 30000 g for 30 min. The cleared lysates were mixed with 1.2 ml Ni-NTA agarose beads (Qiagen) that were equilibrated with buffer B2, and incubated with gentle agitation for 2 h at 4 ˚C. The mixtures were then washed four times with 10 ml of buffer B3. Proteins were finally eluted with 4 × 3.2 ml elution buffer B4. The elutes were dialyzed against 3 l dialysis buffer B6. Purified proteins were snap-frozen and stored at -80 ˚C until further use.

4.5.4 Antibody synthesis

Purified BacO-His_6 and His_6-$BadA_{\Delta aa1-239}$ were sent for antibody generation (Eurogentec, Belgium).

4.5.5 Co-immunoprecipitation, pull-down and mass spectrometry

Co-IP with BacN-HA: Exponentially growing cells (250 ml) were incubated with 0.6% paraformaldehyde in PBS for 20 min, followed by incubation with 125 mM glycine in PBS for 5 min in order to stop the crosslinking reaction. Cells were then harvested by centrifugation at 4 ˚C, 2000 g for 10 min. Pellets were washed twice with wash buffer 1 (50mM $NaPO_4$, pH 7.4, 5 mM $MgCl_2$). Afterwards, the cells were resuspended in 4 ml RIPA-like buffer (10 mM sodium phosphate, pH 7.2, 0.1% SDS, 1% Triton X-100, 1 mM EDTA), supplied with Complete Mini with EDTA protease inhibitor (Roche). The suspension was incubated on ice for 2 h to lyse the cells. Cell debris was then removed by centrifugation at 6000 rpm for 20 min. The supernatant was incubated overnight with 20 µl EZview™ Red anti-HA affinity gel (Sigma Aldrich) at 4 ˚C, then washed in the following order: twice with Co-IP buffer (20 mM HEPES pH 7.4, 100 mM NaCl, 20% glycerol, 0.5% Triton X-100), three times with wash buffer 2 (50 mM Tris/HCl, pH 7.5, 150 mM NaCl, 1 mM EDTA, 0.5% Triton X-100), and three times with wash buffer 3 (100 mM Tris/HCl, pH 8.0, 750 mM NaCl, 1 mM EDTA, 0.05% Triton X-100). Bound proteins were eluted either in 100 µl of 50 mM glycine/HCl, pH 2.5, or by boiled in SDS sample buffer. The elutes were then subjected for Western blot analysis using α-BacP antibodies.

CO-IP with mCherry-fused BacN-P: Exponentially growing cells (250 ml) were incubated with 0.6% paraformaldehyde in PBS for 20 min, followed by incubation with 125 mM glycine in PBS for 5 min in order to stop the crosslinking reaction. Cells were then harvested by centrifugation at 2000 g and 4 ˚C for 10 min. Pellets were washed twice with wash buffer 1. Afterwards, the cells were resuspended in 4 ml RIPA-like buffer, supplied with Complete Mini with EDTA protease inhibitor (Roche). The resuspension was incubated on ice to lyse the cell for 2 h. Cell walls and debris were then removed by centrifugation at 6000 rpm for 20 min. For Co-IP against BacP-mCherry, BacO-mCherry, and BacN-mCherry, anti-RFP monoclonal antibody (MBL) was first bound to Dynabeads G (Invitrogen) following the manufacturer's protocol. Cell lysates were then incubated overnight at 4 ˚C with the dynabead-antibody complex. Afterwards, the mixtures were washed three times with wash buffer 3 and then eluted with 100 µl of 50 mM glycine-HCl, pH 2.5. Eluted proteins were visualized by silver staining after separation in an 11% SDS–polyacrylamide gel, and identified using matrix-assisted laser desorption/ionization time-of-flight mass spectrometry (MALDI-MS) analysis after excision from the gel.

Pull-down assay with StrepII-ParB: Cell lysates were prepared as follows: 1 L of exponentially growing cells (DK1622) was supplemented with 0.6% paraformaldehyde in PBS for 20-30 min, followed by incubation with 125 mM glycine in PBS for 5-10 min in order to stop the crosslinking reaction. Cells were then harvested by centrifugation at 6500 rpm and 4 ˚C for 10 min. Pellets were washed twice with wash buffer 1. Afterwards, the cells were resuspended in 15 ml of Buffer S (20 mM Tris-HCl, pH 7.6, 200 mM NaCl), supplemented with Complete Mini with EDTA protease inhibitor (Roche). The suspension was lysed by three passages in a French press (18000 psi). Cell debris was then removed by centrifugation at 10000 g for 10 min. The total of 15 ml cleared lysates was then divided into two equal volumes for both experiment and control samples. The Strep-Tactin® Superflow Plus resin was prepared as follows: 200 µl of regenerated Superflow Plus after StrepII-ParB purification were mixed with 1

mg purified StrepII-ParB and gently agitated for 2 h; meanwhile, another 200 µl Superflow Plus was mixed with 1 ml buffer S as a negative control. Resins were then washed twice with buffer S. Resins were then mixed with 7.5 ml DK1622 cleared lysates and incubated overnight at 4 ˚C. The mixtures were washed five times with buffer S. Proteins were eventually eluted with 5 × 200 µl of NPD buffer for 20 minutes. The elutes were subjected for immunoblot analysis using α-ParB antibodies (1:5000). For further detection of BacP, the elutes were concentrated using trichloroacetic acid (TCA) as follows: deoxycholic acid was added to elution samples to a final concentration of 0.1% before mixing with 1/10 vol. of 77% TCA. The mixtures were incubated on ice for 30 min then centrifuged at 13200 rpm for 15 min. Pellets were then washed twice with cold acetone and dried at 95 ºC for 2 min. The final products were resuspended in SDS sample buffer and heated at 95 ºC for 20 min before immunoblot analysis probed with α-BacP antibodies (1:1000).

Pull-down assay with His_6-$BadA_{\Delta aa1-239}$: cell pellets were collected as described in pull-down assay with StrepII-ParB using 2 L of DK1622 cultures in total. The cells were resuspended in 20 ml of buffer S supplemented with Complete Mini without EDTA protease inhibitor (Roche). The suspension was lysed by three passages in a French press (16000 psi). Cell debris was then removed by centrifugation at 10000 g for 30 min. The total of 20 ml cleared lysates was divided into two equal volumes for both experiment and control samples. The Ni-NTA agarose beads were equilibrated with buffer S, and then subjected for the follows: Ni-NTA agarose resins were mixed with 1.5 mg purified His_6-$BadA_{\Delta aa1-239}$ and gently agitated for 1.5 h; meanwhile, same amount of Ni-NTA agarose resin was mixed with 600 µl of buffer S as a negative control. Resins were then washed twice with buffer S and then mixed with 10 ml DK1622 clear lysates. The mixtures were incubated overnight at 4 ˚C and then washed four times with buffer S. Proteins were eventually eluted by 4 × 500 µl buffer B4. The elutes were subjected for SDS-PAGE and Western blot analysis using α-BacP or α-BacO antibodies, as well as matrix-assisted laser desorption/ionization time-of-flight mass spectrometry (MALDI-MS).

4.6 Bioinformatic and Statistic analysis

Nucleotide and amino acid sequences were obtained from the national center for biotechnology information (NCBI) (http://www.ncbi.nlm.nih.gov/). Sequence alignments were conducted using the Blastn- or Blastp- algorithm at NCBI or MUSCLE (MUltiple Sequence Comparison by Log- Expectation) algorithm at EMBL-EBI [37] (http://www.ebi.ac.uk/Tools/msa/muscle/). Conserved domains of proteins were identified using the NCBI website. Secondary structures were predicted using the PSIPRED Protein Sequence Analysis Workbench [13, 70, 96] (UCL; http://bioinf.cs.ucl.ac.uk/psipred/).

All the statistic analyses were performed using Origin 6.1 (OriginLab, USA). For *t*-test analysis, the independent 2-population test with significance level of α=0.001 was used.

APPENDIX

Table 7. Oligonucleotides

Name	Sequences (5'→3')
MXAN4635-down-rev	ATGGTACCAAGAAGAAGGTCGTGGTGAAGAAGA
MXAN4635-down-for	ATATAAGCTTCCTGCCTGGTCCTTCGAACCTTC
MXAN4635-up-for	ATGGATCCGTTGCTGCTCGCTGAGAGCT
MXAN4635-up-rev	ATGAATTCCTCACCATCGAGAGCACCGGC
MXAN4636-down-for	ATATAAGCTTCAGCGGCTTGCTTCCCAGGC
MXAN4636-down-rev	ATGGATCCAAGGGCAACGTCGACATGGAC
MXAN4636-up-for	ATATGGATCCAGGTGTGTGCCGTGCCGT
MXAN4636-up-rev	ATGAATTCCTGTTCGTCCTGTGTGGCGCG
MXAN4637-down-rev	ATGGATCCATCGAGATGGACGTACGGCTTC
MXAN4637-down-for	ATATAAGCTTCTGACGATGGCGTTCTTCACCGC
MXAN4637-up-for	ATGGATCCGCCCTTGCCGATGATGCCC
MXAN4637-up-rev	ATGAATTCCAAGAAGGCCTTCGTGCTGGCG
MXAN4634-down-for	TAGGATCCTCGTCCGAGCTGGTCACCTATCTGG
MXAN4634-down-rev	TTAAGAATTCCTCGCGGAAGGACAGCGTCTGCAGCGTC
MXAN4634-up-For	TATAAAGCTTCCTCCTTCAAGGGCAACGTCGAC
MXAN4634-up-Rev	TAGGATCCCATGGTGGCACCCCTGAAAAGCCCA
MXAN4634down-1-HindIII	GAGCAAGCTTAGAATCTTCCGGTAGGA
MXAN4634down-2-BamHI	AATTGGATCCTCGTCCGAGCTGGTCAC
BacN-up-1-BamHI	AATTGGATCCGCCCTTGCCGATGATGC
BacN-up-2-EcoRI	AATTGAATTCGGCCACGGTAAGGCCGA
MXAN4635-For	TATAGATCTATGGCCACCGCGAAGGAGCTCTCAG
MXAN4635-Rev	TTTTGCTAGCCTAGCGGGTCTTCTTCTTCACCACG
MXAN4636-For	TATAGATCTATGAGCTTCACGCCGCGCACGGCACG
MXAN4636-Rev	TTTTGCTAGCTCAGCGCTCCTTCATGTCCATGTC
MXAN4637-For	TATAGATCTATGGCAACGGGTGAAACGGGCATCAT

MXAN4635C111-240-For	TATAGATCTCGCGTGGACATGGGGGACGTGGAG
MXAN4634-For-new-NdeI	TATACATATGCGGGCGCGTGGGCTTTTCAGGG
MXAN4634-Rev-new-EcoRI	TAGAATTCGACAGCCCCTCCAGATAGGTGACCAG
ccParB-for	AATTCATATGATGTCCGAAGGGCGTCGTGGTCTG
ccParB-Rev	AATTGAATTCCCGATCCCGCGCGTCAGTCGGTTG
MXAN4637-for-2	GCGCGAATTCGGCAACGGGTGAAACGGGCA
MXAN4637-rev-2	GCGCGGATCCTCAAATGTCGTCAGGAAGCC
ParA-for-NdeI	AATTCATATGCACTGCATCACGCGCGGG
ParA-rev-EcoRI	AATTGAATTCCCAGCCACGCGCCTGCGA
mxan4634c-for	AATTCATATGCCCTCCGACGGCGAGGCCCG
mxan4634c-rev	AGTCGAATTCTTACAGCCCCTCCAGATAGG
parA(R209A)-for	ACCATGTTCGACTCGGCGGCGAACATTGCCCA
parA(R209A)-rev	TGGGCAATGTTCGCCGCCGAGTCGAACATGGT
parA(R238E)-for	GTGCCGCGCAACGTGGAGCTGTCCGAGTGCCCC
parA(R238E)-rev	GGGGCACTCGGACAGCTCCACGTTGCGCGGCAC
MXAN4635-HA-1	TATAAAGCTTGTGGCCACCGCGAAGGAGCTCTCAG
MXAN4635-HA-2	TAGGATCCCTAAGCGTAGTCTGGGACGTCGTATGGGTAGCGGGTCTTCTTCTTCACCA
MXAN4635HA-down-for	TAGGATCCCGCGCACCGCCCGCGCCGCCAGTCG
MXAN4635HA-down-rev	TTAAGAATTCACTGCTCGGCGCGCGCCTCCTCGTT
MXAN4636HA-1	TATAAAGCTTATGGCAACGGGTGAAACGGGCATCA
MXAN4636-HA-2	TAGGATCCCTAAGCGTAGTCTGGGACGTCGTATGGGTAGCGCTCCTTCATGTCCATGT
MXAN4636down-1	TTAAGAATTCCGGTGCTCACCACCGGACTCCGGTG
MXAN4636down-2	TAGGATCCATGGACATGAAGGAGCGCTGATTCGTGG
MXAN4637-HA-1	TATAAAGCTTCGTGCTGCTGGCGCCGAAGATTCAA
MXAN4637-HA-2	TAGGATCCCTAAGCGTAGTCTGGGACGTCGTATGGGTAAATGTCGTCAGGAAGCCGTAC
MXAN4637HA-down-for	TAGGATCCCGGCTTCCTGACGACATTTGAGCTTCAC
MXAN4637HA-down-rev	TTAAGAATTCGGCAGCGGCTTGCTTCCCAGGCCAC
MXAN4635-up-for-2	TTGCGGCCGCGAGGAGCTGGCGCTGGGTGAGGTCA
MXAN4635-up-rev-2	TTTTCATATGGAATCAGCGCTCCTTCATGTCCATGT
mxan4635upFor-EcoRI	TAGAATTCGAGGAGCTGGCGCTGGGTGAGGTCA

MXAN4635Rev-HindIII	TATAAAGCTTCTAGCGGGTCTTCTTCTTCACCACG
MXAN4634down-For-2	TATAGCTAGCGCCATGGCGGAACCTCTCGTGCG
MXAN4634down-rev-2	TTAAGAATTCCTCGCGGAAGGACAGCGTCTGCAGCGTC
MXAN4634-For-XbaI	TTAATCTAGAATGCGGGCGCGTGGGCTTTTC
MXAN4634down-Rev-NheI	TTAAGCTAGCCTCGCGGAAGGACAGCGTCTG
MXAN4635-for-XbaI	AATTCTAGAATGGCCACCGCGAAGGAGCTC
MXAN4636-for-XbaI	AATTCTAGAATGAGCTTCACGCCGCGCACG
MXAN4637-for-XbaI	AATTCTAGAATGGCAACGGGTGAAACGGGC
mCherry-for-XbaI	AATTCTAGAATGGTGAGCAAGGGCGAGGAGGATAAC
MXAN4635-rev-HindIII	TATAAAGCTTCTAGCGGGTCTTCTTCTTCACCACG
MXAN4636-rev-HindIII	TATAAAGCTTTCAGCGCTCCTTCATGTCCATGTC
MXAN4637-rev-HindIII	TATAAAGCTTTCAAATGTCGTCAGGAAGCCGTACG
Comp MXAN4635-for	TTATCTAGAATGGCCACCGCGAAGGAGCTCTCA
Comp MXAN4635-Rev	TTAAAGCTTCTAGCGGGTCTTCTTCTTCACCAC
MXAN4637TC-rev	ATATGGATCCTCAGGGCTCCATACAGCAGCCCGGGCAACAGTTCAGGAAAATGTCGTCAGGAAGCCG
MXAN4635TC2-for	ATATGGATCCGTGGCCACCGCGAAGGAGCTCTC
MXAN4635TC2-rev	ATATCCCGGGCAACAGTTCAGGAAGACCACCGCGGGGCGCTCGG
MXAN4635TC2down-for	ATATCCCGGGCTGCTGTATGGAGCCCCGCCCCACGGCGGTGA
MXAN4635TC2down-rev	ATATGAATTCGGGCCCCCCGAAGCGTGCAGCTC
mCherry-Rev-NheI	TATAGCTAGCTTACTTGTACAGCTCGTCCATGCCGCCG
eYFP-for-BamHI	AATTGGATCCATGGTGAGCAAGGGCGA
eYFP-rev-HindIII	GGCCAAGCTTTTACTTGTACAGCTCGTC
mCherry-For-NdeI	AGCTCATATGATGGTGAGCAAGGGCGAGGAG
mCherry-MXAN4635-Rev-XhoI	AATTCTCGAGCTAGCGGGTCTTCTTCTTCACCA
NcoI-CFP-For	AATTCCATGGTGAGCAAGGGCGAGGAGCTGTTCA
CFP-MXAN4636-Rev-EcoRI	AGCTGAATTCTCAGCGCTCCTTCATGTCCATGTC
parB-yfp-for-XbaI	AATTTCTAGAAGGAGGAATTCACCATGGTGAAAGCAGACATGCAGAAGC
parB-yfp-rev-XmaI	GCGCCCCGGGTTACTTGTACAGCTCGTCCATGCCG
mCherry-MXAN4635rev-MfeI	AATTCAATTGCTAGCGGGTCTTCTTCTTCACCA

mCherry-MXAN4636rev-MfeI	AATTCAATTGTCAGCGCTCCTTCATGTCCATGTC
mCherry-for-NdeI-2	AATTCATATGGTGAGCAAGGGCGAGGAGG
mCherry-MXAN4635N-rev	AATTCAATTGCTACAGACGTCCCGGCTCCACGTC
XbaI-RBS-eYFP-for	TCTAGAAGGAGGAATTCACCATGGTGAGCAAGGGCGAGGAGC
ccParB-YFP-for-xbaI	AATTTCTAGAAGGAGGAATTCACCATGTCCGAAGGGCGTCG
ParB-for-BamHI strep	TGTAGGATCCGATGGTGAAAGCAGACATG
ParB-rev-NotI strep	AATTGCGGCCGCCTACTCCTTCCTGAGAAGC
YFP-MXAN4637-For	GCGCCCCGGGAGGAGGAATTCACCATGGTGAGCAAGGGCGAGGAGCTGT
YFP-MXAN4637-Rev	GCGCGGATCCTCAAATGTCGTCAGGAAGCCG
ParA-yfp-for-XbaI	AATTCTAGAAGGAGGAATTCACCATGCACTGCATCACGCGCGGGGCC
ParA-yfp-rev-XmaI	AATTCCCGGGTTACTTGTACAGCTCGTCCAT
mCherry-rev-HindIII	ATAAGCTTTTACTTGTACAGCTCGTCCATGCCGCCG
eyfp-rev-NheI	AGCTGCTAGCTTACTTGTACAGCTCGTC
ParA-rev-EcoRI-2	AATTGAATTCTCAAGCCACGCGCCTGCGAG
Commonly used oligonucleotides for sequencing and colony PCR	
eCFP-1	GTTTACGTCGCCGTCCAGCTCGAC
eCFP-2	ATGGTCCTGCTGGAGTTCGTGACC
M13for	GCCAGGGTTTTCCCAGTCACGA
M13rev	GAGCGGATAACAATTTCACACAGG
PvanA-for	GACGTCCGTTTGATTACGATCAAGATTGG
Pxyl-1	CCCACATGTTAGCGCTACCAAGTGC
T7 rev	GCTAGTTATTGCTCAGCGG
pET-for	CACGATGCGTCCGGCGTAGAGGATC
Pxyl-for	TGTCGGCGGCTTCTAGCATGGACCG
Pvan-for	TGGACTCTAGCCGACCGACTGAGACGC
mCherry-up	CTCGCCCTCGCCCTCGATCTCGAAC
mCherry-down	GGCGCCTACAACGTCAACATCAAGTTGG
REV-uni	GGGGATGTGCTGCAAGGCGATTAAGTTG
pET-rev	CCTTTCAGCAAAAAACCCCTCAAGACCCG
Duet1-MCSI-fw	GGATCTCGACGCTCTCCCTTATGC

Duet1-MCSI-rev	GATTATGCGGCCGTGTACAATACG
Duet1-MCSII-fw	TTGTACACGGCCGCATAATCG
attB right	GGAATGATCGGACCAGCTGAA
attB left	CGGCACACTGAGGCCACATA
attP right	GCTTTCGCGACATGGAGGA
attP left	GGGAAGCTCTGGGTGACGAA
KA-231FOR	GGATGTGCTGCAAGGCGATTAAGTTGG
KA-232REV	GCTTTACACTTTATGCTTCCGGCTCG
CuoA-F	CCGAGGTCACGCGCCTC
pSW105fwd	GGCTTGGAGTGCGCACCT
pSW105rev	ACGACGTTGTAAAACGAC
HA-1	ATGTACCCATACGACGTCCCAGACTACGCTTCG
HA tag-2	CTACCATGGAAGCGTAGTCTGGGACGTCGTATGGGTA

Table 8. Plasmids and strains.

Plasmid	**Description**	**Reference/ source**
Basic vectors		
pBJ114	*galK*-containing suicide vector for double homologous recombination in *M. xanthus*, Kan^R	[72]
pSWU30	Vector for interacting at *M. xanthus* chromosomal Mx8 *attB* site, Tet^R	[152]
pKO1Km	*galK*-containing suicide vector for double homologous recombination in *M. xanthus*, Kan^R	[137]
pMAT4	Vector for genes ligated to *cuoA* promoter interacting at *M. xanthus* chromosomal Mx8 *attB* site, Kan^R	[51]
pMAT15	Vector for genes ligated to *cuoA* promoter interacting at *M. xanthus PcuoA* site, Kan^R	[51]
pSW105	Vector for genes ligated to *pilA* promoter interacting at *M. xanthus* chromosomal Mx8 *attB* site, Kan^R	[69]; S.Weiss
pMT325	pASK-IBA3plus derivative with pBBR1MCS-5 backbone, Amp^R, Gm^R	[130]
pETDuet-1	Vector for coexpression of two target genes, Amp^R	Novagen
pRSFDuet-1	Vector for coexpression of two target genes, Kan^R	Novagen
pET21a+	Vector for overexpression of C-terminally His_6-tagged proteins, Amp^R	Novagen
pET28a+	Vector for overexpression of N-terminally His_6-tagged proteins, Kan^R	Novagen
pET51b+	Vector for overexpression of N-terminally StrepII-tagged proteins, Amp^R	Novagen
pXCHYN-2	Integration plasmid to fuse 5' end of a target gene to *mCherry* under the control of P_{xyl}, Kan^R	[131]
pXYFPN-1	Integration plasmid to fuse 5' end us of a target gene to *eyfp* under the control of P_{xyl}, $Strep/Spec^R$	[131]
pVCFPN-4	Integration plasmid to fuse 5' end us of a target gene to *cfp* under the control of P_{van}, $Gent^R$	[131]
pXCHYC-1	Integration plasmid to fuse 3' end us of a target gene to *mCherry* under the control of P_{xyl}, $Strep/Spec^R$	[131]
pXYFPC-2	Integration plasmid fuse 3' end us of a target gene to *eyfp* under the control of P_{xyl}, Kan^R	[131]
pXVENN-2	Integration plasmid to fuse 5' end us of a target gene to *venus* under the control of P_{xyl}, Kan^R	[131]
pMR3690	Vector for the expression of a gene under the control of the *vanA* promoter, integrating at the *M. xanthus* Mxan18_19 chromosomal locus, Kan^R	[65]
pMR3691	Vector for the expression of a gene under the control of the *vanA* promoter, integrating at the *M. xanthus* Mxan18_19 chromosomal locus, tet^R	[65]
pLL1	pBJ114 derivative used to generate an in-frame deletion in *bacP* in *M. xanthus*	this study
pLL2	pBJ114 derivative used to generate an in-frame deletion in *bacO* in *M. xanthus*	this study
pLL3	pBJ114 derivative used to generate an in-frame deletion in *bacN* in *M. xanthus*	this study

pLL9	pBJ114 derivative used to replace native *bacP* with *bacP*-HA in *M. xanthus*	this study
pLL10	pBJ114 derivative used to replace native *bacO* with *bacO*-HA in *M. xanthus*	this study
pLL11	pBJ114 derivative used to replace native *bacN* with *bacN*-HA in *M. xanthus*	this study
pLL14	pMAT4 bearing *bacP-mCherry*	this study
pLL15	pMAT4 bearing *bacO-mCherry*	this study
pLL16	pMAT4 bearing *bacN-mCherry*	this study
pLL17	pXCHYN-2 bearing *bacP*	this study
pLL18	pXCHYN-2 bearing *bacO*	this study
pLL19	pXCHYN-2 bearing *bacN* fused with *bacO*	this study
pLL20	pLL17 carrying the upstream region of *bacP*	this study
pLL23	pBJ114 derivative used to replace the native *bacP* with *mCherry-bacP* in *M. xanthus*	this study
pLL30	pSW105 bearing *mCherry-bacP*	this study
pLL31	pSW105 bearing *mCherry-bacO*	this study
pLL32	pSW105 bearing *mCherry-bacN*	this study
pLL33	pSW105 bearing *bacP*	this study
pLL38	pBJ114 derivative used to generate in-frame deletion of *badA* in *M. xanthus*	this study
pLL42	pBJ114 derivative used to replace native *bacN* with *bacN*-TC in *M. xanthus*	this study
pLL45	pBJ114 derivative used to replace native *bacP* with *bacP*-TC in *M. xanthus*	this study
pLL47	pVCFPN-4 bearing *bacO*	this study
pLL48	pETDuet-1carrying *mCherry-bacP*	this study
pLL51	pETDuet-1carrying *cfp-bacO*	this study
pLL52	pMT325 carrying *parB-eyfp*	this study
pLL53	pXCHYN-2 bearing $bacP_{\Delta aa1\text{-}110}$	this study
pLL54	pETDuet-1 carrying *cfp-bacO* and *mCherry-bacP*	this study
pLL55	pETDuet-1 carrying *mCherry-bacO*	this study
pLL57	pETDuet-1 carrying *mCherry-*$bacP_{\Delta aa1\text{-}110}$	this study
pLL60	pETDuet-1 carrying *mCherry-*$bacP_{\Delta aa123\text{-}240}$	this study
pLL61	pMT325 carrying *eyfp*	this study
pLL64	pXCHYC-1 bearing *badA*	this study

pLL65	pXYFPC-2 bearing *parB (C. crescentus)*	this study
pLL66	pLL64 carrying downstream region of *badA*	this study
pLL69	pMT325 carrying *ccparB-eyfp*	this study
pLL72	pBJ114 derivative used to replace the native *badA* with *badA-mCherry* in *M. xanthus*	this study
pLL73	pSW105 bearing *badA-mCherry*	this study
pLL74	pMAT4 bearing *badA-mCherry*	this study
pLL80	pET51b(+) bearing *parB*	this study
pLL85	pXYFPC-2 bearing *parA*	this study
pLL86	pMT325 carrying *parA-eyfp*	this study
pLL87	pXYFPC-2 bearing *badA*	this study
pLL89	pSWU30 carrying P_{parA}-*parA-eyfp*	this study
pLL93	pMAT4 bearing *badA-eyfp*	this study
pLL97	pET21a(+) bearing *badA*	this study
pLL100	pMT325 carrying *parA-mCherry*	this study
pLL101	pRSFDuet-1 carrying *badA-eyfp*	this study
pLL104	pBJ114 derivative used to generate in-frame deletion of MXAN4634-7 in *M. xanthus*	this study
pLL105	pET28a(+) bearing $badA_{\Delta aa1-239}$	this study
pLL116	pMR3691 carrying *parA-eyfp*	this study
pLL117	pXYFPC-2 bearing $parA^{R238E}$	this study
pLL118	pXVENN-2 bearing $badA_{\Delta aa1-239}$	this study
pLL119	pXYFPC-2 bearing $parA^{R209A}$	this study
pLL120	pRSFDuet-1 carrying *venus-* $badA_{\Delta aa1-239}$	this study
pLL121	pXCHYC-1 bearing $parA^{R238E}$	this study
pLL122	pMT325 carrying $parA_{R238E}$-*mCherry*	this study
pLL123	pXCHYC-1 bearing $parA^{R209A}$	this study
pLL124	pMT325 carrying $parA_{R209A}$-*mCherry*	this study
pLL126	pMR3690 carrying *badA*	this study
pLL131	pET28a(+) bearing *badA*	this study
pLL132	pMR3691 carrying *parA*	this study

pLL137	pRSFDuet-1 carrying *eyfp*	this study
pPS17	pXYFPN-2 bearing *bacN*	P. Schall
pPS20	pMT325 carrying *eyfp-bacN*	P. Schall
pSW17	pET21a(+) bearing *bacO*	[82]
pMT978	pKO1Km derivative used to replace the native *bacP* with *bacP-mCherry* in *M. xanthus*	[82]
pMT979	pKO1Km derivative used to replace the native *bacO* with *bacO-mCherry* in *M. xanthus*	[82]
pMT980	pKO1Km derivative used to replace the native *bacN* with *bacN-mCherry* in *M. xanthus*	[82]
pAH7	pSWU30 carrying P_{parB}-*parB-yfp*	[133]
pAH59	pSWU30 fused with P_{parA}-*parA-mCherry*	[57]
pAH73	pMAT15 bearing *parB-yfp*	[57]

Strains

DK1622	*M. xanthus* wild type	[74]
Rosetta™(DE 3)pLysS	F^- *ompT hsdS*$_B$(r_B^- m_B^-) *gal dcm* (DE3) pLysSRARE (Cam^R)	Novagen
BL21(DE3)	F^- *omp*T *hsd*SB(rB–, mB–) *gal dcm* (DE3)	Novagen
TOP10	F^- *mcr*A Δ(*mrr-hsd*RMS-*mcr*BC) Φ80*lac*ZΔM15 Δ*lac*X74 *rec*A1 *ara*D139 Δ(*ara leu*) 7697 *gal*U *gal*K *rps*L (StrR) *end*A1 *nup*G	Invitrogen
DK1300	Δ*sglG*	[62]
DK5208	*CsgA::Tn5-132 Ω LS205*	[80]
MT295	In-frame deletion of *bacN-P* in DK1622 using pMT982	[82]
MT296	Substitution of the native *bacP* gene of DK1622 with *bacP-mCherry* by double homologous recombination using pMT978	[82]
MT297	Substitution of the native *bacO* gene of DK1622 with *bacO-mCherry* by double homologous recombination using pMT979	[82]
MT298	Substitution of the native *bacN* gene of DK1622 with *bacN-mCherry* by double homologous recombination using pMT980	[82]
MT300	In-frame deletion of *bacM* in DK1622 using pMT981	[82]
JK328	In-frame deletion of *bacM* in MT295 using pMT981	[82]
LL001	In-frame deletion of *bacP* in DK1622 using pLL1	this study
LL002	In-frame deletion of *bacO* in DK1622 using pLL2	this study
LL003	In-frame deletion of *bacN* in DK1622 using pLL3	this study
LL012	Integration of a *parB-eyfp* fusion under P_{parB} at the *attB* site of DK1622 using pAH7	this study

LL013	Integration of a *parB-eyfp* fusion under P_{parB} at the *attB* site of MT300 using pAH7	this study
LL014	Integration of a *parB-eyfp* fusion under P_{parB} at the *attB* site of LL003 using pAH7	this study
LL015	Integration of a *parB-eyfp* fusion under P_{parB} at the *attB* site of LL001 using pAH7	this study
LL016	Integration of a *parB-eyfp* fusion under P_{parB} at the *attB* site of JK328 using pAH7	this study
LL018	Integration of a *parB-eyfp* fusion under P_{parB} at the *attB* site of LL002 using pAH7	this study
LL019	Integration of a *parB-eyfp* fusion under P_{parB} at the *attB* site of MT295 using pAH7	this study
LL028	Integration of *bacP-mCherry* under P_{cuoA} at the *attB* site of LL001 using pLL14	this study
LL032	Substitution of the native *bacP* gene of DK1622 with a *bacP*-HA fusion by double homologous recombination using pLL9	this study
LL033	Substitution of the native *bacN* gene of DK1622 with a *bacN*-HA fusion by double homologous recombination using pLL11	this study
LL034	Integration of *bacP-mCherry* under P_{cuoA} at the *attB* site of DK1622 using pLL14	this study
LL035	Integration of *bacN-mCherry* under P_{cuoA} at the *attB* site of DK1622 using pLL16	this study
LL037	Integration of *bacO-mCherry* under P_{cuoA} at the *attB* site of LL002 using pLL15	this study
LL038	Integration of *bacO-mCherry* under P_{cuoA} at the *attB* site of DK1622 using pLL15	this study
LL040	Integration of a *parB-eyfp* fusion under P_{parB} at the *attB* site of LL033 using pAH7	this study
LL046	Integration of a *parB-eyfp* fusion under P_{parB} at the *attB* site of LL032 using pAH7	this study
LL048	Substitution of the native *bacO* gene of DK1622 with a *bacO*-HA fusion by double homologous recombination using pLL10	this study
LL061	Substitution of *bacP* of DK1622 with *mCherr-bacP* by double homologous recombination using pLL23	this study
LL067	Integration of a *parB-eyfp* fusion under P_{parB} at the *attB* site of LL061 using pAH7	this study
LL074	Integration of *mCherry-bacO* under P_{pilA} at the *attB* site of LL002 using pLL31	this study
LL080	Integration of *mCherry-bacP* under P_{pilA} at the *attB* site of LL001 using pLL30	this study
LL084	Integration of *mCherry-bacP* under P_{pilA} at the *attB* site of DK1622 using pLL30	this study
LL085	Integration of *mCherry-bacO* under P_{pilA} at the *attB* site of DK1622 using pLL31	this study
LL086	Integration of *mCherry-bacN* under P_{pilA} at the *attB* site of DK1622 using pLL32	this study
LL101	In-frame deletion of *badA* in DK1622 using pLL38	this study
LL102	Integration of a *parB-eyfp* fusion under P_{parB} at the *attB* site of LL101 using pAH7	this study
LL104	Substitution of the native *bacP* gene of DK1622 with a *bacP*-TC fusion by double homologous recombination using pLL45	this study

LL110	In-frame deletion of *badA* in LL033 using pLL38	this study
LL116	Substitution of the native *badA* gene of DK1622 with a *badA-mCherry* fusion by double homologous recombination using pLL72	this study
LL117	Substitution of the native *badA* gene of MT295 with a *badA-mCherry* fusion by double homologous recombination using pLL72	this study
LL118	Integration of a *parB-eyfp* fusion under P_{parB} at the *attB* site of LL116 using pAH7	this study
LL122	Substitution of the native *badA* gene of LL033 with a *badA-mCherry* fusion by double homologous recombination using pLL72	this study
LL124	Integration of *badA-mCherry* under P_{pilA} at the *attB* site of LL101 using pLL73	this study
LL130	Substitution of the native *badA* gene of LL001 with a *badA-mCherry* fusion by double homologous recombination using pLL72	this study
LL133	Integration of *badA-mCherry* under P_{pilA} at the *attB* site of DK1622 using pLL73	this study
LL134	Integration of *badA-mCherry* under P_{cuoA} at the *attB* site of DK1622 using pLL74	this study
LL135	Integration of *bacP* under P_{pilA} at the *attB* site of LL130 using pLL33	this study
LL140	Integration of *badA-mCherry* under P_{cuoA} at the *attB* site of LL033 using pLL74	this study
LL141	Substitution of the native *badA* gene of LL002 with a *badA-mCherry* fusion by double homologous recombination using pLL72	this study
LL142	Substitution of the native *badA* gene of LL003 with a *badA-mCherry* fusion by double homologous recombination using pLL72	this study
LL145	Integration of a *parA-mCherry* fusion under P_{parA} at the *attB* site of DK1622 using pAH59	this study
LL146	Substitution of the native *bacN* gene of DK1622 with a *bacN*-TC fusion by double homologous recombination using pLL42	this study
LL147	Integration of a *parA-mCherry* fusion under P_{parA} at the *attB* site of MT295 using pAH59	this study
LL148	Integration of a *parA-mCherry* fusion under P_{parA} at the *attB* site of LL002 using pAH59	this study
LL149	Integration of a *parA-mCherry* fusion under P_{parA} at the *attB* site of LL003 using pAH59	this study
LL150	Integration of a *parA-mCherry* fusion under P_{parA} at the *attB* site of LL032 using pAH59	this study
LL151	Integration of a *parA-mCherry* fusion under P_{parA} at the *attB* site of MT300 using pAH59	this study
LL152	Integration of a *parA-mCherry* fusion under P_{parA} at the *attB* site of LL001 using pAH59	this study
LL153	Integration of a *parA-mCherry* fusion under P_{parA} at the *attB* site of LL033 using pAH59	this study
LL154	Integration of a *parA-mCherry* fusion under P_{parA} at the *attB* site of LL101 using pAH59	this study
LL155	Integration of a *parA-mCherry* fusion under P_{parA} at the *attB* site of LL048 using pAH59	this study
LL156	Integration of a *parA-eyfp* fusion under P_{parA} at the *attB* site of DK1622 using pLL89	this study

LL158	Integration of a *parA-mCherry* fusion under P_{parA} at the *attB* site of LL104 using pAH59	this study
LL159	Integration of a *parA-mCherry* fusion under P_{parA} at the *attB* site of LL146 using pAH59	this study
LL162	Integration of a *parB-eyfp* fusion at the native *cuoA* site of LL145 using pAH73	this study
LL163	Integration of a *parA-eyfp* fusion under P_{parA} at the *attB* site of LL061 using pLL89	this study
LL167	Integration of *badA-eyfp* under P_{cuoA} at the *attB* site of LL061 using pLL93	this study
LL168	Integration of a *parB-eyfp* fusion at the native *cuoA* site of LL154 using pAH73	this study
LL172	Integration of a *parA-eyfp* fusion under P_{parA} at the *attB* site of LL116 using pLL89	this study
LL174	In-frame deletion of MXAN4634-7 in DK1622 using pLL104	this study
LL175	Integration of a *parA-mCherry* fusion under P_{parA} at the *attB* site of LL174 using pAH59	this study
LL176	Integration of a *parB-yfp* fusion under P_{parB} at the *attB* site of LL174 using pAH7	this study
LL182	Integration of a *parA-eyfp* fusion under P_{van} at the Mxan18_19 chromosomal locus of DK1622 using pLL116	this study
LL185	Integration of a *parA-eyfp* fusion under P_{van} at the Mxan18_19 chromosomal locus of LL174 using pLL116	this study
LL186	Integration of a *parA-eyfp* fusion under P_{van} at the Mxan18_19 chromosomal locus of LL001 using pLL116	this study
LL188	Integration of *bacP* under P_{pilA} at the at the *attB* site of LL186 using pLL33	this study
LL192	Integration of *badA* under P_{van} at the Mxan18_19 chromosomal locus of LL154 using pLL126	this study
LL195	Integration of a *parA-eyfp* fusion under P_{van} at the Mxan18_19 chromosomal locus of LL124 using pLL116	this study
LL196	Integration of *parA* under P_{van} at the Mxan18_19 chromosomal locus of DK1622 using pLL132	this study

REFERENCES

1. Anderson, D.E., Gueiros-Filho, F.J., and Erickson, H.P. (2004) Assembly dynamics of FtsZ rings in *Bacillus subtilis* and *Escherichia coli* and effects of FtsZ-regulating proteins. *J Bacteriol* 186, 5775-5781.

2. Ausmees, N., Kuhn, J.R., and Jacobs-Wagner, C. (2003) The bacterial cytoskeleton: an intermediate filament-like function in cell shape. *Cell* 115, 705-713.

3. Ausubel, F., Brent, R., Kingston, R., Moore, D., Seidman, J., Smith, J., and Struhl, K. (2002) *Short protocols in molecular biology: A Compendium of methods from current protocols in molecular biology.* John Wiley & Sons Inc..

4. Begg, K.J., Dewar, S.J., and Donachie, W.D. (1995) A new *Escherichia coli* cell division gene, ftsK. *J Bacteriol* 177, 6211-6222.

5. Ben-Yehuda, S., Rudner, D.Z., and Losick, R. (2003) RacA, a bacterial protein that anchors chromosomes to the cell poles. *Science* 299, 532-536.

6. Ben-Yehuda, S., Fujita, M., Liu, X.S., Gorbatyuk, B., Skoko, D., Yan, J., Marko, J.F., Liu, J.S., Eichenberger, P., Rudner, D.Z., and Losick, R. (2005) Defining a centromere-like element in *Bacillus subtilis* by Identifying the binding sites for the chromosome-anchoring protein RacA. *Mol Cell* 17, 773-782.

7. Bertsche, U., Kast, T., Wolf, B., Fraipont, C., Aarsman, M.E., Kannenberg, K., von Rechenberg, M., Nguyen-Disteche, M., den Blaauwen, T., Holtje, J.V., and Vollmer, W. (2006) Interaction between two murein (peptidoglycan) synthases, PBP3 and PBP1B, in *Escherichia coli*. *Mol Microbiol* 61, 675-690.

8. Bi, E.F. and Lutkenhaus, J. (1991) FtsZ ring structure associated with division in *Escherichia coli*. *Nature* 354, 161-164.

9. Bigot, S., Sivanathan, V., Possoz, C., Barre, F.X., and Cornet, F. (2007) FtsK, a literate chromosome segregation machine. *Mol Microbiol* 64, 1434-1441.

10. Bowman, G.R., Comolli, L.R., Zhu, J., Eckart, M., Koenig, M., Downing, K.H., Moerner, W.E., Earnest, T., and Shapiro, L. (2008) A polymeric protein anchors the chromosomal origin/ParB complex at a bacterial cell pole. *Cell* 134, 945-955.

11. Bowman, G.R., Comolli, L.R., Gaietta, G.M., Fero, M., Hong, S.H., Jones, Y., Lee, J.H., Downing, K.H., Ellisman, M.H., McAdams, H.H., and Shapiro, L. (2010) *Caulobacter* PopZ forms a polar subdomain dictating sequential changes in pole composition and function. *Mol Microbiol* 76, 173-189.

12. Bramkamp, M., Emmins, R., Weston, L., Donovan, C., Daniel, R.A., and Errington, J. (2008) A novel component of the division-site selection system of *Bacillus subtilis* and a new mode of action for the division inhibitor MinCD. *Mol Microbiol* 70, 1556-1569.

13. Buchan, D.W., Ward, S.M., Lobley, A.E., Nugent, T.C., Bryson, K., and Jones, D.T. (2010) Protein annotation and modelling servers at University College London. *Nucleic Acids Res* 38, W563-568.

14. Buddelmeijer, N. and Beckwith, J. (2004) A complex of the *Escherichia coli* cell division proteins FtsL, FtsB and FtsQ forms independently of its localization to the septal region. *Mol Microbiol* 52, 1315-1327.

15. Bulyha, I., Schmidt, C., Lenz, P., Jakovljevic, V., Hone, A., Maier, B., Hoppert, M., and Sogaard-Andersen, L. (2009) Regulation of the type IV pili molecular machine by dynamic localization of two motor proteins. *Mol Microbiol* 74, 691-706.

16. Bulyha, I., Lindow, S., Lin, L., Bolte, K., Wuichet, K., Kahnt, J., van der Does, C., Thanbichler, M., and Sogaard-Andersen, L. (2013) Two small GTPases act in concert with the bactofilin cytoskeleton to regulate dynamic bacterial cell polarity. *Dev Cell* 25, 119-131.

17. Cabeen, M.T. and Jacobs-Wagner, C. (2010) The bacterial cytoskeleton. *Annu Rev Genet* 44, 365-392.

18. Carballido-Lopez, R. and Errington, J. (2003) The bacterial cytoskeleton: in vivo dynamics of the actin-like protein Mbl of *Bacillus subtilis*. *Dev Cell* 4, 19-28.

19. Carballido-Lopez, R. (2006) Orchestrating bacterial cell morphogenesis. *Mol Microbiol* 60, 815-819.

20. Carballido-Lopez, R., Formstone, A., Li, Y., Ehrlich, S.D., Noirot, P., and Errington, J. (2006) Actin homolog MreBH governs cell morphogenesis by localization of the cell wall hydrolase LytE. *Dev Cell* 11, 399-409.

21. Carballido-Lopez, R. and Formstone, A. (2007) Shape determination in *Bacillus subtilis*. *Curr Opin Microbiol* 10, 611-616.

22. Charbon, G., Cabeen, M.T., and Jacobs-Wagner, C. (2009) Bacterial intermediate filaments: *in vivo* assembly, organization, and dynamics of crescentin. *Gene Dev* 23, 1131-1144.

23. Chen, J.C., Viollier, P.H., and Shapiro, L. (2005) A membrane metalloprotease participates in the sequential degradation of a *Caulobacter* polarity determinant. *Mol Microbiol* 55, 1085-1103.

24. Dai, K. and Lutkenhaus, J. (1992) The proper ratio of FtsZ to FtsA is required for cell division to occur in *Escherichia coli*. *J Bacteriol* 174, 6145-6151.

25. Daniel, R.A. and Errington, J. (2003) Control of cell morphogenesis in bacteria: two distinct ways to make a rod-shaped cell. *Cell* 113, 767-776.

26. Davis, M.A., Martin, K.A., and Austin, S.J. (1992) Biochemical activities of the parA partition protein of the P1 plasmid. *Mol Microbiol* 6, 1141-1147.

27. den Blaauwen, T., de Pedro, M.A., Nguyen-Disteche, M., and Ayala, J.A. (2008) Morphogenesis of rod-shaped sacculi. *FEMS Microbiol Rev* 32, 321-344.

28. Ditkowski, B., Holmes, N., Rydzak, J., Donczew, M., Bezulska, M., Ginda, K., Kedzierski, P., Zakrzewska-Czerwinska, J., Kelemen, G.H., and Jakimowicz, D. (2013) Dynamic interplay of ParA with the polarity protein, Scy, coordinates the growth with chromosome segregation in *Streptomyces coelicolor*. *Open biology* 3, 130006.

29. Dominguez-Escobar, J., Chastanet, A., Crevenna, A.H., Fromion, V., Wedlich-Soldner, R., and Carballido-Lopez, R. (2011) Processive movement of MreB-associated cell wall biosynthetic complexes in bacteria. *Science* 333, 225-228.

30. Donovan, C., Schwaiger, A., Kramer, R., and Bramkamp, M. (2010) Subcellular localization and characterization of the ParAB system from *Corynebacterium glutamicum*. *J Bacteriol* 192, 3441-3451.

31. Donovan, C., Sieger, B., Kramer, R., and Bramkamp, M. (2012) A synthetic *Escherichia coli* system identifies a conserved origin tethering factor in actinobacteria. *Mol Microbiol* 84, 105-116.

32. Donovan, C., Schauss, A., Kramer, R., and Bramkamp, M. (2013) Chromosome segregation impacts on cell growth and division site selection in *Corynebacterium glutamicum*. *PLoS One* 8, e55078.

33. dos Santos, V.T., Bisson-Filho, A.W., and Gueiros-Filho, F.J. (2012) DivIVA-mediated polar localization of ComN, a posttranscriptional regulator of *Bacillus subtilis*. *J Bacteriol* 194, 3661-3669.

34. Durand-Heredia, J.M., Yu, H.H., De Carlo, S., Lesser, C.F., and Janakiraman, A. (2011) Identification and characterization of ZapC, a stabilizer of the FtsZ ring in *Escherichia coli*. *J Bacteriol* 193, 1405-1413.

35. Ebersbach, G. and Gerdes, K. (2005) Plasmid segregation mechanisms. *Annu Rev Genet* 39, 453-479.

36. Ebersbach, G., Briegel, A., Jensen, G.J., and Jacobs-Wagner, C. (2008) A self-associating protein critical for chromosome attachment, division, and polar organization in *Caulobacter*. *Cell* 134, 956-968.

37. Edgar, R.C. (2004) MUSCLE: multiple sequence alignment with high accuracy and high throughput. *Nucleic Acids Res* 32, 1792-1797.

38. Edwards, D.H. and Errington, J. (1997) The *Bacillus subtilis* DivIVA protein targets to the division septum and controls the site specificity of cell division. *Mol Microbiol* 24, 905-915.

39. Esue, O., Rupprecht, L., Sun, S.X., and Wirtz, D. (2010) Dynamics of the bacterial intermediate filament crescentin *in vitro* and *in vivo*. *PLoS One* 5, e8855.

40. Fadda, D., Santona, A., D'Ulisse, V., Ghelardini, P., Ennas, M.G., Whalen, M.B., and Massidda, O. (2007) *Streptococcus pneumoniae* DivIVA: localization and interactions in a MinCD-free context. *J Bacteriol* 189, 1288-1298.

41. Figge, R.M., Divakaruni, A.V., and Gober, J.W. (2004) MreB, the cell shape-determining bacterial actin homologue, co-ordinates cell wall morphogenesis in *Caulobacter crescentus*. *Mol Microbiol* 51, 1321-1332.

42. Fletcher, D.A. and Mullins, R.D. (2010) Cell mechanics and the cytoskeleton. *Nature* 463, 485-492.

43. Fogel, M.A. and Waldor, M.K. (2005) Distinct segregation dynamics of the two *Vibrio cholerae* chromosomes. *Mol Microbiol* 55, 125-136.

44. Fogel, M.A. and Waldor, M.K. (2006) A dynamic, mitotic-like mechanism for bacterial chromosome segregation. *Genes Dev* 20, 3269-3282.

45. Fraipont, C., Alexeeva, S., Wolf, B., van der Ploeg, R., Schloesser, M., den Blaauwen, T., and Nguyen-Disteche, M. (2011) The integral membrane FtsW protein and peptidoglycan synthase PBP3 form a subcomplex in *Escherichia coli*. *Microbiology* 157, 251-259.

46. Garner, E.C., Campbell, C.S., and Mullins, R.D. (2004) Dynamic instability in a DNA-segregating prokaryotic actin homolog. *Science* 306, 1021-1025.

47. Garner, E.C., Bernard, R., Wang, W., Zhuang, X., Rudner, D.Z., and Mitchison, T. (2011) Coupled, circumferential motions of the cell wall synthesis machinery and MreB filaments in *B. subtilis*. *Science* 333, 222-225.

48. Ginda, K., Bezulska, M., Ziolkiewicz, M., Dziadek, J., Zakrzewska-Czerwinska, J., and Jakimowicz, D. (2013) ParA of *Mycobacterium smegmatis* co-ordinates chromosome segregation with the cell cycle and interacts with the polar growth determinant DivIVA. *Mol Microbiol* 87, 998-1012.

49. Gode-Potratz, C.J., Kustusch, R.J., Breheny, P.J., Weiss, D.S., and McCarter, L.L. (2011) Surface sensing in *Vibrio parahaemolyticus* triggers a programme of gene expression that promotes colonization and virulence. *Mol Microbiol* 79, 240-263.

50. Goehring, N.W. and Beckwith, J. (2005) Diverse paths to midcell: assembly of the bacterial cell division machinery. *Curr Biol* 15, R514-526.

51. Gomez-Santos, N., Treuner-Lange, A., Moraleda-Munoz, A., Garcia-Bravo, E., Garcia-Hernandez, R., Martinez-Cayuela, M., Perez, J., Sogaard-Andersen, L., and Munoz-Dorado, J. (2012) Comprehensive set of integrative plasmid vectors for copper-inducible gene expression in *Myxococcus xanthus*. *Appl Environ Microbiol* 78, 2515-2521.

52. Green, M.R.a.S., J. (2012) *Molecular Cloning: A Laboratory Manual (Fourth Edition)*. Cold Spring Harbor Laboratory Press.

53. Gruber, S. and Errington, J. (2009) Recruitment of condensin to replication origin regions by ParB/SpoOJ promotes chromosome segregation in *B. subtilis*. *Cell* 137, 685-696.

54. Gueiros-Filho, F.J. and Losick, R. (2002) A widely conserved bacterial cell division protein that promotes assembly of the tubulin-like protein FtsZ. *Genes Dev* 16, 2544-2556.

55. Hale, C.A. and de Boer, P.A. (1997) Direct binding of FtsZ to ZipA, an essential component of the septal ring structure that mediates cell division in *E. coli*. *Cell* 88, 175-185.

56. Hale, C.A., Shiomi, D., Liu, B., Bernhardt, T.G., Margolin, W., Niki, H., and de Boer, P.A. (2011) Identification of *Escherichia coli* ZapC (YcbW) as a component of the division apparatus that binds and bundles FtsZ polymers. *J Bacteriol* 193, 1393-1404.

57. Harms, A., Treuner-Lange, A., Schumacher, D., and Søgaard-Andersen, L. (2013) Tracking of chromosome and replisome dynamics in *Myxococcus xanthus* reveals a novel chromosome arrangement. *PLoS Genet* 9, e1003802.

58. Hay, N.A., Tipper, D.J., Gygi, D., and Hughes, C. (1999) A novel membrane protein influencing cell shape and multicellular swarming of *Proteus mirabilis*. *J Bacteriol* 181, 2008-2016.

59. Hempel, A.M., Wang, S.B., Letek, M., Gil, J.A., and Flardh, K. (2008) Assemblies of DivIVA mark sites for hyphal branching and can establish new zones of cell wall growth in *Streptomyces coelicolor*. *J Bacteriol* 190, 7579-7583.

60. Hester, C.M. and Lutkenhaus, J. (2007) Soj (ParA) DNA binding is mediated by conserved arginines and is essential for plasmid segregation. *P Natl Acad Sci USA* 104, 20326-20331.

61. Hodgkin, J. and Kaiser, D. (1977) Cell-to-cell stimulation of movement in nonmotile mutants of *Myxococcus*. *Proc Natl Acad Sci U S A* 74, 2938-2942.

62. Hodgkin, J. and Kaiser, D. (1979) Genetics of Gliding Motility in *Myxococcus xanthus* (Myxobacterales) - 2 Gene Systems Control Movement. *Molecular & General Genetics* 171, 177-191.

63. Holmes, N.A., Walshaw, J., Leggett, R.M., Thibessard, A., Dalton, K.A., Gillespie, M.D., Hemmings, A.M., Gust, B., and Kelemen, G.H. (2013) The coiled-coil protein Scy is a key component of a multi-protein assembly controlling polarised growth in *Streptomyces*. *Proc Natl Acad Sci U S A*.

64. Hwang, L.C., Vecchiarelli, A.G., Han, Y.W., Mizuuchi, M., Harada, Y., Funnell, B.E., and Mizuuchi, K. (2013) ParA-mediated plasmid partition driven by protein pattern self-organization. *EMBO J* 32, 1238-1249.

65. Iniesta, A.A., Garcia-Heras, F., Abellon-Ruiz, J., Gallego-Garcia, A., and Elias-Arnanz, M. (2012) Two systems for conditional gene expression in *Myxococcus xanthus* inducible by isopropyl-beta-D-thiogalactopyranoside or vanillate. *J Bacteriol* 194, 5875-5885.

66. Ireton, K., Gunther, N.W.t., and Grossman, A.D. (1994) spo0J is required for normal chromosome segregation as well as the initiation of sporulation in *Bacillus subtilis*. *J Bacteriol* 176, 5320-5329.

67. Ishino, F., Park, W., Tomioka, S., Tamaki, S., Takase, I., Kunugita, K., Matsuzawa, H., Asoh, S., Ohta, T., Spratt, B.G., and et al. (1986) Peptidoglycan synthetic activities in membranes of *Escherichia coli* caused by overproduction of penicillin-binding protein 2 and rodA protein. *J Biol Chem* 261, 7024-7031.

68. Jakimowicz, D., Brzostek, A., Rumijowska-Galewicz, A., Zydek, P., Dolzblasz, A., Smulczyk-Krawczyszyn, A., Zimniak, T., Wojtasz, L., Zawilak-Pawlik, A., Kois, A., Dziadek, J., and Zakrzewska-Czerwinska, J. (2007) Characterization of the mycobacterial chromosome segregation protein ParB and identification of its target in *Mycobacterium smegmatis*. *Microbiology* 153, 4050-4060.

69. Jakovljevic, V., Leonardy, S., Hoppert, M., and Sogaard-Andersen, L. (2008) PilB and PilT are ATPases acting antagonistically in type IV pilus function in *Myxococcus xanthus*. *J Bacteriol* 190, 2411-2421.

70. Jones, D.T. (1999) Protein secondary structure prediction based on position-specific scoring matrices. *J Mol Biol* 292, 195-202.

71. Jones, L.J., Carballido-Lopez, R., and Errington, J. (2001) Control of cell shape in bacteria: helical, actin-like filaments in *Bacillus subtilis*. *Cell* 104, 913-922.

72. Julien, B., Kaiser, A.D., and Garza, A. (2000) Spatial control of cell differentiation in *Myxococcus xanthus*. *P Natl Acad Sci USA* 97, 9098-9103.

73. Kadoya, R., Baek, J.H., Sarker, A., and Chattoraj, D.K. (2011) Participation of chromosome segregation protein ParAI of *Vibrio cholerae* in chromosome replication. *J Bacteriol* 193, 1504-1514.

74. Kaiser, D. (1979) Social Gliding Is Correlated with the Presence of Pili in *Myxococcus xanthus*. *P Natl Acad Sci USA* 76, 5952-5956.

75. Kim, H.J., Calcutt, M.J., Schmidt, F.J., and Chater, K.F. (2000) Partitioning of the linear chromosome during sporulation of *Streptomyces coelicolor* A3(2) involves an oriC-linked parAB locus. *J Bacteriol* 182, 1313-1320.

76. Kim, S.K. and Kaiser, D. (1990) Cell Motility Is Required for the Transmission of C-Factor, an Intercellular Signal That Coordinates Fruiting Body Morphogenesis of *Myxococcus xanthus*. *Gene Dev* 4, 896-904.

77. Kim, S.K. and Kaiser, D. (1990) C-factor: a cell-cell signaling protein required for fruiting body morphogenesis of *M. xanthus*. *Cell* 61, 19-26.

78. Koch, M.K., McHugh, C.A., and Hoiczyk, E. (2011) BacM, an N-terminally processed bactofilin of *Myxococcus xanthus*, is crucial for proper cell shape. *Mol Microbiol* 80, 1031-1051.

79. Konovalova, A., Petters, T., and Sogaard-Andersen, L. (2010) Extracellular biology of *Myxococcus xanthus*. *FEMS Microbiol Rev* 34, 89-106.

80. Kroos, L. and Kaiser, D. (1987) Expression of many developmentally regulated genes in *Myxococcus* depends on a sequence of cell interactions. *Genes Dev* 1, 840-854.

81. Kruse, T., Bork-Jensen, J., and Gerdes, K. (2005) The morphogenetic MreBCD proteins of *Escherichia coli* form an essential membrane-bound complex. *Mol Microbiol* 55, 78-89.

82. Kühn, J., Briegel, A., Morschel, E., Kahnt, J., Leser, K., Wick, S., Jensen, G.J., and Thanbichler, M. (2010) Bactofilins, a ubiquitous class of cytoskeletal proteins mediating polar localization of a cell wall synthase in *Caulobacter crescentus*. *EMBO J* 29, 327-339.

83. Kuner, J.M. and Kaiser, D. (1982) Fruiting body morphogenesis in submerged cultures of *Myxococcus xanthus*. *J Bacteriol* 151, 458-461.

84. Laemmli, U.K. (1970) Cleavage of structural proteins during the assembly of the head of bacteriophage T4. *Nature* 227, 680-685.

85. Laloux, G. and Jacobs-Wagner, C. (2013) Spatiotemporal control of PopZ localization through cell cycle-coupled multimerization. *J Cell Biol* 201, 827-841.

86. Lam, H., Schofield, W.B., and Jacobs-Wagner, C. (2006) A landmark protein essential for establishing and perpetuating the polarity of a bacterial cell. *Cell* 124, 1011-1023.

87. Lee, P.S. and Grossman, A.D. (2006) The chromosome partitioning proteins Soj (ParA) and Spo0J (ParB) contribute to accurate chromosome partitioning, separation of replicated sister origins, and regulation of replication initiation in *Bacillus subtilis*. *Mol Microbiol* 60, 853-869.

88. Lenarcic, R., Halbedel, S., Visser, L., Shaw, M., Wu, L.J., Errington, J., Marenduzzo, D., and Hamoen, L.W. (2009) Localisation of DivIVA by targeting to negatively curved membranes. *EMBO J* 28, 2272-2282.

89. Leonardy, S., Miertzschke, M., Bulyha, I., Sperling, E., Wittinghofer, A., and Sogaard-Andersen, L. (2010) Regulation of dynamic polarity switching in bacteria by a Ras-like G-protein and its cognate GAP. *EMBO J* 29, 2276-2289.

90. Letek, M., Ordonez, E., Vaquera, J., Margolin, W., Flardh, K., Mateos, L.M., and Gil, J.A. (2008) DivIVA is required for polar growth in the MreB-lacking rod-shaped actinomycete *Corynebacterium glutamicum*. *J Bacteriol* 190, 3283-3292.

91. Li, Z., Trimble, M.J., Brun, Y.V., and Jensen, G.J. (2007) The structure of FtsZ filaments *in vivo* suggests a force-generating role in cell division. *EMBO J* 26, 4694-4708.

92. Lin, L. and Thanbichler, M. (2013) Nucleotide-independent cytoskeletal scaffolds in bacteria. *Cytoskeleton (Hoboken)* 70, 409-423.

93. Lobedanz, S. and Sogaard-Andersen, L. (2003) Identification of the C-signal, a contact-dependent morphogen coordinating multiple developmental responses in *Myxococcus xanthus*. *Gene Dev* 17, 2151-2161.

94. Lowe, J. and Amos, L.A. (1998) Crystal structure of the bacterial cell-division protein FtsZ. *Nature* 391, 203-206.

95. Lutkenhaus, J., Pichoff, S., and Du, S. (2012) Bacterial cytokinesis: From Z ring to divisome. *Cytoskeleton (Hoboken)* 69, 778-790.

96. McGuffin, L.J., Bryson, K., and Jones, D.T. (2000) The PSIPRED protein structure prediction server. *Bioinformatics* 16, 404-405.

97. Miertzschke, M., Koerner, C., Vetter, I.R., Keilberg, D., Hot, E., Leonardy, S., Sogaard-Andersen, L., and Wittinghofer, A. (2011) Structural analysis of the Ras-like G protein MglA and its cognate GAP MglB and implications for bacterial polarity. *EMBO J* 30, 4185-4197.

98. Minnen, A., Attaiech, L., Thon, M., Gruber, S., and Veening, J.W. (2011) SMC is recruited to oriC by ParB and promotes chromosome segregation in *Streptococcus pneumoniae*. *Mol Microbiol* 81, 676-688.

99. Mohammadi, T., van Dam, V., Sijbrandi, R., Vernet, T., Zapun, A., Bouhss, A., Diepeveen-de Bruin, M., Nguyen-Disteche, M., de Kruijff, B., and Breukink, E. (2011) Identification of FtsW as a transporter of lipid-linked cell wall precursors across the membrane. *EMBO J* 30, 1425-1432.

100. Mohl, D.A. and Gober, J.W. (1997) Cell cycle-dependent polar localization of chromosome partitioning proteins in *Caulobacter crescentus*. *Cell* 88, 675-684.

101. Mohl, D.A., Easter, J., Jr., and Gober, J.W. (2001) The chromosome partitioning protein, ParB, is required for cytokinesis in *Caulobacter crescentus*. *Mol Microbiol* 42, 741-755.

102. Nogales, E., Downing, K.H., Amos, L.A., and Lowe, J. (1998) Tubulin and FtsZ form a distinct family of GTPases. *Nat Struct Biol* 5, 451-458.

103. Ogura, Y., Ogasawara, N., Harry, E.J., and Moriya, S. (2003) Increasing the ratio of Soj to Spo0J promotes replication initiation in *Bacillus subtilis*. *J Bacteriol* 185, 6316-6324.

104. Oliva, M.A., Cordell, S.C., and Lowe, J. (2004) Structural insights into FtsZ protofilament formation. *Nat Struct Mol Biol* 11, 1243-1250.

105. Oliva, M.A., Halbedel, S., Freund, S.M., Dutow, P., Leonard, T.A., Veprintsev, D.B., Hamoen, L.W., and Löwe, J. (2010) Features critical for membrane binding revealed by DivIVA crystal structure. *EMBO J* 29, 1988-2001.

106. Osborn, M.J. and Rothfield, L. (2007) Cell shape determination in *Escherichia coli*. *Curr Opin Microbiol* 10, 606-610.

107. Paradis-Bleau, C., Markovski, M., Uehara, T., Lupoli, T.J., Walker, S., Kahne, D.E., and Bernhardt, T.G. (2010) Lipoprotein cofactors located in the outer membrane activate bacterial cell wall polymerases. *Cell* 143, 1110-1120.

108. Patrick, J.E. and Kearns, D.B. (2008) MinJ (YvjD) is a topological determinant of cell division in *Bacillus subtilis*. *Mol Microbiol* 70, 1166-1179.

109. Pichoff, S. and Lutkenhaus, J. (2002) Unique and overlapping roles for ZipA and FtsA in septal ring assembly in *Escherichia coli*. *EMBO J* 21, 685-693.

110. Pichoff, S. and Lutkenhaus, J. (2007) Overview of cell shape: cytoskeletons shape bacterial cells. *Curr Opin Microbiol* 10, 601-605.

111. Pogliano, J., Pogliano, K., Weiss, D.S., Losick, R., and Beckwith, J. (1997) Inactivation of FtsI inhibits constriction of the FtsZ cytokinetic ring and delays the assembly of FtsZ rings at potential division sites. *Proc Natl Acad Sci U S A* 94, 559-564.

112. Ptacin, J.L., Lee, S.F., Garner, E.C., Toro, E., Eckart, M., Comolli, L.R., Moerner, W.E., and Shapiro, L. (2010) A spindle-like apparatus guides bacterial chromosome segregation. *Nat Cell Biol* 12, 791-798.

113. Rajagopala, S.V., Titz, B., Goll, J., Parrish, J.R., Wohlbold, K., McKevitt, M.T., Palzkill, T., Mori, H., Finley, R.L., Jr., and Uetz, P. (2007) The protein network of bacterial motility. *Mol Syst Biol* 3, 128.

114. Ramamurthi, K.S. and Losick, R. (2009) Negative membrane curvature as a cue for subcellular localization of a bacterial protein. *Proc Natl Acad Sci U S A* 106, 13541-13545.

115. Reyes-Lamothe, R., Nicolas, E., and Sherratt, D.J. (2012) Chromosome replication and segregation in bacteria. *Annu Rev Genet* 46, 121-143.

116. Rico, A.I., Garcia-Ovalle, M., Palacios, P., Casanova, M., and Vicente, M. (2010) Role of *Escherichia coli* FtsN protein in the assembly and stability of the cell division ring. *Mol Microbiol* 76, 760-771.

117. Ringgaard, S., van Zon, J., Howard, M., and Gerdes, K. (2009) Movement and equipositioning of plasmids by ParA filament disassembly. *Proc Natl Acad Sci U S A* 106, 19369-19374.

118. Romberg, L. and Levin, P.A. (2003) Assembly dynamics of the bacterial cell division protein FtsZ: poised at the edge of stability. *Annu Rev Microbiol* 57, 125-154.

119. Rosario, C.J. and Singer, M. (2007) The *Myxococcus xanthus* developmental program can be delayed by inhibition of DNA replication. *J Bacteriol* 189, 8793-8800.

120. Salje, J., van den Ent, F., de Boer, P., and Lowe, J. (2011) Direct membrane binding by bacterial actin MreB. *Mol Cell* 43, 478-487.

121. Schmidt, K.L., Peterson, N.D., Kustusch, R.J., Wissel, M.C., Graham, B., Phillips, G.J., and Weiss, D.S. (2004) A predicted ABC transporter, FtsEX, is needed for cell division in *Escherichia coli*. *J Bacteriol* 186, 785-793.

122. Schofield, W.B., Lim, H.C., and Jacobs-Wagner, C. (2010) Cell cycle coordination and regulation of bacterial chromosome segregation dynamics by polarly localized proteins. *EMBO J* 29, 3068-3081.

123. Shebelut, C.W., Guberman, J.M., van Teeffelen, S., Yakhnina, A.A., and Gitai, Z. (2010) *Caulobacter* chromosome segregation is an ordered multistep process. *Proc Natl Acad Sci U S A* 107, 14194-14198.

124. Sievers, J., Raether, B., Perego, M., and Errington, J. (2002) Characterization of the parB-like yyaA gene of *Bacillus subtilis*. *J Bacteriol* 184, 1102-1111.

125. Soufo, H.J.D. and Graumann, P.L. (2004) Dynamic movement of actin-like proteins within bacterial cells. *Embo Rep* 5, 789-794.

126. Stahlberg, H., Kutejova, E., Muchova, K., Gregorini, M., Lustig, A., Muller, S.A., Olivieri, V., Engel, A., Wilkinson, A.J., and Barak, I. (2004) Oligomeric structure of the *Bacillus subtilis* cell division protein DivIVA determined by transmission electron microscopy. *Mol Microbiol* 52, 1281-1290.

127. Stricker, J., Maddox, P., Salmon, E.D., and Erickson, H.P. (2002) Rapid assembly dynamics of the *Escherichia coli* FtsZ-ring demonstrated by fluorescence recovery after photobleaching. *Proc Natl Acad Sci U S A* 99, 3171-3175.

128. Sullivan, N.L., Marquis, K.A., and Rudner, D.Z. (2009) Recruitment of SMC by ParB-parS organizes the origin region and promotes efficient chromosome segregation. *Cell* 137, 697-707.

129. Sycuro, L.K., Pincus, Z., Gutierrez, K.D., Biboy, J., Stern, C.A., Vollmer, W., and Salama, N.R. (2010) Peptidoglycan crosslinking relaxation promotes *Helicobacter pylori*'s helical shape and stomach colonization. *Cell* 141, 822-833.

130. Thanbichler, M. and Shapiro, L. (2006) MipZ, a spatial regulator coordinating chromosome segregation with cell division in *Caulobacter*. *Cell* 126, 147-162.

131. Thanbichler, M., Iniesta, A.A., and Shapiro, L. (2007) A comprehensive set of plasmids for vanillate- and xylose-inducible gene expression in *Caulobacter crescentus*. *Nucleic Acids Res* 35, e137.

132. Thomaides, H.B., Freeman, M., El Karoui, M., and Errington, J. (2001) Division site selection protein DivIVA of *Bacillus subtilis* has a second distinct function in chromosome segregation during sporulation. *Genes Dev* 15, 1662-1673.

133. Treuner-Lange, A., Aguiluz, K., van der Does, C., Gomez-Santos, N., Harms, A., Schumacher, D., Lenz, P., Hoppert, M., Kahnt, J., Munoz-Dorado, J., and Sogaard-Andersen, L. (2013) PomZ, a ParA-like protein, regulates Z-ring formation and cell division in *Myxococcus xanthus*. *Mol Microbiol* 87, 235-253.

134. Typas, A., Banzhaf, M., van den Berg van Saparoea, B., Verheul, J., Biboy, J., Nichols, R.J., Zietek, M., Beilharz, K., Kannenberg, K., von Rechenberg, M., Breukink, E., den Blaauwen, T., Gross, C.A., and Vollmer, W. (2010) Regulation of peptidoglycan synthesis by outer-membrane proteins. *Cell* 143, 1097-1109.

135. Typas, A., Banzhaf, M., Gross, C.A., and Vollmer, W. (2012) From the regulation of peptidoglycan synthesis to bacterial growth and morphology. *Nat Rev Microbiol* 10, 123-136.

136. Tzeng, L., Ellis, T.N., and Singer, M. (2006) DNA replication during aggregation phase is essential for *Myxococcus xanthus* development. *J Bacteriol* 188, 2774-2779.

137. Ueki, T., Inouye, S., and Inouye, M. (1996) Positive-negative KG cassettes for construction of multi-gene deletions using a single drug marker. *Gene* 183, 153-157.

138. Ursinus, A., van den Ent, F., Brechtel, S., de Pedro, M., Holtje, J.V., Lowe, J., and Vollmer, W. (2004) Murein (peptidoglycan) binding property of the essential cell division protein FtsN from *Escherichia coli*. *J Bacteriol* 186, 6728-6737.

139. Vallet-Gely, I. and Boccard, F. (2013) Chromosomal organization and segregation in *Pseudomonas aeruginosa*. *PLoS Genet* 9, e1003492.

140. van den Ent, F., Amos, L.A., and Lowe, J. (2001) Prokaryotic origin of the actin cytoskeleton. *Nature* 413, 39-44.

141. van den Ent, F., Johnson, C.M., Persons, L., de Boer, P., and Lowe, J. (2010) Bacterial actin MreB assembles in complex with cell shape protein RodZ. *EMBO J* 29, 1081-1090.

142. van Teeffelen, S., Wang, S., Furchtgott, L., Huang, K.C., Wingreen, N.S., Shaevitz, J.W., and Gitai, Z. (2011) The bacterial actin MreB rotates, and rotation depends on cell-wall assembly. *Proc Natl Acad Sci U S A* 108, 15822-15827.

143. Vaughan, S., Wickstead, B., Gull, K., and Addinall, S.G. (2004) Molecular evolution of FtsZ protein sequences encoded within the genomes of archaea, bacteria, and eukaryota. *J Mol Evol* 58, 19-29.

144. Vecchiarelli, A.G., Han, Y.W., Tan, X., Mizuuchi, M., Ghirlando, R., Biertumpfel, C., Funnell, B.E., and Mizuuchi, K. (2010) ATP control of dynamic P1 ParA-DNA interactions: a key role for the nucleoid in plasmid partition. *Mol Microbiol* 78, 78-91.

145. Vecchiarelli, A.G., Mizuuchi, K., and Funnell, B.E. (2012) Surfing biological surfaces: exploiting the nucleoid for partition and transport in bacteria. *Mol Microbiol* 86, 513-523.

146. Vecchiarelli, A.G., Hwang, L.C., and Mizuuchi, K. (2013) Cell-free study of F plasmid partition provides evidence for cargo transport by a diffusion-ratchet mechanism. *Proc Natl Acad Sci U S A* 110, E1390-1397.

147. Watanabe, E., Wachi, M., Yamasaki, M., and Nagai, K. (1992) ATPase activity of SopA, a protein essential for active partitioning of F plasmid. *Mol Gen Genet* 234, 346-352.

148. White, C.L. and Gober, J.W. (2012) MreB: pilot or passenger of cell wall synthesis? *Trends Microbiol* 20, 74-79.

149. Wu, L.J. and Errington, J. (2003) RacA and the Soj-Spo0J system combine to effect polar chromosome segregation in sporulating *Bacillus subtilis*. *Mol Microbiol* 49, 1463-1475.

150. Wu, L.J. and Errington, J. (2004) Coordination of cell division and chromosome segregation by a nucleoid occlusion protein in *Bacillus subtilis*. *Cell* 117, 915-925.

151. Wu, L.J., Ishikawa, S., Kawai, Y., Oshima, T., Ogasawara, N., and Errington, J. (2009) Noc protein binds to specific DNA sequences to coordinate cell division with chromosome segregation. *EMBO J* 28, 1940-1952.

152. Wu, S.S., Wu, J., and Kaiser, D. (1997) The *Myxococcus xanthus* pilT locus is required for social gliding motility although pili are still produced. *Mol Microbiol* 23, 109-121.

153. Yamaichi, Y., Fogel, M.A., and Waldor, M.K. (2007) par genes and the pathology of chromosome loss in *Vibrio cholerae*. *Proc Natl Acad Sci U S A* 104, 630-635.

154. Yamaichi, Y., Bruckner, R., Ringgaard, S., Moll, A., Cameron, D.E., Briegel, A., Jensen, G.J., Davis, B.M., and Waldor, M.K. (2012) A multidomain hub anchors the chromosome segregation and chemotactic machinery to the bacterial pole. *Genes Dev* 26, 2348-2360.

155. Zhang, Y., Franco, M., Ducret, A., and Mignot, T. (2010) A bacterial Ras-like small GTP-binding protein and its cognate GAP establish a dynamic spatial polarity axis to control directed motility. *PLoS Biol* 8, e1000430.

156. Zhang, Y., Ducret, A., Shaevitz, J., and Mignot, T. (2012) From individual cell motility to collective behaviors: insights from a prokaryote, *Myxococcus xanthus*. *FEMS Microbiol Rev* 36, 149-164.

ACKNOWLEDGEMENT

As scientists, we usually have to be very professional and rational at writing. However, the acknowledgement is probably the only chance when we can emotionally express our gratitude without concerning too much on grammar and formats. I am very grateful that I have this opportunity to thank a lot of people here. Without them, this doctoral thesis will not be presented here.

First of all, I would like to thank my supervisor, Dr. Martin Thanbichler. I still can remember how excited I was when I got the chance to have an interview in the group. And you are such a wonderful advisor with brilliant scientific ideas that you provide tons of smart advices about my work. More importantly, you are always very nice and supportive. I also greatly appreciate the chance to have nice "debates" with you over the data from time to time, which helped me a lot to enrich my thoughts on this project. Last but not least, thank you for helping out with all the official documents when I just arrived here. Thank you for being such a wonderful supervisor.

I also want to express my gratitude to my doctoral thesis committee members: Prof. Dr. MD Lotte Søgaard-Andersen, Prof. Dr. Uwe Maier, and Prof. Dr. Hans-Ulrich Mösch. In particular, thank Prof. Dr. MD Lotte Søgaard-Andersen for being my second reviewer. I also want to thank Dr. Christof Taxis, who is one of my graduate school committee members.

I want to thank the DFG graduate school 'Intra- and Intercellular Transport and Communication' for funding. Especially, I want to thank Prof. Dr. Uwe Maier, the graduate school speaker, as well as our secretary of the school, Mrs. Lucette Claudet, for her extremely helpful assistance.

I would not be able to have this project work out without collaboration with many people. First, I want to thank our collaborator, Prof. Dr. MD Lotte Søgaard-Andersen and her group. Special thanks go to Andrea Harms, who first observed the link between bactofilins and chromosome segregation and provided all the necessary tools for ParAB localization and detection. I am also grateful to Dr. Iryna Bulyha for her help and communication on the social motility aspects of bactofilins. She also provided the anti-BacP antibodies. I thank Edina Hot for her help with co-immunoprecipitation and help within the graduate school. I also thank Jörg Kahnt for the MALDI/MS analyses. Secondly, I need to thank Dr. Adam Lange and Dr. Suresh Kumar Vasa from MPI for biophysical chemistry in Göttingen, for our successful collaboration on resolving the structure of bactofilins.

I always enjoyed my time working in the lab, with such a pleasant and inspiring working environment that helped me a lot to go through this stressful Ph. D life. For this, I want to express my great thanks to all the past and current lab members. In particular, I want to thank Dr. Juliane Kühn for her supervision when I first started my work here. I thank Julia Rosum and Marlina Bischoff for excellent technical assistance. I also thank my former bachelor student, Patrick Schall for his work within this project. Special thanks to our "postdoc community", Susan, Maria and Dani for their helpful suggestions and encouragement all the time. Also, I want to take this chance to thank Binbin He, not only for her great help, but also for sharing our

difficulties as friends on this way ever since we started our work here. Last but not least, I have to thank many of my colleagues, especially Alex, Emőke, Anne, Ola, Till, Sabrina, Wolle and Olli, who helped me with my many problems during my stay in Germany. Danke schön!

It has been very enjoyable to work with the Ecophysiology department, especially our 'A2' community (AG Thormann, AG Higgs and AG van der Does), for the comfortable and inspiring working environment. Thanks to all the nice people I have been working with. I also appreciate Manfred and Reinhard for their IT support all the time.

I also want to thank all my friends here, in China, in Hongkong or in the USA. Even though we may be far apart from each other, but we still talk and share our life from time to time. Thank you all for your precious friendships.

There are people who I always miss and love, no matter where I am. They are my family members. I need to apologize to my parents and grandma for not calling so often and not visiting them enough. This thesis is also your work. Without your love, none of my work could be done. Thank you so much for understanding and endless love. Last but not least, this is a thesis dedicated to all the people I love. No matter how far I am away from you, my love is always with all of you.

To this end, I also want to thank all the artists who produced wonderful music and movies. Their work becomes my best friend when life gets very tough. But as written, 'everything that kills me makes me feel alive.' (From 'Counting stars' by OneRepublic)

'So we beat on, boats against the current, borne back ceaselessly into the past.'

- From 'The Great Gatsby'

ERKLÄRUNG

Ich versichere, dass ich meine Dissertation:

„Cytoskeletons as polar landmarks: characterization of bactofilin homologs in *Myxococcus xanthus*“

selbstständig, ohne unerlaubte Hilfe angefertigt und mich dabei keiner anderen als der von mir ausdrücklich bezeichneten Quellen und Hilfen bedient habe.

Die Dissertation wurde in der jetzigen oder einer ähnlichen Form noch bei keiner anderen Hochschule eingereicht und hat noch keinen sonstigen Prüfungszwecken gedient.

Marburg, den _____

Lin Lin